



Development and Semi-Automated Analysis of an *in vitro* Dissemination Model
for Myeloma Cells Interacting with Mesenchymal Stromal Cells

Entwicklung und semi-automatisierte Analyse eines *in vitro* Modells
für die Disseminierung von Myelomzellen in Interaktion mit mesenchymalen Stromazellen

Doctoral Thesis for a Doctoral Degree

at the

GRADUATE SCHOOL OF LIFE SCIENCES,
JULIUS-MAXIMILIANS-UNIVERSITÄT WÜRZBURG,
SECTION BIOMEDICINE

submitted by

Martin Kuric

from

Bad Neustadt a.d. Saale

Würzburg, 2024

Submitted on:
Office stamp

Members of the *Promotionskomitee*:

Chairperson: Prof. Dr. Uwe Gbureck
Primary Supervisor: Prof. Dr. rer. nat. Regina Ebert
Supervisor (Second): Prof. Dr. med. Franziska Jundt
Supervisor (Third): Prof. Dr. rer. nat. Torsten Blunk

Date of Public Defense:

Date of Receipt of Certificates:

This work was conducted at the Department of Musculoskeletal Tissue Regeneration (Bernhard-Heine-Centre for Locomotive Research), University of Würzburg from 08.04.2018 to 31.03.2024 under the supervision of Prof Dr. rer. nat. Regina Ebert.

Acknowledgements

Lorem Ipsum dolor sit amet, consetetur sadipscing elitr, sed diam nonumy eirmod tempor invidunt ut labore et dolore magna aliquyam erat, sed diam voluptua. At vero eos et accusam et justo duo dolores et ea rebum. Stet clita kasd gubergren, no sea takimata sanctus est Lorem ipsum dolor sit amet. Lorem ipsum dolor sit amet, consetetur sadipscing elitr, sed diam nonumy eirmod tempor invidunt ut labore et dolore magna aliquyam erat, sed diam voluptua. At vero eos et accusam et justo duo dolores et ea rebum. Stet clita kasd gubergren, no sea takimata sanctus est Lorem ipsum

Summary

 Lorem Ipsum dolor sit amet, consetetur sadipscing elitr, sed diam nonumy eirmod tempor invidunt ut labore et dolore magna aliquyam erat, sed diam voluptua. At vero eos et accusam et justo duo dolores et ea rebum. Stet clita kasd gubergren, no sea takimata sanctus est Lorem ipsum dolor sit amet. Lorem ipsum dolor sit amet, consetetur sadipscing elitr, sed diam nonumy eirmod tempor invidunt ut labore et dolore magna aliquyam erat, sed diam voluptua. At vero eos et accusam et justo duo dolores et ea rebum. Stet clita kasd gubergren, no sea takimata sanctus est Lorem ipsum

Zusammenfassung

 Lorem Ipsum dolor sit amet, consetetur sadipscing elitr, sed diam nonumy eirmod tempor invidunt ut labore et dolore magna aliquyam erat, sed diam voluptua. At vero eos et accusam et justo duo dolores et ea rebum. Stet clita kasd gubergren, no sea takimata sanctus est Lorem ipsum dolor sit amet. Lorem ipsum dolor sit amet, consetetur sadipscing elitr, sed diam nonumy eirmod tempor invidunt ut labore et dolore magna aliquyam erat, sed diam voluptua. At vero eos et accusam et justo duo dolores et ea rebum. Stet clita kasd gubergren, no sea takimata sanctus est Lorem ipsum bla

Contents

Summary	ii
Introduction	1
Human Mesenchymal Stem/Stromal Cells	2
Multiple Myeloma	3
Myeloma-hMSC Interactions	3
Myeloma Bone Disease	3
Dissemination of Myeloma Cells	4
Code-Automation as a Standard in Modern Biosciences	5
How Code Quality Improves Scientific Reproducibility	6
Python as a Programming Language	8
Data Science with Python	12
Aims	14
Chapter 1: Modelling Myeloma Dissemination <i>in vitro</i>	15
Abstract	15
Introduction	16
Materials and Methods	18
Results	22
Discussion	35
Chapter 2: Semi-Automating Data Analysis with <code>plotastic</code>	36
Abstract	36
Introduction	37
Statement of Need	39
Example	40
Overview	42
Discussion	44
Summarising Discussion	46
Time Lapse	46
Myeloma	46
Semi-Automated Analysis Improves Agility During Establishing new <i>in vitro</i> Methods	46
References	47
Appendices	56
A Supplementary Data & Methods	56
A.1 Figures	56
A.2 Tables	74
A.3 Materials & Methods	82
B Documentation of <code>plotastic</code>	99
B.1 Class Diagram	100
B.2 Readme	102
B.3 Example Analysis “qpcr”	115
C Submission Forms & Documents	122

Contents

C.1	Author Contributions	122
C.2	Affidavit	129
C.3	Curriculum Vitae	131

Introduction

To provide a comprehensive background for the following chapters that focus on the interaction of human mesenchymal stromal cells (hMSCs) with multiple myeloma (MM) cells, this

Human Mesenchymal Stem/Stromal Cells

Explaining what a mesenchymal stromal cell (MSC) is, is not such an easy task as one might expect. MSCs are derived from multiple MSCs different sources, serve a wide array of functions and are always isolated as a heterogenous group of cells. This makes it particularly challenging to find a consensus on their exact definition, nomenclature, exact function and *in vivo* differentiation potential. Therefore, the most effective approach to describe hMSCs is to present their historical context.

hMSCs first gained popularity as a stem cell. Stem cells lay the foundation of multicellular organisms. Embryonic stem cells orchestrate the growth and patterning during embryonic development, while adult stem cells are responsible for regeneration during adulthood. The classical definition of a stem cell is that of a relatively undifferentiated cell that divides asymmetrically, producing another stem cell and a differentiated cell (Cooper, 2000; Shenghui et al., 2009). Because of their significance in biology and regenerative medicine, stem cells have become a prominent subject in modern research. Especially human mesenchymal stromal cells (hMSCs) have proven to be a promising candidate in this context (Ullah et al., 2015).

Mesenchyme first appears in embryonic development during gastrulation. There, cells that are committed to a mesodermal fate, lose their cell junctions and exit the epithelial layer in order to migrate freely. This process is called epithelial-mesenchymal transition (Tam & Beddington, 1987; Nowotschin & Hadjantonakis, 2010). Hence, the term mesenchyme describes non-epithelial embryonic tissue differentiating into mesodermal lineages such as bone, muscles and blood. Interestingly, it was shown nearly twenty years earlier that cells within adult bone marrow seemed to have mesenchymal properties as they were able to differentiate into bone tissue (A. J. Friedenstein et al., 1966; A. Friedenstein & Kuralesova, 1971; Bianco, 2014). This was the origin of the “mesengenic process”-hypothesis: This concept states that mesenchymal stem cells serve as progenitors for multiple mesodermal tissues (bone, cartilage, muscle, marrow stroma, tendon, fat, dermis and connective tissue) during both adulthood and embryonic development (A. Caplan, 1991; A. I. Caplan, 1994). The mesenchymal nature of these cells (termed bone marrow stromal cells: BMSCs) was confirmed later when they were shown to differentiate into adipocytic (fat) and chondrocytic (cartilage) lineages (Pittenger et al., 1999). Since then, the term “mesenchymal stem cell” (MSC) has grown popular as an adult multipotent precursor to a couple of mesodermal tissues. hMSCs derived from bone marrow (hMSCs) were shown to differentiate into osteocytes, chondrocytes, adipocytes and cardiomyocytes (Gronthos et al., 1994; Muruganandan et al., 2009; Xu et al., 2004) Most impressively, these cells also exhibited ectodermal and endodermal differentiation potential, as they produced neuronal cells, pancreatic cells and hepatocytes (Barzilay et al., 2009; Wilkins et al., 2009; Gabr et al., 2013; Stock et al., 2014).

Furthermore, cultures with MSC properties can be established from “virtually every post-natal organs and tissues”, and not just bone marrow (da Silva Meirelles et al., 2006). However, it has to be noted that hMSCs can differ greatly in their transcription profile and *in vivo* differentiation potential depending on which tissue they originated from (Jansen et al., 2010; Sacchetti et al., 2016).

Since “hMSCs” are a heterogenous group of cells, they were defined by their *in vitro* characteristics. A minimal set of criteria are the following (Dominici et al., 2006): First, hMSCs must be plastic adherent. Second, they must express or lack a set of specific surface antigens (positive for CD73, CD90, CD105; negative for CD45, CD34, CD11b, CD19). Third, hMSCs must differentiate to osteoblasts, adipocytes and chondroblasts *in vitro*. Together, hMSCs exhibit diverse differentiation potentials and can be isolated from multiple sources of the body. This offers great opportunity for regenerative medicine, if the particular hMSC-subtype is properly characterized.

Multiple Myeloma

Multiple myeloma arises from clonal expansion of malignant plasma cells in the bone marrow (BM). At diagnosis, myeloma cells have disseminated to multiple sites in the skeleton and, in some cases, to virtually any tissue (Rajkumar & Kumar, 2020; Bladé et al., 2022).

Myeloma-hMSC Interactions

Since plasma cells can not survive outside the bone marrow, MM cells also require survival signals for growth and disease progression. These signals are produced by the bone marrow microenvironment, including ECM, MSCs and ACs (Kibler et al., 1998; García-Ortiz et al., 2021).

Myeloma Bone Disease

Bone is a two-phase system in which the mineral phase provides the stiffness and the collagen fibers provide the ductility and ability to absorb energy (Viguet-Carrin et al., 2006). On a molecular level, bone tissue is composed of extracellular matrix (ECM) proteins that are calcified by hydroxyapatite crystals. This ECM consists mostly of collagen type I, but also components with major regulatory activity, such as fibronectin and proteoglycans that are essential for healthy bone physiology (Alcorta-Sevillano et al., 2020). Bone tissue is actively remodeled by bone-forming osteoblasts and bone-degrading osteoclasts. Osteoblasts are derived from mes-

enchymal stromal cells (MSCs) that reside in the bone marrow (A. J. Friedenstein et al., 1966; Pittenger et al., 1999). MSCs also give rise to adipocytes (ACs) to form Bone Marrow Adipose Tissue (BMAT), which can account for up to 70% of bone marrow volume (Fazeli et al., 2013).

MM indirectly degrades bone tissue by stimulating osteoclasts and inhibiting osteoblast differentiation, which leads to MM-related bone disease (MBD) (Glavey et al., 2017). MBD is present in 80% of patients at diagnosis and is characterized by osteolytic lesions, osteopenia and pathological fractures (Terpos et al., 2018).

Dissemination of Myeloma Cells

dissemination is still widely unclear - multistep process - invasion, intravasation, intravascular arrest, extravasation, colonization - overcome adhesion, retention, and dependency on the BM microenvironment - loss of adhesion factors such as CD138

Code-Automation as a Standard in Modern Biosciences

Beschreibe die Situation. - Big Data in Biosciences - what is big data, examples - Define citable challenges: - reproducibility crisis - lack of tools

In recent years, the biosciences have evolved dramatically, with a marked increase in the volume and complexity of data generated (Yang et al., 2017; Ekmekci et al., 2016). This transformation necessitates robust software tools, many of which require coding skills to use effectively. Here we summarize standard tools used by biosciences today and show their reliance on coding. The author argues that the role of a modern independent researcher is now intertwined with coding skills similar to a role of “precision medicine bioninformatician” (Gómez-López et al., 2019).

Statistical analysis in biosciences has traditionally been reliant on user-friendly tools like Excel and GraphPad Prism. While Excel by itself is recognized as limited for complex data analysis (Tanavalee et al., 2016; Incerti et al., 2019), GraphPad Prism offers more advanced statistical models .

However, increasingly demands more sophisticated approaches as data sets grow in size and complexity.

R and Python scripts offer more efficient and versatile solutions, enabling complex analyses with a few lines of code (R Core Team, 2018; Vallat, 2018).

Recognizing this trend, Microsoft has integrated a Python interpreter into Excel to computations more accessible within a widely used platform (?).

Next-generation sequencing, such as bulk RNAseq, has become affordable, allowing for larger sample sets during a single PhD project. This technology offers advanced tools that are most efficiently used through scripting in R or Python. In the absence of a dedicated statistician, researchers are compelled to learn coding.

In gene ontology, tools such as Metascape facilitate the integration of vast datasets and outputs multiple useful data visualizations. Metascape also provides multiple excel sheets, containing all results, sometimes in a nested format, which provides even further information that's adaptable for specific hypotheses, but given the sheer amount of data, is impractical to analyze manually.

since Metascape returns large Excel sheets with complex nested information, a researcher without coding skills requires manual work to adapt the results to specific research hypotheses.

its true potential is unlocked only when researchers can manipulate and analyze these data through scripting.

Modern gene ontology tools like Metascape offer powerful graphical user interfaces. However, their effectiveness is only possible through standardizing multiple large datasets.

The output from Metascape, large Excel sheets with complex nested information, is more efficiently analyzed through scripting, which is often necessary to adapt metascape results to specific research hypotheses.

Image analysis is another area where coding skills are essential. ImageJ/FIJI, a standard tool in the field, requires scripting for batch processing of multiple images and automating multiple processing steps into a pipeline. While macros can be recorded, understanding the underlying code is necessary for troubleshooting and adapting the macro to new datasets.

In the field of protein structural biology, Pymol is a standard tool that also has a Python command interface.

Similarly, artificial intelligence (AI), a game-changer in biomedicine, primarily uses Python due to its extensive libraries for machine learning and scientific computing. Python is also a standard for integrative biomedicine simulations.

Finally, databases and repositories are essential for storing, retrieving, and sharing data. Researchers need to understand common file formats to adhere to standards that ensure re-usability and interoperability. Scripting helps automate the process of formatting data for submission to these databases.

In conclusion, the integration of coding in bioscience research is not just a trend but a necessity. As the field continues to evolve, the demarcation between biologists and computational scientists blurs, underscoring the importance of coding skills for the next generation of researchers. The ability to code is fast becoming an indispensable asset, as integral to bioscience as traditional laboratory skills.

How Code Quality Improves Scientific Reproducibility

A main reason to write software is to define re-usable instructions for task automation (Narzt et al., 1998). However, the complexity of the code makes it prone to errors and can prevent usage by persons other than the author himself. This is a problem for the general scientific community, as the software is often the only way to reproduce the results of a study (Sandve et al., 2013). Hence, modern journals aim to enforce standards to software development, including software written and used by biological researchers (Smith et al., 2018). Here, we provide a brief overview of the standards utilized by `plotastic` that to ensure its reliability and reproducibility by the scientific community (Peng, 2011).

Modern software development is a long-term commitment of maintaining and improving

code after initial release (Boswell & Foucher, 2011). Hence, it is good practice to write the software such that it is scalable, maintainable and usable. Scalability or, to be precise, structural scalability means that the software can easily be expanded with new features without major modifications to its architecture (Bondi, 2000). This is achieved by writing the software in a modular fashion, where each module is responsible for a single function. Maintainability means that the software can easily be fixed from bugs and adapted to new requirements (Kazman et al., 2020). This is achieved by writing the code in a clear and readable manner, and by writing tests that ensure that the code works as expected (Boswell & Foucher, 2011). Usability is hard to define (Brooke, 1996), yet one can consider a software as usable if the commands have intuitive names and if the software’s manual, termed “documentation”, is up-to-date and easy to understand for new users with minimal coding experience. A software package that has not received an update for a long time (approx. one year) could be considered abandoned. Abandoned software is unlikely to be fully functional, since it relies on other software (dependencies) that has changed in functionality or introduce bugs that were not expected by the developers of all dependencies. Together, software that’s scalable, maintainable and usable requires continuous changes to its codebase. There are best practices that standardize the continuous change of the codebase, including version control, continuous integration (often referred to as CI), and software testing.

Version control is a system that records changes to the codebase line by line, allowing the documentation of the history of the codebase, including who made which changes and when. This is required to isolate new and experimental features into newer versions and away from the stable version that’s known to work. The most popular version control system is Git, which is considered the industry standard for software development (Chacon & Straub, 2024). Git can use GitHub.com as a platform to store and host codebases in the form of software repositories. GitHub’s most famous feature is called “pull request”. A pull request is a request from anyone registered on GitHub to include their changes to the codebase (as in “please pull this into your main code”). One could see pull requests as the identifying feature of the open source community, since it exposes the codebase to potentially thousands of independent developers, reaching a workforce that is impossible to achieve with closed source models used by paid software companies.

Continuous integration (CI) is a software development practice in which developers integrate code changes into a shared repository several times a day (Duvall et al., 2007). Each integration triggers the test suite, aiming to detect errors as soon as possible. The test suite includes building the software, setting up an environment for the software to run and then executing the programmed tests, ensuring that the software runs as a whole. Continuous integration is often used together with software branches. Branches are independent copies of the codebase that are meant to be merged back into the original code once the changes are finished. Since branches

accumulate multiple changes over time, this can lead to minor incompatibilities between the branches of all developers (integration conflicts), which is something that CI helps to prevent.

Continuous integration especially relies on a thorough software testing suite. Software testing is the practice of writing code that checks if the codebase works as expected (Myers et al., 2011). The main type of software testing is unit testing, which tests the smallest units of the codebase (functions and classes) in isolation (Listing 1).

Listing 1: Example of an arbitrary python function and its respective unit test function. The first function simply returns the number 5. The second function tests if the first function indeed returns the number 5. The test function is named with the prefix “test_” and is placed in a file that ends with the suffix “_test.py”. The test function is executed by the testing framework pytest. Note that code after “#” is considered a comment and won’t be executed.

```
1 # Define a function called "give_me_five" that returns the number 5
2 def give_me_five():
3     return 5
4 # Define a test function asserting that "give_me_five" returns 5
5 def test_give_me_five():
6     assert give_me_five() == 5
```

The quality of the software testing suite is measured by the code coverage, the precision of the tests, and the number of test-cases that are checked. The code coverage is the percentage of the codebase that is called by the testing functions, which should be as close to 100% as possible, although it does not measure how well the code is tested. The precision of the test is not a measurable quantity, but it represents if the tests truly checks if the code works as expected. The number of test-cases is the number of different scenarios that are checked by the testing functions, for example testing every possible option or combinations of options for functions that have multiple options. The most popular software testing framework for python is pytest, which is utilized by plotastic (Krekel et al., 2004).

Together, the standards of software development, including version control, continuous integration, and software testing, ensure that the software is scalable, maintainable, and usable. This is especially important for software that is used by the scientific community, as it ensures that the software is working as expected at defined versions years after publishing scientific results.

Python as a Programming Language

Here, we provide a general overview of the python programming language, explaining terms like “*type*”, “*method*”, etc., in order to prepare readers without prior programming experience for the following chapters. We also describe the design principles of python to lay out the key concepts that differentiate python compared to other programming languages. A more detailed tutorial on python that’s specialized for bioscientists is found in Ekmekci et al. 2016

Listing 2: Example of readable python code. This one-line code returns the words (string) 'Hello, World!' when executed. The command is straightforward and easy to understand.

```
1 print("Hello, World!")
2 // Output: Hello, World!
```

Languages such as python are considered “*high-level*”, which means that it is designed to be easy to read and write, but also independent of hardware by hiding (“*abstracting*”) underlying details (*The Python Language Reference*, n.d.). A key principle of python is the emphasis on implementing a syntax that is concise and close to human language (Listing 2, Listing 3).

Listing 3: Example of less readable code written in the low-level programming language C. This code is doing exactly the same as the python code in Listing 2. The command is harder to understand because more steps are needed to access the same functionality, including the definition of a function

```
1 #include <stdio.h>
2 int main() {
3     printf("Hello, World!");
4     return 0;
5 }
6 // Output: Hello, World!
```

Furthermore, python is an *interpreted* language, which means that the code is executed line by line. This makes coding easier because the programmer can see the results of the code immediately after writing it, and error messages point to the exact line where the error occurred. This is in contrast to *compiled* languages, where the code has to be compiled into machine code before it can be executed. The advantage of compiled languages is that the code runs faster, because the machine code is optimized for the hardware.

Python automates tasks that would otherwise require an advanced understanding of computer hardware, like the need for manual allocation of memory space. This is achieved by using a technique called “*garbage collection*”, which automatically frees memory space that is no longer needed by the program. This is a feature that is not present in low-level programming languages like C or C++, that were designed to maximize control over hardware.

Another hallmark of python is its *dynamic typing system*. In python the type is inferred automatically during code execution (Listing 4). This is in contrast to *statically typed* languages like C, where the type of a variable has to be declared explicitly and cannot be changed during code execution (Listing 5) (*The Python Language Reference*, n.d.).

Dynamic typing makes python a very beginner-friendly language, since one does not have to keep track of the type of each variable. However, this also makes python a slower language, because the interpreter has to check the type of each variable during code execution. Also, developing code with dynamic typing systems is prone to introducing bugs (“*type errors*”), because it allows unexperienced developers to convert variables from one type to another without noticing, leading to unexpected behavior. Hence, larger python projects require disciplined

Listing 4: Example of dynamic typing in python. The variable “a” is assigned the value 5, which is of type integer. The variable “a” is then assigned the value “Hello, World!”, which is of type string. Python allows dynamic re-assignment of variables with different types. Note that code after “#” is considered a comment and won’t be executed.

```
1 a = 5 # Type integer
2 a = 5.0 # Type float
3 a = 'Hello, World!' # Type string
4 a = True # Type boolean
5 a = False # Type boolean
6 a = [1, 2, 3] # Type list of integers
7 a = {'name': 'Regina'} # Type dictionary
```

Listing 5: Example of static typing in C. The variable “a” is declared as an integer (int), and can only store integers. The variable “a” is then assigned the value 5, which is an integer. The variable “a” is then assigned the value ‘Hello, World!’, which is a string. This results in a compilation error, because the variable “a” can only store integers. Note that code after “//” is considered a comment and won’t be executed.

```
1 int a; // Declare type as integer
2 a = 5;
3 a = 'Hello, World!'; // Compilation error!
```

adherence to programming conventions. One such convention is *type hinting*, which is a way to explicitly note the type of a variable. Type hinting does not have an effect on the code, but it makes the code more readable and understandable for other developers, and allows for development environments to detect type errors before execution (Listing 6) (van Rossum et al., 2014).

Listing 6: Example of type hints used in python. Explicitly stating the type of the variable is optional and does not change the behavior of the code as shown in Listing 4.

```
1 a: int = 5
2 a: str = 'Hello, World!'
```

Python supports both functional and object-oriented programming paradigms. In functional programming, the code is written in a way that the program is a sequence of function calls, where each function call returns a value that is used in the next function call (Listing 7). This approach is useful when multiple actions have to be performed on the same data and the structure of the data is relatively simple, for example a string of a gene sequence.

When the data itself gains in complexity, for example when storing not just the gene sequence, but also the promotor sequence, an object-oriented approach is more suitable (Listing 8). Object-oriented programming is a programming paradigm that uses objects and classes. An object is a collection of both data and functions, and a class is a blueprint for creating objects. The data of an object is stored as attributes. Functions that are associated with an object are called methods.

Listing 7: Example of functional programming in Python. The code defines a function called “find_restriction_site” that finds the position of a restriction site in a gene. The function “cut” uses the function “find_restriction_site” to cut the gene at the restriction site.

```

1 def find_restriction_site(gene: str):
2     return gene.find('GCGC')
3
4 def cut(gene: str):
5     position = find_restriction_site(gene)
6     return gene[:position]
7
8 gene1 = 'TGAGCTGAGCTGATGCGCTATATTAGGCG'
9 gene1_cut = cut(gene1)
10 print(gene1_cut)
11 # Output: GCGCTATATTAGGCG

```

Listing 8: Example of object oriented programming in python. The class is called “Gene” and has four methods, “__init__”, “find_promotor”, “find_restriction_site” and “cut”. The method “__init__” is called when creating (“initializing”) an object, which fills the object with user-defined data. The parameter “self” is used to reference the object itself internally. “find_promotor” is a method that finds the position of the promotor in the gene and is called during object initialization.

```

1 class Gene:
2     def __init__(self, sequence: str):
3         self.sequence: str = sequence # Save sequence as attribute
4         self.promotor: str = self.find_promotor()
5     def find_promotor(self):
6         return self.sequence.find('TATA')
7     def find_restriction_site(self):
8         return self.sequence.find('GCGC')
9     def cut(self):
10        position = self.find_restriction_site()
11        return self.sequence[:position]
12
13 gene1 = Gene(sequence='TGAGCTGAGCTGATGCGCTATATTAGGCG') # Create object
14 gene1_cut = gene1.cut() # Call the method cut
15 print(gene1_cut) # Show result
16 # Output: GCGCTATATTAGGCG

```

A major benefit of using an object oriented versus a functional approach is that the data itself is programmable, enabling the programmer to define the behavior of the data itself through methods. This is achieved by using the keyword “self” to reference the object itself inside the class. For example, one could extend the class “Gene” with a method that finds the promotor of the gene and stores it as an attribute (Listing 8).

When designing software, both functional and object oriented programming can be used together, where object oriented programming is often used to design the program’s overall architecture, and functional programming is used to implement the algorithms of the program’s features. This allows for scalability of the software, as every single class is extended through the

addition of new methods. Furthermore, classes can be expanded in their functionalities through inheritance (Listing 9).

Listing 9: Example of inheritance in python. The class “mRNA” inherits from the class “Gene”. The class “mRNA” has two methods, “__init__” and “find_stopcodon”. The method “find_stopcodon” finds the position of stop codons.

```
1 # Define a class called mRNA inheriting from the class Gene
2 class mRNA(Gene):
3     def __init__(self, sequence: str):
4         super().__init__(sequence) # Get attributes from parent class
5         self.sequence.replace('T', 'U') # Replace thymine with uracil
6     def find_stopcodons(self):
7         return self.sequence.find('UGA')
8
9 mRNA1 = mRNA(sequence='TGAGCTGAGCTGATGCGCTATTTAGGGC') # Create object
10 print(mRNA1.find_stopcodons()) # Call the method translate
11 # Output: [0, 5, 10]
```

Inheritance is a feature of object-oriented programming that allows a class to access every attribute and method of a parent class. For example, one could extend the class “Gene” with a class “mRNA”, by writing a class “mRNA” that inherits from the class “Gene”.

Together, python is not just beginner-friendly, but also well respected for its ease in development, which is why it is widely used in professional settings for web development, data analysis, machine learning, biosciences and more (Ekmekci et al., 2016).

Data Science with Python

the ease of use has made python a very popular language (Rayhan & Gross, 2023)

Like any other programming language, python alone does not provide specialized tools like those used for data analysis (*The Python Language Reference*, n.d.). However, python was designed to be extended by packages developed by its users. A python package consists of multiple python modules, where each module is a text-file with a .py ending containing python code. Famous examples of such packages are pytorch and tensorflow, that are used to build models of artificial intelligence, including ChatGPT (Paszke et al., 2019; Abadi et al., 2016; Radford et al., 2019). Here, we outlay the most important packages used for plotastic.

Interactive Python - Jupyter

Python overcame the issues of interpreted language by utilizing Code written in C numpy:

- Acceleration, - SIMD instructions

Tabular operations - pandas

Data visualization - matplotlib - seaborn

Inferential Statistics - pingouin

AI: - pytorch and tensorflow - example: VGG19 is just a few lines of code (??) asdfdf

Aims

This project defines these aims:

- Characterize the interaction between myeloma cells and mesenchymal stromal cells
- Aim 2
- Aim 3

Chapter 1: Modelling Myeloma Dissemination *in vitro*

Abstract

Multiple myeloma involves early dissemination of malignant plasma cells across the bone marrow; however, the initial steps of dissemination remain unclear. Human bone marrow- derived mesenchymal stromal cells (hMSCs) stimulate myeloma cell expansion (e.g., IL-6) and simultaneously retain myeloma cells via chemokines (e.g., CXCL12) and adhesion factors. Hence, we hypothesized that the imbalance between cell division and retention drives dissemination. We present an *in vitro* model using primary hMSCs co-cultured with INA-6 myeloma cells. Time-lapse microscopy revealed proliferation and attachment/detachment dynamics. Separation techniques (V-well adhesion assay and well plate sandwich centrifugation) were established to isolate MSC-interacting myeloma sub-populations that were characterized by RNAseq, cell viability and apoptosis. Results were correlated with gene expression data ($n = 837$) and survival of myeloma patients ($n = 536$). On dispersed hMSCs, INA-6 saturate hMSC-surface before proliferating into large homotypic aggregates, from which single cells detached completely. On confluent hMSCs, aggregates were replaced by strong heterotypic hMSC-INA-6 interactions, which modulated apoptosis time-dependently. Only INA-6 daughter cells (nMA-INA6) detached from hMSCs by cell division but sustained adherence to hMSC-adhering mother cells (MA-INA6). Isolated nMA-INA6 indicated hMSC-autonomy through superior viability after IL-6 withdrawal and upregulation of proliferation-related genes. MA-INA6 upregulated adhesion and retention factors (CXCL12), that, intriguingly, were highly expressed in myeloma samples from patients with longer overall and progression-free survival, but their expression decreased in relapsed myeloma samples. Altogether, *in vitro* dissemination of INA-6 is driven by detaching daughter cells after a cycle of hMSC-(re)attachment and proliferation, involving adhesion factors that represent a bone marrow-retentive phenotype with potential clinical relevance.

Statement of Significance

Novel methods describe *in vitro* dissemination of myeloma cells as detachment of daughter cells after cell division. Myeloma adhesion genes were identified that counteract *in vitro* detachment with potential clinical relevance.

Introduction

Multiple myeloma arises from clonal expansion of malignant plasma cells in the bone marrow (BM). At diagnosis, myeloma cells have disseminated to multiple sites in the skeleton and, in some cases, to “virtually any tissue” (Bladé et al., 2022; Rajkumar et al., 2014). However, the mechanism through which myeloma cells initially disseminate remains unclear. Dissemination is a multistep process involving invasion, intravasation, intravascular arrest, extravasation, and colonization (Zeissig et al., 2020). To initiate dissemination, myeloma cells overcome adhesion, retention, and dependency on the BM microenvironment, which could involve the loss of adhesion factors such as CD138 (Akhmetzyanova et al., 2020; García-Ortiz et al., 2021). BM retention is mediated by multiple factors: First, chemokines (CXCL12 and CXCL8) produced by mesenchymal stromal cells (MSCs), which attract plasma cells and prime their cytoskeleton and integrins for adhesion (Aggarwal et al., 2006; Alsayed et al., 2007). Second, myeloma cells must overcome the anchorage and physical boundaries of the extracellular matrix (ECM), consisting of e.g. fibronectin, collagens, and proteoglycans such as decorin (Hu et al., 2021; Huang et al., 2015; Katz, 2010; Kibler et al., 1998). Simultaneously, ECM provides signals inducing myeloma cell cycle arrest or progression the cell cycle (Hu et al., 2021; Katz, 2010). ECM is also prone to degradation, which is common in several osteotropic cancers, and is the cause of osteolytic bone disease. This is driven by a ‘vicious cycle’ that maximizes bone destruction by extracting growth factors (EGF and TGF-) that are stored in calcified tissues (Glavey et al., 2017). Third, direct contact with MSCs physically anchors myeloma cells to the BM (Zeissig et al., 2020; Sanz-Rodríguez et al., 1999). Fourth, to disseminate to distant sites, myeloma cells require, at least partially, independence from essential growth and survival signals provided by MSCs in the form of soluble factors or cell adhesion signaling (García-Ortiz et al., 2021; Chatterjee et al., 2002; Hideshima et al., 2007). For example, the VLA4 (Myeloma)-VCAM1 (MSC)-interface activates NF- B in both myeloma and MSCs, inducing IL-6 expression in MSCs. The independence from MSCs is then acquired through autocrine survival signaling (Frassanito et al., 2001; Urashima et al., 1995). In short, anchorage of myeloma cells to MSCs or ECM is a ‘double-edged sword’: adhesion counteracts dissemination, but also presents signaling cues for growth, survival, and drug resistance (Solimando et al., 2022).

To address this ambiguity, we developed an *in vitro* co-culture system modeling diverse adhesion modalities to study dissemination, growth, and survival of myeloma cells and hMSCs. Co-cultures of hMSCs and the myeloma cell line INA-6 replicated tight interactions and aggregate growth, akin to “micrometastases” in Ghobrial’s metastasis concept (Ghobrial, 2012). We characterized the growth conformations of hMSCs and INA-6 as homotypic aggregation *vs.* heterotypic hMSC adherence and their effects on myeloma cell survival. We tracked INA-6 detachments from aggregates and hMSCs, thereby identifying a potential “disseminated” sub-

population lacking strong adhesion. We developed innovative techniques (V-well adhesion assay and well plate sandwich centrifugation) to separate weakly and strongly adherent subpopulations for the subsequent analysis of differential gene expression and cell survival. Notably, our strategy resolves the differences in gene expression and growth behavior between cells of one cell population in “direct” contact with MSCs. In contrast, previous methods differentiated between “direct” and “indirect” cell-cell contact using transwell inserts (Dziadowicz et al., 2022). To evaluate whether genes mediating adhesion and growth characteristics of INA-6 were associated with patient survival, we analyzed publicly available datasets (Seckinger et al., 2017, 2018).

Materials and Methods

See Appendix A.3 for a complete method list and description.

Ethics Statement

Primary human MSCs were collected with the written informed consent of all patients. The procedure was conducted in accordance with recognized ethical guidelines (Helsinki Declaration) and approved by the local Ethics Committee of the University of Würzburg (186/18).

Cultivation and Co-Culturing of primary hMSCs and INA-6

Primary human MSCs were obtained from the femoral head of 34 non-myeloma patients (Appendix A: Table 1: 21 male and 13 female, mean age 68.9 ± 10.6) undergoing elective hip arthroplasty. The INA-6 cell line (*DSMZ Cat# ACC-862, RRID:CVCL_5209*, link) was initially isolated from a pleural effusion sample obtained from an 80-year-old male with multiple myeloma (Burger, Günther, et al., 2001; Gramatzki et al., 1994). hMSCs were not tested for mycoplasma, whereas stocks of INA-6 were tested in this study (Appendix A: Table 1) using the *Venor GEM OneStep* kit (Minerva Biolabs, Berlin, Germany). For each co-culture, hMSCs were seeded 24 h before INA-6 addition to generate the MSC-conditioned medium (CM). INA-6 cells were washed with PBS, resuspended in MSC medium, and added to hMSCs so that the co-culture comprised 33 % (v/v) of CM gathered directly from the respective hMSC donor. The co-cultures were not substituted for IL-6 (Chatterjee et al., 2002).

Cell Viability and Apoptosis Assay

Cell viability and apoptosis rates were measured using *CellTiter-Glo Luminescent Cell Viability Assay* and *Caspase-Glo 3/7 Assay*, respectively (Promega GmbH, Mannheim, Germany).

Automated Fluorescence Microscopy

Microscopic images were acquired using an Axio Observer 7 (Zeiss) with a COLIBRI LED light source and motorized stage top using 5x and 10x magnification. The tiled images had an automatic 8–10 % overlap and were not stitched.

Live Cell Imaging

hMSCs (stained with PKH26) were placed into an ibidi Stage Top Incubation System and equilibrated to 80 % humidity and 5% CO₂. INA-6 (2×10^3 cells/cm²) were added directly before the start of acquisition. Brightfield and fluorescence images of up to 13 mm² of the co-culture area were acquired every 15 min for 63 h. Each event of interest was manually analyzed and categorized into defined event parameters.

V-well Adhesion Assay

INA-6 cells were arrested during mitosis by two treatments with thymidine, followed by nocodazole. Arrested INA-6 were released and added to 96 V-well plates (10⁴ cells/cm²) on top of confluent hMSCs and adhered for 1–3 h. The co-culture was stained with calcein-AM (Thermo Fisher Scientific, Darmstadt, Germany) before non-adherent INA-6 were pelleted into the tip of the V-well (2000 rpm, 5–10 min). MSC-adhering INA-6 cells were manually detached by rapid pipetting. The pellet brightness was measured microscopically and the pellet was isolated by pipetting.

Cell Cycle Profiling by Image Cytometry

Isolated INA-6 cells were fixed in 70 % ice-cold ethanol, washed, resuspended in PBS, distributed in 96-well plates, and stained with Hoechst 33342. The plates were scanned at 5x magnification. A pre-trained convolutional neural network (Intellesis, Zeiss) was fine-tuned to segment the scans into single nuclei and exclude fragmented nuclei. Nuclei were filtered to exclude extremes of size and roundness. The G0/G1 frequency was determined by Gaussian curve fitting.

Well Plate Sandwich Centrifugation (WPSC)

hMSCs were grown to confluence in 96-well plates coated with collagen I (rat tail; Corning, NY, USA). INA-6 cells were added and the cells were allowed to adhere for 24 h. A second plate (“catching plate”) was attached upside down to the top of the co-culture plate. That “well plate sandwich” was turned around and the content of the co-culture plate was centrifuged into the catching plate three times (40 s at 110 g) while gently adding 30 µL of medium in between centrifugation steps. Non-MSC-adhering INA-6 cells were collected from the catching plate, whereas MSC-adhering INA-6 cells were isolated by digesting the co-culture with accutase. For RNA sequencing (RNAseq), all samples were purified using anti-CD45 magnetic-assisted cell sorting (Miltenyi Biotec B.V. & Co. KG, Bergisch Gladbach).

RNA Isolation

RNA was isolated using the *NucleoSpin RNA II Purification Kit* (Macherey-Nagel) according to the manufacturer's instructions. RNA was isolated from INA-6 cells co-cultured with a unique hMSC donor ($n = 5$ for RNA sequencing, $n = 11$ for qPCR).

RNA sequencing, Differential Expression, and Functional Enrichment Analysis

RNA sequencing (RNAseq) was performed at the Core Unit Systems Medicine, University of Würzburg. mRNA was enriched with polyA beads. Fastq files were aligned to the GRCh38 reference genome using STAR (*RRID:SCR_004463*, link) and raw read counts were generated using HTseq (*RRID:SCR_005514*, link) (Anders et al., 2015; Dobin et al., 2013; Zerbino et al., 2018). Differential gene expression was analyzed using edgeR in R (version 3.6.3) (*RRID:SCR_012802*, link). Functional enrichment analysis was performed using Metascape (*RRID:SCR_016620*, link) (Zhou et al., 2019).

RT-qPCR

RNA (1 µg) was reverse transcribed using *SuperScript IV reverse transcriptase* (Thermo Fisher Scientific). qPCR was performed using 10 µL *GoTaq qPCR Master Mix* (Promega), 1 :10 diluted cDNA, and 5 pmol of primers obtained from Biomers.net or Qiagen (Appendix A: Table 3).

Statistical Analysis

Inferential statistics were performed using Python (IPython, *RRID:SCR_001658*, link) (3.10) packages *pingouin* (0.5.1) and *statsmodels* (0.14.0) (Vallat, 2018; Seabold & Perktold, 2010). The figures were plotted using *plotastic* (0.0.1) (Kuric & Ebert, 2024). Normality (for $n \geq 4$) and sphericity were ensured using Mauchly's and Shapiro-Wilk tests, respectively. Data points were \log_{10} transformed to convert the scale from multiplicative to additive or to fulfill sphericity requirements. $p = 0.05 > * > 0.01 > ** > 10^{-3} > *** > 10^{-4} > ****$. p -values were either adjusted (*p-adj*) or not adjusted (*p-unc*) for family wise error rate. Power calculations were not performed to determine the sample size.

Patient Cohort, Analysis of Survival and Expression

Survival and gene expression data were obtained as previously described (Seckinger et al., 2017, 2018) and are available at the European Nucleotide Archive (ENA) under accession numbers

PRJEB36223 and PRJEB37100. The expression level was categorized into “high” and “low” using maxstat (Maximally selected Rank Statistics) thresholds (Hothorn & Lausen, n.d.).

Data Availability Statement

A detailed description of the methods is provided in the Supplementary Material section. Raw tabular data and examples of analyses and videos are available in the github repository, [link](#). Raw RNAseq data are available from the NCBI Gene Expression Omnibus (GEO) (*RRID:SCR_005012*, [link](#)) (GSE261423). Microscopy data are available at BioStudies (EMBL-EBI) (*RRID:SCR_004727*, [link](#)) (S-BIAD1092).

Results

INA-6 Cells Saturate hMSC-Interaction to Proliferate into Aggregates

hMSCs are isolated as a heterogeneous cell population. To analyze whether INA-6 cells could adhere to every hMSC, we saturated hMSCs with INA-6. A seeding ratio of 1:4 (hMSC:INA-6) resulted in the occupation of $93 \pm 6\%$ of single hMSCs by one or more INA-6 cells within 24 hours after INA-6 addition, escalating to 6% after 48 hours (Figure 1A, B). Therefore, most hMSCs provide an interaction surface for INA-6 cells.

INA-6 exhibits homotypic aggregation when cultured alone, a phenomenon observed in some freshly isolated myeloma samples (up to 100 cells after 6 hours) (Kawano et al., 1991; Okuno et al., 1991). Adding hMSCs at a 1:1 ratio led to smaller aggregates after 24 hours (size 1–5 cells), all of which were distributed over $52 \pm 2\%$ of all hMSCs (Figure 1A, B). Intriguingly, INA-6 aggregation was notably absent when grown on confluent hMSCs, and occurred only when heterotypic interactions were limited to 0.2 hMSCs per INA-6 cell (Figure 1C). We concluded that INA-6 cells prioritize heterotypic over homotypic interactions.

To monitor the formation of such aggregates, we conducted live-cell imaging of hMSC/INA-6 co-cultures for 63 hours. We observed that INA-6 cells adhered long after cytokinesis, constituting $55 \pm 12\%$ of all homotypic interactions between 13 hours and 26 hours, increasing to more than 75% for the remainder of the co-culture (Figure 1D). Therefore, homotypic INA-6 aggregates were mostly formed by cell division.

Apoptosis of INA-6 Depends on Ratio Between Heterotypic and Homotypic Interaction

Although direct interaction with hMSCs has been shown to enhance myeloma cell survival through NF- κ B signaling (Hideshima et al., 2007), the impact of aggregation on myeloma cell viability during hMSC interaction remains unclear. To address this, we measured the cell viability (ATP) and apoptosis rates of INA-6 cells growing as homotypic aggregates compared to those in heterotypic interactions with hMSCs by modulating hMSC density (Figure 1E). To equalize the background signaling caused by soluble MSC-derived factors, all cultures were incubated in hMSC-conditioned medium and the results were normalized to INA-6 cells cultured without direct hMSC contact (Figure 1E, left).

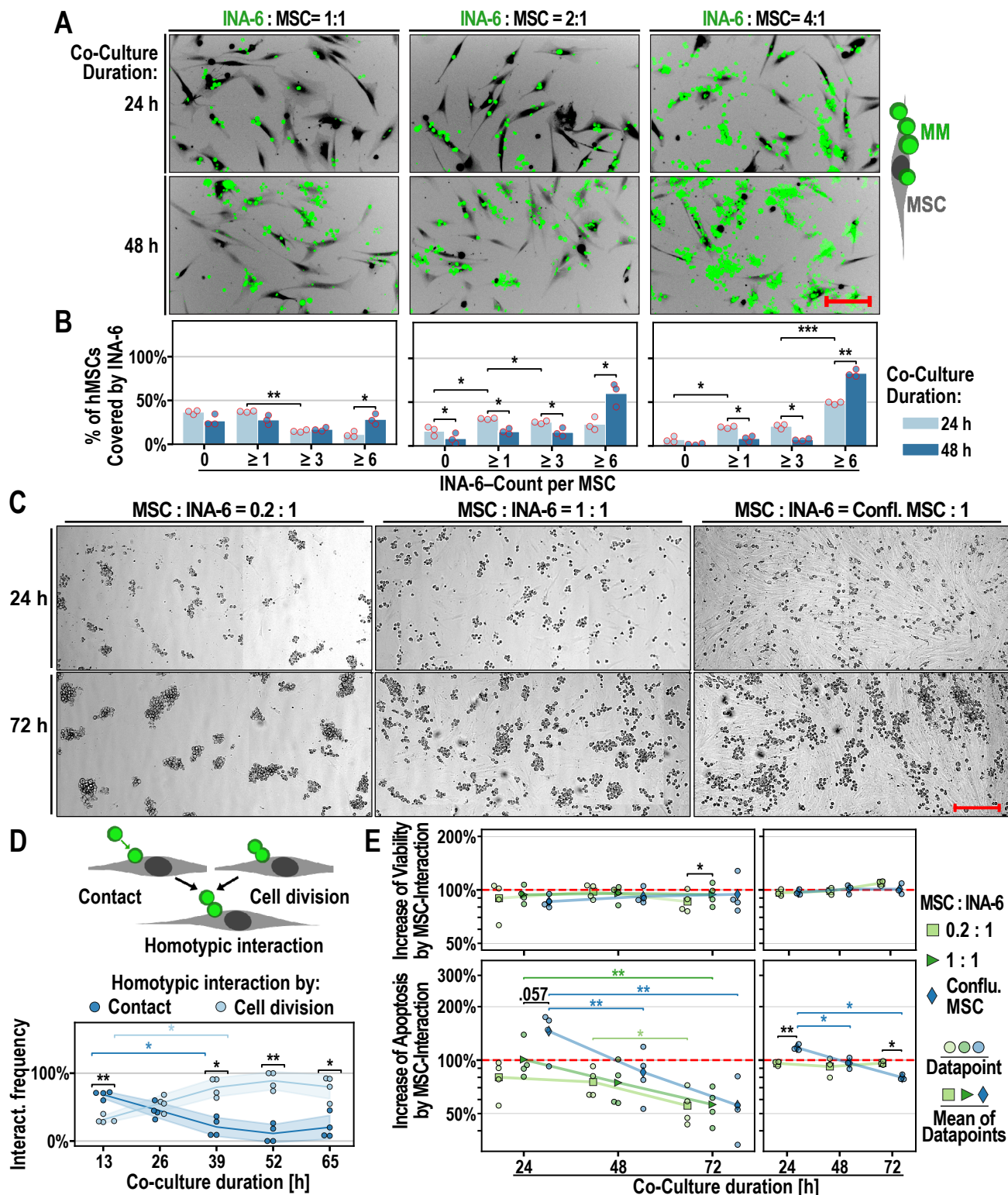


Figure 1: INA-6 growth conformations and survival on hMSCs. **A:** Interaction of INA-6 (green) with hMSCs (black, negative staining) at different INA-6 densities (constant hMSC densities). Scale bar = 200 μ m. **B:** Frequency of single hMSCs (same as A) that are covered by INA-6 of varying group sizes. Technical replicates = three per datapoint; 100 single hMSCs were evaluated per technical replicate. **C:** Interaction of INA-6 – continued on next page

Figure 1: continued from previous page – with hMSCs at different hMSC densities (constant INA-6 densities). Scale bar = 300 µm. **D:** Two types of homotypic interaction: Attachment after cell contact and sustained attachment of daughter cells after cell division. Datapoints represent one of four independent time-lapse recordings, each evaluating 116 interaction events. **E:** Effects of hMSC-density on the viability (ATP, top) and apoptosis (Caspase3/7 activity, bottom). INA-6:MSC ratio = 4:1; Technical replicates = four per datapoint; **E left:** Signals were measured in INA-6 washed off from hMSCs and normalized by INA-6 cultured in MSC-conditioned medium (= red line) ($n = 4$). **E right:** Signals were measured in co-cultures and normalized by the sum of the signals measured in hMSC and INA-6 cultured separately (= red line) ($n = 3$). **Statistics:** Paired t-test, two-factor RM-ANOVA. Datapoints represent independent co-cultures with hMSCs from three (A, B, D, E right), four (E left) unique donors. Confl. = Confluent.

INA-6 viability (ATP) was not affected by the direct adhesion of hMSCs at any density. However, apoptosis rates decreased over time [$F(2, 6) = 23.29, p\text{-unc} = 1.49 \times 10^{-3}$] (Two-factor RM-ANOVA), interacting significantly with MSC density [$F(4, 12) = 6.98, p\text{-unc} = 3.83 \times 10^{-3}$] For example, 24 hours of adhesion to confluent MSCs increased apoptosis rates by 1.46 ± 0.37 fold, while culturing INA-6 cells on dispersed hMSCs (ratio 1:1) did not change the apoptosis rate (1.01 ± 0.26 fold).

We presumed that sensitive apoptotic cells might have been lost when harvesting INA-6 cells from hMSCs. Hence, we measured survival parameters in the co-culture and in hMSC and INA-6 cells cultured separately (Figure 1E, right). We defined MSC interaction effects when the survival measured in the co-culture differed from the sum of the signals measured from INA-6 and hMSCs alone. RM-ANOVA confirmed that adherence to confluent MSCs increased apoptosis rates of INA-6 cells 24 hours after adhesion and decreased after 72 hours [$F(2, 4) = 26.86, p\text{-unc} = 4.80 \times 10^{-3}$] (interaction between MSC density and time, Two-factor RM-ANOVA), whereas INA-6 cells were unaffected when grown on dispersed hMSCs. In summary, the growth conformation of INA-6 cells, measured as the ratio between homotypic aggregation and heterotypic MSC interactions, affected apoptosis rates of INA-6 cells.

Single INA-6 Cells Detach Spontaneously from Aggregates of Critical Size

Using time-lapse microscopy, we observed that $26 \pm 8\%$ of INA-6 aggregates growing on single hMSCs spontaneously shed INA-6 cells (Figure 2A, B; Supplementary Video 1). Notably, all detached cells exhibited similar directional movements, suggesting entrainment in convective streams generated by temperature gradients within the incubation chamber. INA-6 predominantly detached from other INA-6 cells or aggregates (Figure 2C), indicating weaker adhesive forces in homotypic interactions than in heterotypic interactions. The detachment frequency increased after 52 hours, when most aggregates that shed INA-6 cells were categorized as large (greater than 30 cells) (Figure 2D). Since approximately 10-20 INA-6 cells already fully covered a single hMSC, we suggest that myeloma cell detachment depended not only on hMSC saturation but also required a minimum aggregate size. Interestingly, INA-6 detached mostly as

single cells, independent of aggregate size categories [$F(2, 6) = 4.68, p\text{-unc} = 0.059$] (Two-factor RM-ANOVA) (Figure 2E), showing that aggregates remained mostly stable despite losing cells.

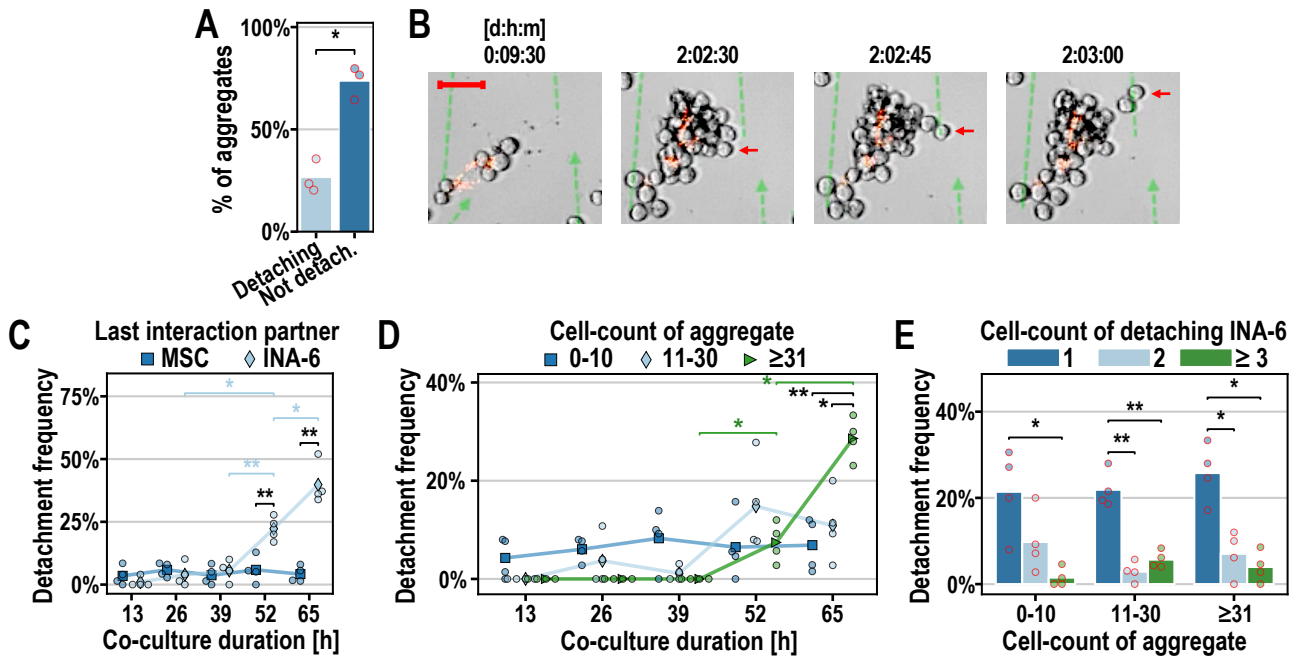


Figure 2: Time-lapse analysis of INA-6 detachment from INA-6 aggregates and hMSCs. **A:** Frequency of observed INA-6 aggregates that did or did not lose INA-6 cell(s). 87 aggregates were evaluated per datapoint. **B:** Example of a “disseminating” INA-6 aggregate growing on fluorescently (PKH26) stained hMSC (from A-D). Dashed green lines are trajectories of detached INA-6 cells. Scale bar = 50 µm. **C-E:** Quantitative assessment of INA-6 detachments. 45 detachment events were evaluated per datapoint. Seeding ratio INA-6:MSC = 4:1. **C:** Most INA-6 cells dissociated from another INA-6 cell and not from an hMSC [$F(1, 3) = 298, p\text{-unc} = 4.2 \times 10^{-4}$]. **D:** Detachment frequency of aggregate size categories. **E:** Detachment frequency of INA-6 cells detaching as single, pairs or more than three cells. **Statistics:** (A): Paired-t-test; (C-E): Paired-t-test, Two-factor RM-ANOVA; Datapoints represent three (A) or four (C-E) independent time-lapse recordings of co-cultures with hMSCs from two (A) or three (C-E) unique donors.

Cell Division Generates a Daughter Cell Detached from hMSC

We suspected that cell division drives detachment because we observed that MSC-adhering INA-6 cells could generate daughter cells that “roll over” the mother cell (Figure 3A; Supplementary Video 2). We recorded and categorized the movement of INA-6 daughter cells in confluent hMSCs after cell division. Half of all INA-6 divisions yielded two daughter cells that remained stationary, indicating hMSC adherence (Figure 3B, C; Supplementary Video 3). The other half of division events generated one hMSC-adhering (MA-INA6) cell and one non-hMSC-adhering (nMA-INA6) cell, which rolled around the MA-INA6 cell for a median time of 2.5 hours post division (Q1=1.00 hour, Q3=6.25 hours) until it stopped and re-adhered to the hMSC monolayer (Figure 3D; Supplementary Video 2, Supplementary Video 4). Thus, cell division establishes a time window in which one daughter cell can detach.

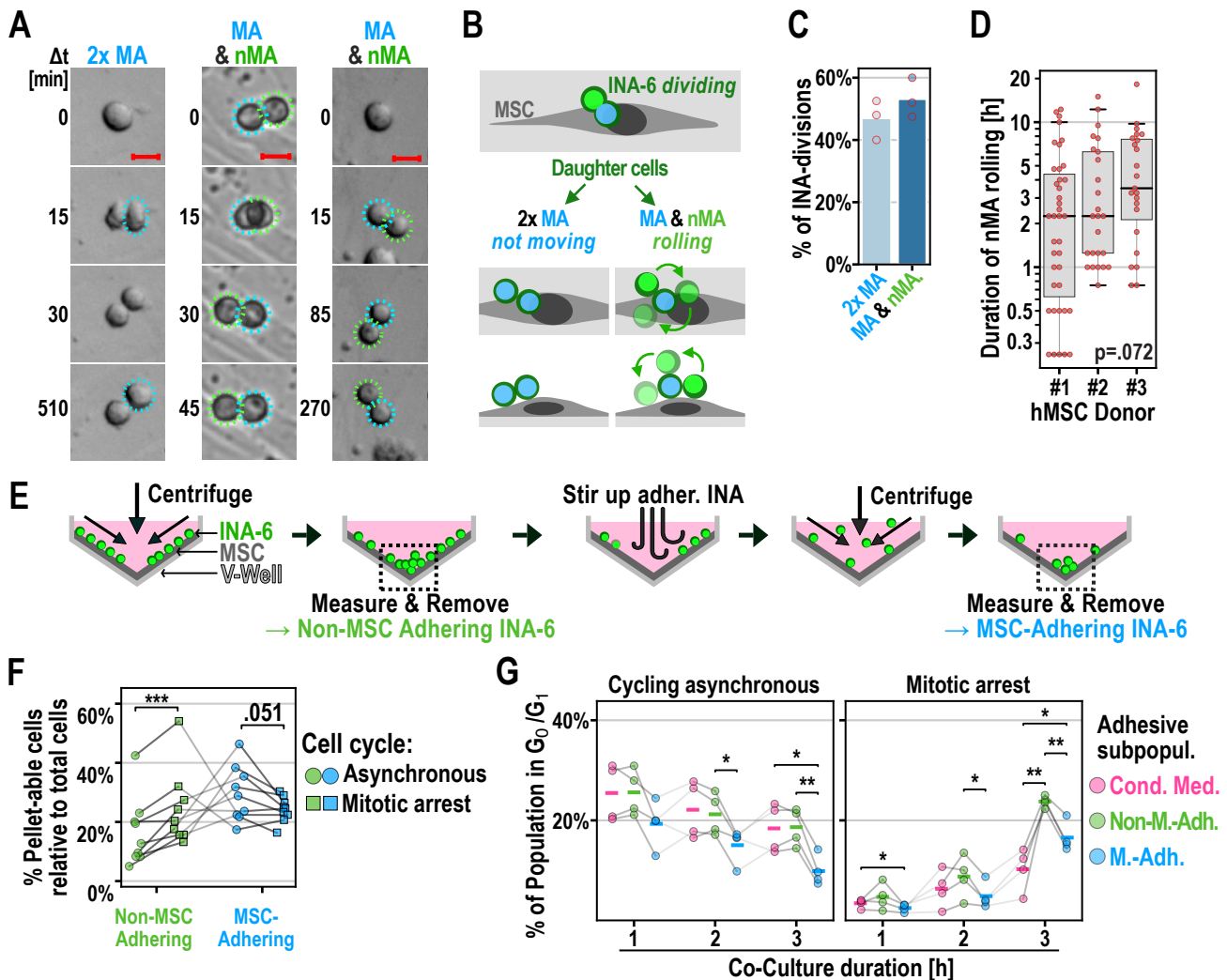


Figure 3: Detachment of INA-6 daughter cells after Cell Division. **A-D:** INA-6 divisions in interaction with confluent hMSCs. Seeding ratio INA-6:MSC = 4:20. **A:** Three examples of dividing INA-6 cells generating either two MA, or one MA and one nMA daughter cells as described in (G). Dashed circles mark mother cells (white), MA cell (blue), and first position of nMA cell (green). Scale bar: 20 µm. **B:** Cell division of MSC-adhering (MA) mother cell can yield one mobile non-MSC-adhering (nMA) daughter cell. **C:** Frequencies of INA-6 pairs defined in (A, B) per observed cell division. 65 divisions were evaluated for each of three independent time-lapse recordings. **D:** Rolling duration of nMA cells after division did not depend on hMSC donor [$H(2) = 5.250$, $p\text{-unc} = .072$]. Datapoints represent single nMA-cells after division. **E-G:** Adhesive and cell cycle assessment of MSC-interacting INA-6 subpopulations using the V-Well assay. **E:** Schematic of V-Well Assay (see Appendix A: Figure 1 for detailed analysis). MSC-interacting subpopulations were separated by subsequent centrifugation and removal of the pellet. The pellet size was quantified by its total fluorescence brightness. Adhering subpopulations were resuspended by rough pipetting. **F:** Relative cell pellet sizes of adhesive INA-6 subpopulations that cycle either asynchronously or were synchronized at mitosis. Gray lines in-between points connect dependent measurements of co-cultures ($n = 9$) that shared the same hMSC-donor and INA-6 culture. Co-cultures were incubated for three different durations (1 h, 2 h and 3 h after INA-6 addition). Time points were pooled, since time did not show an effect on cell adhesion [$F(2, 4) = 1.414$, $p\text{-unc} = 0.343$] Factorial RM-ANOVA shows an interaction between cell cycle and the kind of adhesive subpopulation [$F(1, 8) = 42.67$, $p\text{-unc} = 1.82 \times 10^{-4}$]. Technical replicates = 4 per datapoint. **G:** Cell cycles were profiled in cells gathered from the pellets of four independent co-cultures ($n = 4$) and the frequency of G₀/G₁ cells are displayed depending on co-culture duration (see Appendix A: Figure 3 for cell cycle profiles). Four technical replicates were pooled after pelleting. **Statistics:** (D): Kruskal-Wallis H-test. (F): Paired t-test, (G): Paired t-test, two-factor RM-ANOVA. Datapoints represent INA-6 from independent co-cultures with hMSCs from three unique donors.

To validate that cell division reduced adhesion, we measured both the size and cell cycle profile of the nMA-INA6 and MA-INA6 populations using an enhanced V-well assay (method described in Figure 3E, Appendix A: Figure 1, 2). For comparison, we fully synchronized and arrested INA-6 cells at mitosis and released their cell cycle immediately before addition to the hMSC monolayer, rendering them more likely to divide while adhering. Mitotic arrest significantly increased the number of nMA-INA6 cells and decreased the number of MA-INA6 cells (Figure 3F). Furthermore, the nMA-INA6 population contained significantly more cells cycling in the G0/G1 phase than the MA-INA6 population, both in synchronously and asynchronously cycling INA-6 (Figure 3G, Appendix A: Figure 3, 4). The number of nMA-INA6 INA-6 cells increased due to a higher cell division frequency. Taken together, we showed that INA-6 detach from aggregates by generating one temporarily detached daughter cell after cell division, a process that potentially contributes to the initiation of dissemination.

RNAseq of Non-MSC-Adhering and MSC-Adhering Subpopulations

To characterize the subpopulations separated by WPSC, we conducted RNAseq, revealing 1291 differentially expressed genes between nMA-INA6 *vs.* CM-INA6, 484 between MA-INA6 *vs.* CM-INA6, and 195 between MA-INA6 *vs.* nMA-INA6. We validated RNAseq and found that the differential expression of 18 genes correlated with those measured with qPCR for each pairwise comparison (Figure 4C–E, Appendix A: Figure 5): nMA-INA6 *vs.* CM-INA6 [$\rho(16) = .803, p = 6.09 \times 10^{-5}$], MA-INA6 *vs.* CM-INA6 [$\rho(16) = .827, p = 2.30 \times 10^{-5}$], and MA-INA6 *vs.* nMA-INA6 [$\rho(16) = .746, p = 3.74 \times 10^{-4}$] (Spearman’s rank correlation). One of the 18 genes (*MUC1*) measured by qPCR showed a mean expression opposite to that obtained by RNAseq (nMA-INA6 *vs.* CM-INA6), although the difference was insignificant (Figure 4C). For nMA-INA6 *vs.* CM-INA6, the difference in expression measured by qPCR was significant for only two of the 11 genes (*DKK1*, *OPG*), whereas the other genes (*DKK1*, *OPG*, *BCL6*, *BMP4*, *BTG2*, *IL10RB*, *IL24*, *NOTCH2*, *TNFRSF1A*, *TRAF5*) only confirmed the tendency measured by RNAseq (Figure 4C–E). For MA-INA6 *vs.* CM-INA6, qPCR validated the significant upregulation of seven genes (*DKK1*, *OPG*, *BCL6*, *BMP4*, *BTG2*, *IL10RB*, *IL24*, *NOTCH2*, *TNFRSF1A*, *TRAF5*, *TGM2*, *DCN*, *LOX*, *MMP14*, *MMP2*, *CXCL12*, *CXCL8*), whereas the downregulation of *BMP4* was insignificant.

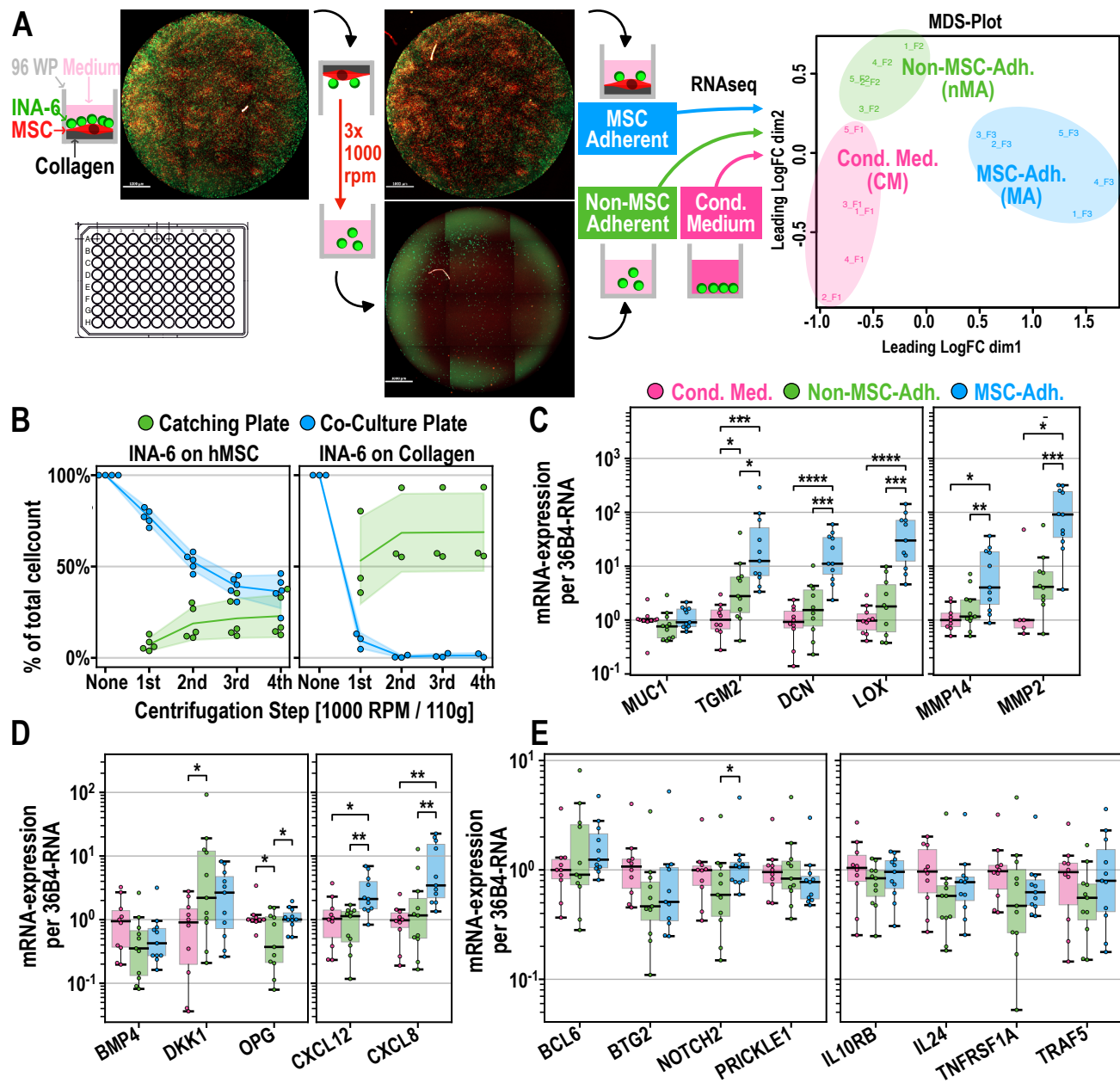


Figure 4: Separation and gene expression of INA-6 subpopulations. **A:** Schematic of “Well-Plate Sandwich Centrifugation” (WPSC) separating nMA- from MA-INA6. A co-culture 96-well plate is turned upside down and attached on top of a “catching plate”, forming a “well-plate sandwich”. nMA-INA6 cells are collected in the catching plate by subsequent rounds of centrifugation and gentle washing. MA-INA6 are enzymatically dissociated from hMSCs or by rough pipetting. Subsequent RNAseq of MSC-interacting subpopulations reveals distinct expression clusters [right, multidimensional scaling plot (MDS)] ($n = 5$). **B:** Separation was microscopically tracked after each centrifugation step. **C-E:** RT-qPCR of genes derived from RNAseq results. Expression was normalized to the median of CM-INA6. Samples include those used for RNAseq and six further co-cultures ($n = 11$; non-detects were discarded). **C:** Adhesion factors, ECM proteins, and matrix metalloproteinases. **D:** Factors involved in bone remodeling and bone homing chemokines. **E:** Factors involved in (immune) signaling. **Statistics:** (C-E): Paired t-test. Datapoints represent the mean of three (B-E) technical replicates. INA-6 were isolated from independent co-cultures with hMSCs from five (A, B), nine (C-E) unique donors.

Non-MSC-Adhering INA-6 and MSC-Adhering INA-6 Have Distinct Expression Patterns of Proliferation or Adhesion, Respectively

To functionally characterize the unique transcriptional patterns in nMA-INA6 and MA-INA6, we generated lists of genes that were differentially expressed *vs.* the other two subpopulations [termed nMA *vs.* (MA & CM) and MA *vs.* (nMA & CM)]. Functional enrichment analysis was performed, and the enriched terms were displayed as ontology clusters (Figure 5A). nMA-INA6 upregulated genes enriched with loosely connected term clusters associated with proliferation (e.g., “positive regulation of cell cycle”). MA-INA6 upregulated genes enriched with tightly connected term clusters related to cell adhesion and the production of ECM factors (e.g., “cell-substrate adhesion”). Similar ontology terms were enriched in the gene lists obtained from pairwise comparisons nMA *vs.* CM, MA *vs.* CM, and MA *vs.* nMA (Figure 5B). In particular, nMA *vs.* CM (but not MA *vs.* CM) upregulated genes that were enriched with “G1/S transition”, showing that WPSC isolated nMA-INA6 daughter cells after cell division.

To check for similarities between lists of differentially expressed genes from hMSC-interacting subpopulations, we performed enrichment analysis on gene lists from the overlaps (“ \cap ”) between all pairwise comparisons (Figure 5B, Appendix A: Figure 6), and showed the extent of these overlaps in circos plots (Figure 5C). The overlap between MA-INA6 *vs.* CM-INA6 and nMA-INA6 *vs.* CM-INA6 showed neither enrichment with proliferation- nor adhesion-related terms but with apoptosis-related terms. A direct comparison of MSC-interacting subpopulations (MA-INA6 *vs.* nMA-INA6) showed a major overlap with MA-INA6 *vs.* CM-INA6 (Figure 5C, middle). This overlap was enriched with terms related to adhesion but not proliferation. Hence, MA-INA6-INA6 and nMA-INA6-INA6 mostly differed in their expression of adhesion genes.

To assess whether nMA-INA6 and MA-INA6 were regulated by separate transcription factors, we examined the enrichment of curated regulatory networks from the TRRUST database (Figure 5B bottom). All the lists were enriched for p53 regulation. E2F1 regulation was observed only in genes upregulated in nMA-INA6 *vs.* CM-INA6 and downregulated in MA-INA6 *vs.* nMA-INA6. Genelists involving MA-INA6 were enriched in regulation by subunits of NF- κ B (NFKB1/p105 and RELA/p65) and factors of immediate early response (SRF, JUN). Correspondingly, NF- κ B and JUN are known to regulate the expression of adhesion factors in multiple myeloma and B-cell lymphoma, respectively (Blonska et al., 2015; Tai et al., 2006).

Taken together, MSC-interacting subpopulations showed unique regulatory patterns, focusing on either proliferation or adhesion.

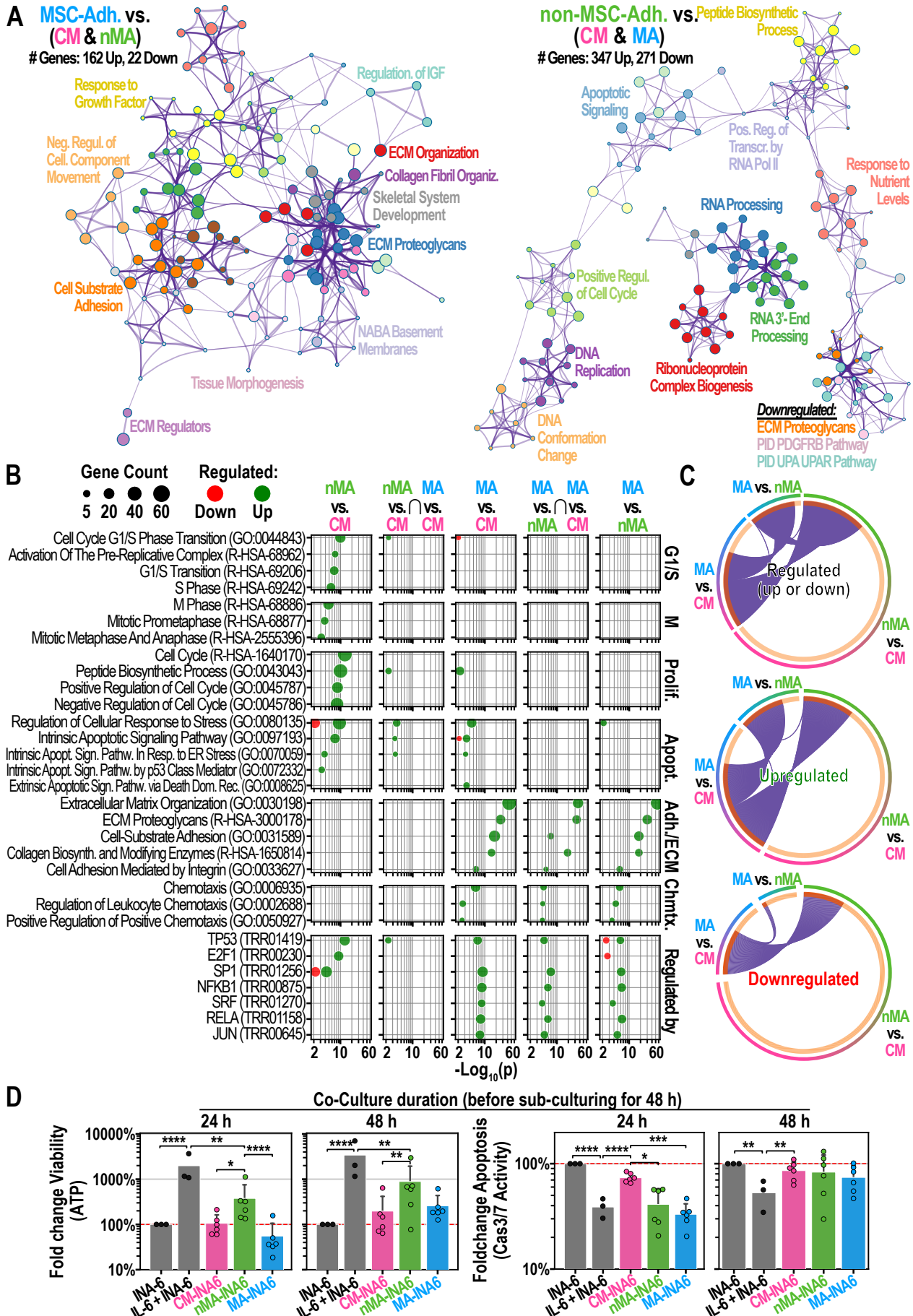


Figure 5: Functional analysis of MSC-interacting subpopulations (**A-C**): Functional enrichment analysis of differentially expressed genes (from RNAseq) using Metascape. **A:** Gene ontology (GO) cluster analysis of gene lists that are unique for MA (left) or nMA (right) INA-6. Circle nodes represent subsets of input genes falling into similar GO-term. Node size grows with the number of input genes. Node color defines a shared parent GO-term. Two nodes with a similarity score > 0.3 are linked. **B:** Enrichment analysis of pairwise comparisons between MA subpopulations and their overlaps (arranged in columns). GO terms were manually picked and categorized (arranged in rows). Raw Metascape results are shown in Appendix A: Figure 6. For each GO-term, the p-values (x-axis) and the counts of matching input genes (circle size) were plotted. The lowest row shows enrichment of gene lists from the TRRUST-database. **C:** Circos plots by Metascape. Sections of a circle represent lists of differentially expressed genes. Purple lines connect same genes appearing in two gene lists. \cap : Overlapping groups, MA: MSC-adhering, nMA: non-MSC-adhering, CM: MSC-Conditioned Medium. **D:** INA-6 were co-cultured on confluent hMSC for 24 h or 48 h, separated by WPSC and sub-cultured for 48 h under IL-6 withdrawal ($n = 6$), except the control (IL-6 + INA-6) ($n = 3$). Signals were normalized (red line) to INA-6 cells grown without hMSCs and IL-6 ($n = 3$). **Statistics:** (D): Paired t-test, two-factor RM-ANOVA. Datapoints represent the mean of four technical replicates. INA-6 were isolated from independent co-cultures with hMSCs from six unique donors.

MSC-Adhering INA-6 Cells Are More Resistant to IL-6 Withdrawal

Lorem ipsum dolor sit amet, consetetur sadipscing elitr, sed diam nonumy eirmod tempor invidunt ut labore et dolore magna aliquyam erat, sed diam Lorem ipsum dolor sit amet, consetetur sadipscing elitr, sed diam nonumy eirmod tempor invidunt ut labore et dolore magna aliquyam erat, sed diam voluptua. At vero eos et accusam et justo duo dolores et ea rebum. Stet Lorem ipsum dolor sit amet, consetetur sadipscing elitr, sed diam nonumy eirmod tempor invidunt ut labore et dolore magna aliquyam erat, sed diam voluptua. At vero eos et accusam et justo duo dolores et ea rebum. Stet

ipsum dolor sit amet, consetetur sadipscing elitr, sed diam nonumy eirmod tempor invidunt ut labore et dolore magna aliquyam erat, sed diam voluptua. At vero eos et accusam et justo duo dolores et ea rebum. Stet

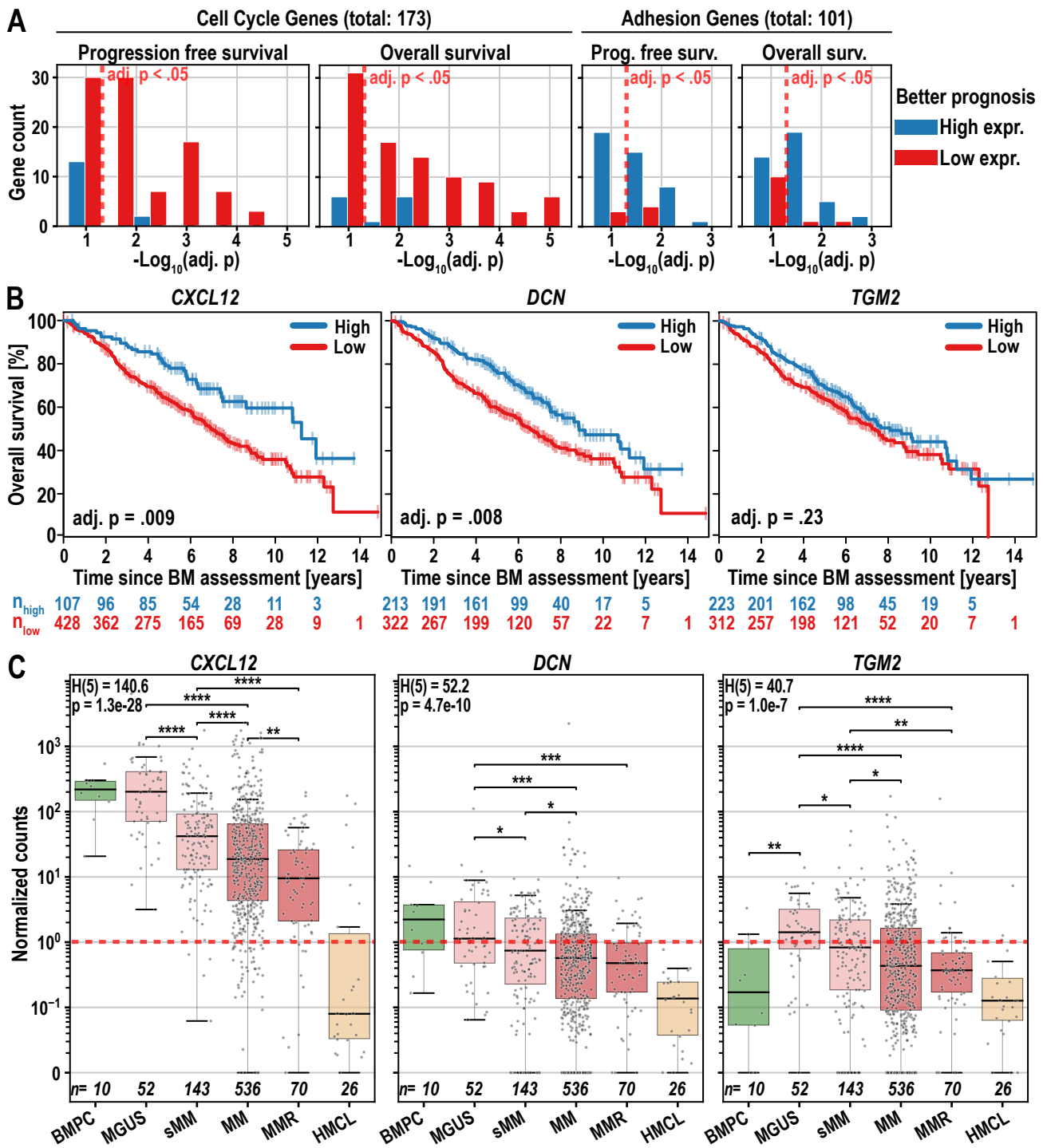


Figure 6: Survival of patients with multiple myeloma regarding the expression levels of adhesion and bone retention genes. **A:** p-value distribution of genes associated with patient survival ($n = 535$) depending on high or low expression levels. Red dashed line marks the significance threshold of $p\text{-adj} = 0.05$. Histogram of p -values was plotted using a bin width of $-\log_{10}(0.05)/2$. Patients with high and low gene expression were delineated using maximally selected rank statistics (maxstat). **B:** Survival curves for three genes taken from the list of adhesion genes shown in (A), maxstat thresholds defining high and low expression were: *CXCL12*: 81.08; *DCN*: 0.75; *TGM2*: 0.66 normalized counts. **C:** Gene expression (RNAseq, $n = 873$) measured in normalized counts (edgeR) of *CXCL12*, *DCN* in Bone Marrow Plasma Cell (BMPC), Monoclonal Gammopathy of Undetermined Significance (MGUS), smoldering Multiple Myeloma (sMM), Multiple Myeloma (MM), Multiple – continued on next page

Figure 6: continued from previous page – Myeloma Relapse (MMR), Human Myeloma Cell Lines (HMCL). The red dashed line marks one normalized read count. **Statistics:** (A, B): Log-rank test; (C): Kruskal-Wallis, Mann–Whitney U Test. All *p*-values were corrected using the Benjamini-Hochberg procedure.

Lorem ipsum dolor sit amet, consetetur sadipscing elitr, sed diam nonumy eirmod tempor invidunt ut labore et dolore magna aliquyam erat, sed diam Lorem ipsum dolor sit amet, consetetur sadipscing elitr, sed diam nonumy eirmod tempor invidunt ut labore et dolore magna aliquyam erat, sed diam voluptua. At vero eos et accusam et justo duo dolores et ea rebum. Stet Lorem ipsum dolor sit amet, consetetur sadipscing elitr, sed diam nonumy eirmod tempor invidunt ut labore et dolore magna aliquyam erat, sed diam voluptua. At vero eos et accusam et justo duo dolores et ea rebum. Stet

Table 1: Adhesion and ECM genes (shown in Figure 6A) were filtered by their association with patient survival (*p*-adj. < 0.01) and were categorized as continuously downregulated during disease progression. The complete list is presented in Appendix A: Table 2. Bone Marrow Plasma Cells (BMPC), Monoclonal Gammopathy of Undetermined Significance (MGUS), smoldering Multiple Myeloma (sMM), Multiple Myeloma (MM), and Multiple Myeloma Relapse (MMR). *p*-unc: unadjusted *p*-values; *p*-adj: *p*-values adjusted using the Benjamini-Hochberg method with 101 genes.

Regulation during disease progression	Gene	Ensemble ID	Progression Free / Overall Survival	Better Prognosis with high/low expression	Association of expression with survival	
					[<i>p</i> -unc]	[<i>p</i> -adj]
Not Downregulated (or overall low expression)	CCNE2	ENSG00000175305	Overall	low	5.34E-04	8.64E-03
	MMP2	ENSG00000087245	Prog. Free	high	2.29E-05	2.32E-03
	OSMR	ENSG00000145623	Prog. Free	high	5.67E-04	7.15E-03
Continuously Downregulated (BMPC > MGUS > sMM > MM > MMR)	AXL	ENSG00000167601	Overall	high	3.64E-05	1.84E-03
	COL1A1	ENSG00000108821	Prog. Free	high	3.03E-04	4.37E-03
			Overall	high	5.93E-04	8.64E-03
	CXCL12	ENSG00000107562	Prog. Free	high	1.16E-04	2.93E-03
			Overall	high	6.48E-04	8.64E-03
	CYP1B1	ENSG00000138061	Overall	high	6.84E-04	8.64E-03
	DCN	ENSG00000011465	Overall	high	2.47E-04	8.33E-03
	LRP1	ENSG00000123384	Overall	high	4.34E-04	8.64E-03
	LTBP2	ENSG00000119681	Prog. Free	high	9.03E-05	2.93E-03
	CYP1B1	ENSG00000138061	Overall	high	6.84E-04	8.64E-03
	DCN	ENSG00000011465	Overall	high	2.47E-04	8.33E-03
	LRP1	ENSG00000123384	Overall	high	4.34E-04	8.64E-03
	LTBP2	ENSG00000119681	Prog. Free	high	9.03E-05	2.93E-03
	MFAP5	ENSG00000197614	Prog. Free	high	2.43E-04	4.09E-03
	MMP14	ENSG00000157227	Prog. Free	high	6.93E-05	2.93E-03
	MYL9	ENSG00000101335	Prog. Free	high	1.46E-04	2.95E-03

continued on next page

Table 1 – continued from previous page

		Overall	high	1.56E-05	1.57E-03

Lorem ipsum dolor sit amet, consetetur sadipscing elitr, sed diam nonumy eirmod tempor invidunt ut labore et dolore magna aliquyam erat, sed diam voluptua. At vero eos et accusam et justo duo dolores et ea rebum. Stet Lorem ipsum dolor sit amet, consetetur sadipscing elitr, sed diam nonumy eirmod tempor invidunt ut labore et dolore magna aliquyam erat, sed diam voluptua. At vero eos et accusam et justo duo dolores et ea rebum. Stet

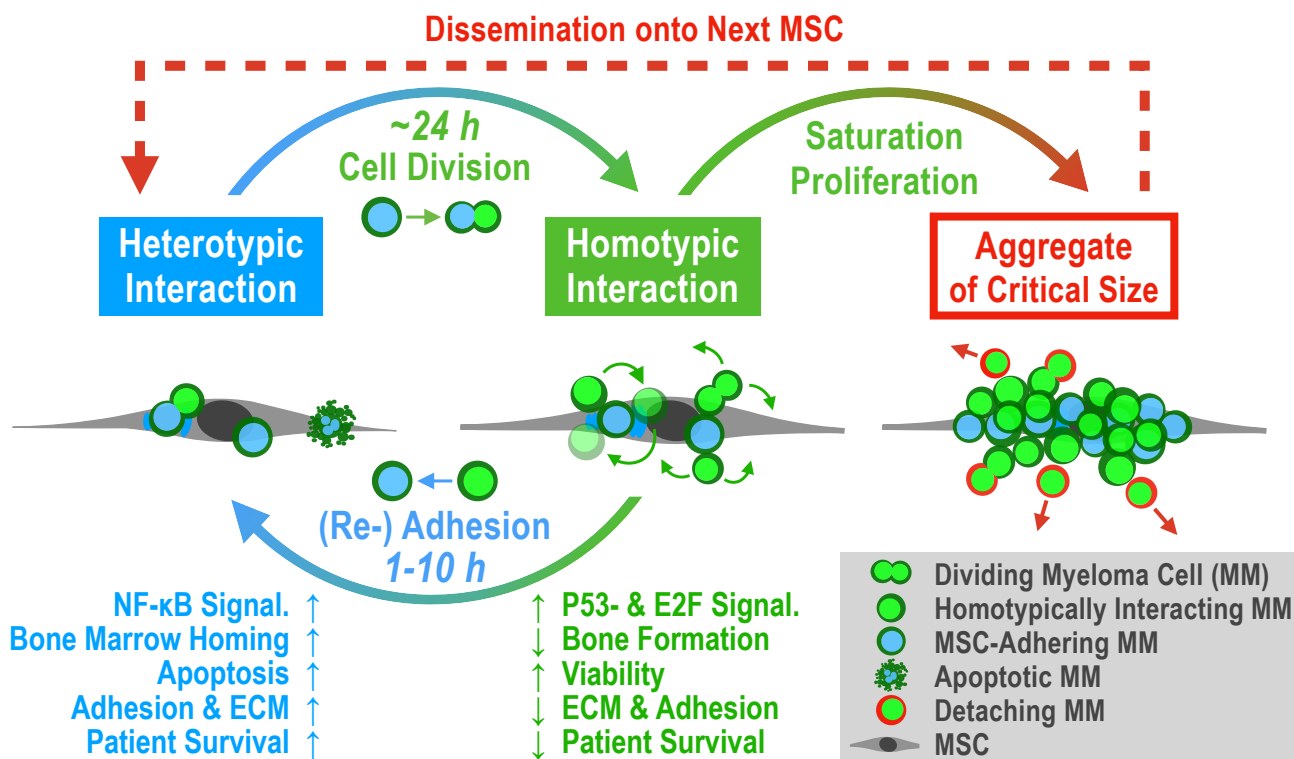


Figure 7: Proposed model of “Detached Daughter Driven Dissemination” (DDDD) in aggregating multiple myeloma. **Heterotypic Interaction:** Malignant plasma cells colonize the bone marrow microenvironment by adhering to an MSC (or osteoblast, ECM, etc.) to maximize growth and survival through paracrine and adhesion mediated signaling, even if contact may trigger initial apoptosis. Gene expression will focus on establishing a strong anchor within the bone marrow, but also on attracting other myeloma cells (via secretion of ECM factors and CXCL12/CXCL8, respectively). **Cell Division:** Cell fission can generate one daughter cell that no longer adheres to the MSC (nMA). **Homotypic Interaction:** If myeloma cells have the capacity to grow as aggregates, the daughter cell stays attached to their MSC-adhering mother cell (MA). **Re-Adhesion:** The daughter cell “rolls around” the mother cell until it re-adheres to the MSC. Our model estimates the rolling duration to be 1–10 h long. **Proliferation & Saturation:** We estimate that a single myeloma cell covers one MSC completely after roughly four population doublings. When heterotypic adhesion is saturated, subsequent daughter cells benefit from a homotypic interaction, since they stay close to growth-factor secreting MSCs and focus gene expression on proliferation (e.g. driven by E2F) and not adhesion (driven by NF- B). **Critical Size:** Homotypic interaction is weaker than heterotypic interaction, and each cell fission destabilizes the aggregate. Hence, detachment of myeloma cells may depend mostly on aggregate size. **Dissemination:** After myeloma cells have detached, they gained a viability advantage through IL-6-independence (with unknown duration), which enhances their survival outside of the bone marrow and allows them to spread throughout the body.

Lorem ipsum dolor sit amet, consetetur sadipscing elitr, sed diam nonumy eirmod tempor invidunt ut labore et dolore magna aliquyam erat, sed diam voluptua. At vero eos et accusam et justo duo dolores et ea rebum. Stet Lorem ipsum dolor sit amet, consetetur sadipscing elitr, sed diam nonumy eirmod tempor invidunt ut labore et dolore magna aliquyam erat, sed diam voluptua. At vero eos et accusam et justo duo dolores et ea rebum. Stet

Discussion

lorem ipsum

Chapter 2: Semi-Automating Data Analysis with `plotastic`

Abstract

`plotastic` addresses the challenges of transitioning from exploratory data analysis to hypothesis testing in Python’s data science ecosystem. Bridging the gap between `seaborn` and `pingouin`, this library offers a unified environment for plotting and statistical analysis. It simplifies the workflow with user-friendly syntax and seamless integration with familiar `seaborn` parameters (`y`, `x`, `hue`, `row`, `col`). Inspired by `seaborn`’s consistency, `plotastic` utilizes a `DataAnalysis` object to intelligently pass parameters to `pingouin` statistical functions. Hence, statistics and plotting are performed on the same set of parameters, so that the strength of `seaborn` in visualizing multidimensional data is extended onto statistical analysis. In essence, `plotastic` translates `seaborn` parameters into statistical terms, configures statistical protocols based on intuitive plotting syntax and returns a `matplotlib` figure with known customization options and more. This approach streamlines data analysis, allowing researchers to focus on correct statistical testing and less about specific syntax and implementations.

Introduction

The reproducibility crisis in research highlights a significant challenge in contemporary biosciences, where a substantial portion of studies faces reproducibility issues (Begley & Ioannidis, 2015). One critical yet often overlooked aspect contributing to this crisis is data management. The literature most often refers to *big data* as the main challenge (Gomez-Cabrero et al., 2014). However, these challenges are also present in smaller datasets, which the author refers to as *semi-big data*. This term describes datasets that, while not extensive enough to necessitate advanced computational tools typically reserved for *big data*, are sufficiently large to render manual analysis very time-intensive. *Semi-big data* is often generated by methods like automated microscopy or multiplex qPCR, which produce volumes of data that are manageable on a surface level, but pose substantial barriers for in-depth, manual reproducibility (Bustin, 2014). This is further complicated by the complexity inherent in multidimensional datasets. For example, the qPCR experiment from Chapter 1, Fig. 4 involves the analysis of 19 genes across three subpopulations, including eleven biological and three technical replicates, resulting in a total of 1881 data points that are all assigned to a complex set of experimental variables. Without a clearly documented data analysis protocol and standardized data formats, the reproduction of such analysis becomes extremely challenging, if not impossible (Bustin, 2014).

The evolving standards in data analysis advocate for the standardization of analytical pipelines, rationalization of sample sizes, and enhanced infrastructure for data storage, addressing some of these challenges (Goodman et al., 2016; Wilkinson et al., 2016). However, these advancements can place undue pressure on researchers, particularly those with limited training in statistics, underscoring the need for intuitive, user-friendly analytical tools (Gosselin, 2021; Armstrong, 2014; Gómez-López et al., 2019)

In this context, *plotastic* emerges as a tool designed to democratize access to sophisticated statistical analysis, offering a user-centric interface that caters to researchers across varying levels of statistical proficiency. By integrating robust statistical methodologies within an accessible framework, *plotastic* aims to contribute to enhancing the reproducibility and integrity of research in the biosciences (Gomez-Cabrero et al., 2014).

initially, the need to develop *plotastic* arose during this project. The first is to address the author's need for a tool that could handle the complex, multidimensional data generated by e.g. qPCR experiments. These experiments typically involve the analysis of multiple genes across several time points and biological replicates, resulting in datasets that are challenging to analyze manually. The author's experience with traditional statistical software, such as Prism, revealed that these tools required extensive manual input, making them unsuitable for the efficient analysis of complex, multidimensional data. - The second was to increase speed. THis

is required for developing methods

Also, Adhesion experiments are highly time-dependent, adding a required factor to every experiment

Since plotastic optimizes the analysis of *semi-big data*, we introduce the term *semi-automation* to distinguish itself from the fully automated pipelines used for *big data*. Semi-automation is defined as the following aspects:

1. **Semi-big input:** The input size is oriented towards *semi-big data*, which is characterized as being manageable by manual analysis, yet highly time inefficient, and probably impossible to re-analyse by someone else than the researcher.
2. **Standardized input** The input follows a standardized format (e.g. long-format)
3. **Minimize user configuration:** User configuration is strictly minimized. The user is never asked to pass the same parameters twice. This reduces the risk of human error and time spent on configuration.
4. **Default configuration provides acceptable results:** If the user does not provide any manual configuration, the pipeline should provide acceptable results. Options should be provided to allow a level of flexibility to adapt the pipeline to the user's needs.
5. **Small Reviewable Processing Steps:** The analysis steps are structured into small processes that can be combined to form a complete analysis pipeline. That way, each step can act as a stage for quality control to improve error detection and troubleshooting. For a statistical analysis, that means the processing steps are separated into 3 steps, those being assumption testing, factor analysis and post-hoc testing.
6. **Isolated Steps:** Processing steps should work independently from another, in the best case only depending on the raw data input. If a processing step depends on the output from other steps, the software should tell the user what exact steps it expects.
7. **Human readable outputs:** Every processing step may provide an output that is not necessarily standardized, but is required to be human readable to ensure reviewability.

Challenges: - Reproducibility crisis? - Data is exploding - Demands for rigorous statistical analysis are increasing - Biologists are not trained in statistics

The demands are rising: (Moreno-Indias et al., 2021)

As laid out in the introduction, one can doubt if a PhD student without coding skills is at its max efficiency.

Why does Biomedicine need plotastic?: - Thorough analysis has become a standard, with assumption testing, omnibus tests and post-hoc analyses for every experiment. - But data is increasing - Example of my data? - The number of dedicated statisticians is limited - The know-how of statistics in biology is limited, for example, Some authors ignored the problem of multiple testing while others used the method uncritically with no rationale or discussion (Perneger, 1998; Armstrong, 2014)

Why did I need plotastic?

Why do biologists need plotastic? - Assays output more data in shorter time, e.g. multiplex qPCR - example: 20 genes, 3 timepoints, 11 biological replicates, (all 3 technical replicates already averaged) - $20 * 3 * 11 = 660$ data points

this is multidimensional data: 660 data points spread across two dimensions: time and gene

-in manual analysis e.g. in Excel, the user has to manually select the data, copy it, paste it into a new sheet, and then perform the statistical test. In Prism, the user has to select the data, click on the statistical test, and then select the data again. This is not only time-consuming, but also prone to

- Re-Analysis: The user has to repeat the process for every gene and timepoint. This is not only time-consuming, but also prone to errors.

shortly Describe Main Packages in more detail: - seaborn: It multidimensional data - pingouin: It's a statistical package

Statement of Need

Python's data science ecosystem provides powerful tools for both visualization and statistical testing. However, the transition from exploratory data analysis to hypothesis testing can be cumbersome, requiring users to switch between libraries and adapt to different syntaxes. `seaborn` has become a popular choice for plotting in Python, offering an intuitive interface. Its statistical functionality focuses on descriptive plots and bootstrapped confidence intervals (Waskom, 2021). The library `pingouin` offers an extensive set of statistical tests, but it lacks integration with common plotting capabilities (Vallat, 2018). `statannotations` integrates statistical testing with plot annotations, but uses a complex interface and is limited to pairwise comparisons (Charlier et al., 2022).

`plotastic` addresses this gap by offering a unified environment for plotting and statistical analysis. With an emphasis on user-friendly syntax and integration of familiar `seaborn` parameters, it simplifies the process for users already comfortable with `seaborn`. The library ensures a smooth workflow, from data import to hypothesis testing and visualization.

Example

The following code demonstrates how plotastic analyzes the example dataset “fmri”, similar to Waskom (2021) (Figure 1).

```
1 ##### IMPORT PLOTASTIC
2 import plotastic as plst
3
4 # IMPORT EXAMPLE DATA
5 DF, _dims = plst.load_dataset("fmri", verbose = False)
6
7 # EXPLICITLY DEFINE DIMENSIONS TO FACET BY
8 dims = dict(
9     y = "signal",      # y-axis, dependent variable
10    x = "timepoint",   # x-axis, independent variable (within-subject factor)
11    hue = "event",     # color, independent variable (within-subject factor)
12    col = "region"     # axes, grouping variable
13 )
14 # INITIALIZE DATAANALYSIS OBJECT
15 DA = plst.DataAnalysis(
16     data=DF,           # Dataframe, long format
17     dims=dims,         # Dictionary with y, x, hue, col, row
18     subject="subject", # Datapoints are paired by subject (optional)
19     verbose=False,     # Print out info about the Data (optional)
20 )
21 # STATISTICAL TESTS
22 DA.check_normality() # Check Normality
23 DA.check_sphericity() # Check Sphericity
24 DA.omnibus_rm_anova() # Perform RM-ANOVA
25 DA.test_pairwise()    # Perform Posthoc Analysis
26
27 # PLOTTING
28 (DA
29 .plot_box_strip()    # Pre-built plotting function initializes plot
30 .annotate_pairwise(  # Annotate results from DA.test_pairwise()
31     include="__HUE" # Use only significant pairs across each hue
32 )
33 )
```

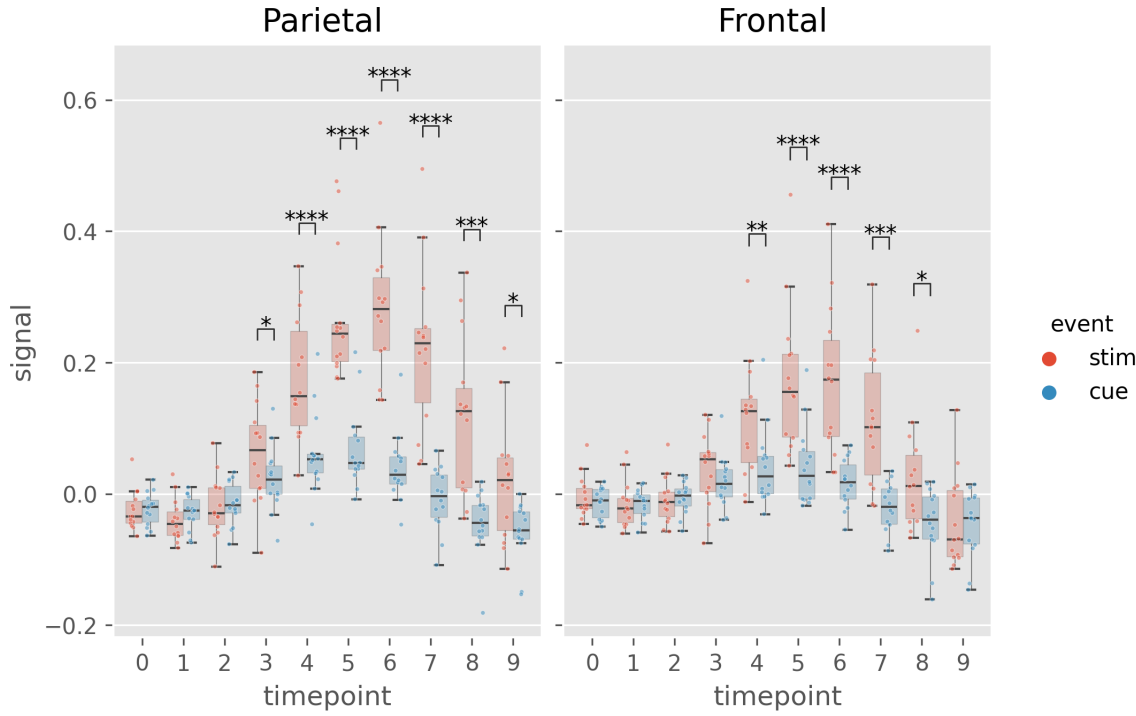


Figure 1: Example figure of plotastic (version 0.1). Image style was set by `plt.style.use('ggplot')`

Table 1: Results from `DA.check_sphericity()`. plotastic assesses sphericity after grouping the data by all grouping dimensions (hue, row, col). For example, `DA.check_sphericity()` grouped the 'fmri' dataset by "region" (col) and "event" (hue), performing four subsequent sphericity tests for four datasets.

'region', 'event'	spher	W	chi2	dof	pval	group count	n per group
'frontal', 'cue'	True	3.26e+20	-462.7	44	1	10	[14]
'frontal', 'stim'	True	2.45e+17	-392.2	44	1	10	[14]
'parietal', 'cue'	True	1.20e+20	-452.9	44	1	10	[14]
'parietal', 'stim'	True	2.44e+13	-301.9	44	1	10	[14]

Table 2: Results of `DA.omnibus_rm_anova()`. plotastic performs one two-factor RM-ANOVA per axis (grouping the data by row and col dimensions) using x and hue as the within-factors. For this example, `DA.omnibus_rm_anova()` grouped the 'fmri' dataset by "region" (col), performing two subsequent two-factor RM-ANOVAs. Within-factors are "timepoint" (x) and "event" (hue). For conciseness, GG-Correction and effect sizes are not shown.

'region'	Source	SS	ddof1	ddof2	MS	F	p-unc	stars
'parietal'	timepoint	1.583	9	117	0.175	26.20	3.40e-24	****
'parietal'	event	0.770	1	13	0.770	85.31	4.48e-07	****
'parietal'	timepoint * event	0.623	9	117	0.069	29.54	3.26e-26	****
'frontal'	timepoint	0.686	9	117	0.076	15.98	8.28e-17	****
'frontal'	event	0.240	1	13	0.240	23.44	3.21e-4	***
'frontal'	timepoint * event	0.242	9	117	0.026	13.031	3.23e-14	****

Overview

The functionality of `plotastic` revolves around a seamless integration of statistical analysis and plotting, leveraging the capabilities of `pingouin`, `seaborn`, `matplotlib` and `statannotations` (Vallat, 2018; Waskom, 2021; Hunter, 2007; Charlier et al., 2022). It utilizes long-format `pandas` `DataFrames` as its primary input, aligning with the conventions of `seaborn` and ensuring compatibility with existing data structures (Wickham, 2014; Team, 2020; McKinney, 2010).

`plotastic` was inspired by `seaborn` using the same set of intuitive and consistent parameters (`y`, `x`, `hue`, `row`, `col`) found in each of its plotting functions (Waskom, 2021). These parameters intuitively delineate the data dimensions plotted, yielding ‘faceted’ subplots, each presenting `y` against `x`. This allows for rapid and insightful exploration of multidimensional relationships. `plotastic` extends this principle to statistical analysis by storing these `seaborn` parameters (referred to as dimensions) in a `DataAnalysis` object and intelligently passing them to statistical functions of the `pingouin` library. This approach is based on the impression that most decisions during statistical analysis can be derived from how the user decides to arrange the data in a plot. This approach also prevents code repetition and streamlines statistical analysis. For example, the `subject` keyword is specified only once during `DataAnalysis` initialisation, and `plotastic` selects the appropriate paired or unpaired version of the test. Using `pingouin` alone requires the user to manually pick the correct test and to repeatedly specify the `subject` keyword in each testing function.

In essence, `plotastic` translates plotting parameters into their statistical counterparts. This translation minimizes user input and also ensures a coherent and logical connection between plotting and statistical analysis. The goal is to allow the user to focus on choosing the correct statistical test (e.g. parametric vs. non-parametric) and worry less about specific implementations.

At its core, `plotastic` employs iterators to systematically group data based on various dimensions, aligning the analysis with the distinct requirements of tests and plots. Normality testing is performed on each individual sample, which is achieved by splitting the data by all grouping dimensions and also the `x`-axis (`hue`, `row`, `col`, `x`). Sphericity and homoscedasticity testing is performed on a complete sampleset listed on the `x`-axis, which is achieved by splitting the data by all grouping dimensions (`hue`, `row`, `col`) (Table 1). For omnibus and posthoc analyses, data is grouped by the `row` and `col` dimensions in parallel to the `matplotlib` axes, before performing one two-factor analysis per axis using `x` and `hue` as the within/between-factors. (Table 2).

`DataAnalysis` visualizes data through predefined plotting functions designed for drawing multi-layered plots. A notable emphasis within `plotastic` is placed on showcasing individual datapoints alongside aggregated means or medians. In detail, each plotting function initializes a `matplotlib` figure and axes using `plt.subplots()` while returning a `DataAnalysis` object for

method chaining. Axes are populated by `seaborn` plotting functions (e.g., `sns.boxplot()`), leveraging automated aggregation and error bar displays. Keyword arguments are passed to these `seaborn` functions, ensuring the same degree of customization. Users can further customize plots by chaining `DataAnalysis` methods or by applying common `matplotlib` code to override `plotastic` settings. Figures are exported using `plt.savefig()`.

`plotastic` also focuses on annotating statistical information within plots, seamlessly incorporating p-values from pairwise comparisons using `statannotations` (Charlier et al., 2022). This integration simplifies the interface and enables options for pair selection in multidimensional plots, enhancing both user experience and interpretability.

For statistics, `plotastic` integrates with the `pingouin` library to support classical assumption and hypothesis testing, covering parametric/non-parametric and paired/non-paired variants. Assumptions such as normality, homoscedasticity, and sphericity are tested. Omnibus tests include two-factor RM-ANOVA, ANOVA, Friedman, and Kruskal-Wallis. Posthoc tests are implemented through `pingouin.pairwise_tests()`, offering (paired) t-tests, Wilcoxon, and Mann-Whitney-U.

To sum up, `plotastic` stands as a unified and user-friendly solution catering to the needs of researchers and data scientists, seamlessly integrating statistical analysis with the power of plotting in Python. It streamlines the workflow, translates `seaborn` parameters into statistical terms, and supports extensive customization options for both analysis and visualization.

Discussion

Is plotastic tested? Coverage? Does it cover every feature? What is not covered
The full code of an example analysis is shown in ??.

Is plotastic USABLE for biologists? - Yes but use is limited by minimal knowledge of Python
- However, that is subject to change as Python is becoming more popular in biology and AI assisted coding decreased the barrier to entry significantly. Tools like github copilot are able to generate code, fix bugs and suggest improvements. This is a game changer for biologists that are not familiar with programming. - Furthermore, installing and using plotastic for biologists is overestimated. These steps re needed:
- Install anaconda from the internet
- Open the terminal
- Type `pip install plotastic` - Check Rea

The evaluation of plotastic within this thesis reflects its potential to address key challenges in the field of data analysis. The software integrates a comprehensive suite of statistical tests, such as ANOVA and t-tests, designed for adaptability and ease of use, leveraging the functionalities of pingouin.

In the context of the reproducibility crisis in scientific research, plotastic offers noteworthy contributions, though it is not positioned as a universal remedy. The tool's unique approach to integrating statistical analysis with visual representation establishes a new paradigm, promoting methodological transparency. By mandating that statistical analyses accompany relevant graphical outputs, plotastic ensures that analyses are not only conducted with proper scientific rigor but also documented in a manner that facilitates replication, provided the user possesses proficiency in Python.

Usability is a critical attribute of analytical software, particularly as researchers confront increasingly complex datasets. While the developer's intimate familiarity with plotastic may bias perceptions of its ease of use, it is recognized that novices may initially encounter challenges. Nevertheless, plotastic is distinguished by its user-friendly interface, enabling users with minimal statistical training to perform sophisticated analyses by intuitively mapping plotting concepts to statistical operations.

The transition to a new analytical framework, especially one that incorporates coding, presents a learning curve. However, the advantages of plotastic in terms of analytical clarity, speed, and depth are anticipated to outweigh these initial challenges. Support mechanisms, such as assistance from advanced AI like ChatGPT, are available to mitigate these hurdles, supporting users across varying levels of expertise.

In conclusion, plotastic is posited as a valuable tool in the landscape of scientific research, offering a means to enhance the reproducibility and efficiency of data analysis. Its development ethos emphasizes simplifying complex analytical tasks, thereby contributing to the broader goal of fostering transparent and reproducible research practices.

DO we apply the principles of Semi-Automation to the software?

what features are missing? - Bivariate analysis - Filer to help save the output? - StatResults: System to suggest the correct test, based on the data

Summarising Discussion

Time Lapse

Lore Ipsum dolor sit amet, consetetur sadipscing elitr, sed diam nonumy eirmod tempor invidunt ut labore et dolore magna aliquyam erat, sed diam voluptua. At vero eos et accusam et justo duo dolores et ea rebum. Stet clita kasd gubergren, no sea takimata sanctus est Lore ipsum dolor sit amet. Lore ipsum dolor sit amet, consetetur sadipscing elitr, sed diam nonumy eirmod tempor invidunt ut labore et dolore magna aliquyam erat, sed diam voluptua. At vero eos et accusam et justo duo dolores et ea rebum. Stet clita kasd gubergren, no sea takimata sanctus est Lore ipsum

Myeloma

Lore Ipsum dolor sit amet, consetetur sadipscing elitr, sed diam nonumy eirmod tempor invidunt ut labore et dolore magna aliquyam erat, sed diam voluptua. At vero eos et accusam et justo duo dolores et ea rebum. Stet clita kasd gubergren, no sea takimata sanctus est Lore ipsum dolor sit amet. Lore ipsum dolor sit amet, consetetur sadipscing elitr, sed diam nonumy eirmod tempor invidunt ut labore et dolore magna aliquyam erat, sed diam voluptua. At vero eos et accusam et justo duo dolores et ea rebum. Stet clita kasd gubergren, no sea takimata sanctus est Lore ipsum

Semi-Automated Analysis Improves Agility During Establishing new *in vitro* Methods

Was plotastic useful for me? - Yes incredibly. I was able to perform the statistical tests and visualize the data in a fraction of the time that I would have needed manually. This allowed me to focus on the interpretation of the results and the writing of the manuscript. There was one particular example where my analysis was so fast, that I fed raw datatables during microscopy into python scripts and was able to adapt the experimental technique during the experiment. This allows for an agile and adaptive work environment that is not possible with manual analysis and proved invaluable during development of *in vitro* methods. - These experiments benefited from the use of plotastic, as the

Further research is needed to assess the true impact of semi-automated analysis on the agility of establishing new *in vitro* methods.

References

- Abadi, M., Agarwal, A., Barham, P., Brevdo, E., Chen, Z., Citro, C., ... Zheng, X. (2016, March). *TensorFlow: Large-Scale Machine Learning on Heterogeneous Distributed Systems* (No. arXiv:1603.04467). arXiv. Retrieved 2024-03-07, from <http://arxiv.org/abs/1603.04467> doi: 10.48550/arXiv.1603.04467
- Aggarwal, R., Ghobrial, I. M., & Roodman, G. D. (2006, October). Chemokines in multiple myeloma. *Experimental hematology*, 34(10), 1289–1295. Retrieved 2023-04-02, from <https://www.ncbi.nlm.nih.gov/pmc/articles/PMC3134145/> doi: 10.1016/j.exphem.2006.06.017
- Akhmetzyanova, I., McCarron, M. J., Parekh, S., Chesi, M., Bergsagel, P. L., & Fooksman, D. R. (2020). Dynamic CD138 surface expression regulates switch between myeloma growth and dissemination. *Leukemia*, 34(1), 245–256. Retrieved 2023-04-04, from <https://www.ncbi.nlm.nih.gov/pmc/articles/PMC6923614/> doi: 10.1038/s41375-019-0519-4
- Alcorta-Sevillano, N., Macías, I., Infante, A., & Rodríguez, C. I. (2020, December). Deciphering the Relevance of Bone ECM Signaling. *Cells*, 9(12), 2630. Retrieved 2023-12-20, from <https://www.ncbi.nlm.nih.gov/pmc/articles/PMC7762413/> doi: 10.3390/cells9122630
- Alsayed, Y., Ngo, H., Runnels, J., Leleu, X., Singha, U. K., Pitsillides, C. M., ... Ghobrial, I. M. (2007, April). Mechanisms of regulation of CXCR4/SDF-1 (CXCL12)-dependent migration and homing in multiple myeloma. *Blood*, 109(7), 2708–2717. doi: 10.1182/blood-2006-07-035857
- Anders, S., Pyl, P. T., & Huber, W. (2015, January). HTSeq—a Python framework to work with high-throughput sequencing data. *Bioinformatics (Oxford, England)*, 31(2), 166–169. doi: 10.1093/bioinformatics/btu638
- Andrews, S. (2010). *FASTQC. A quality control tool for high throughput sequence data*.
- Armstrong, R. A. (2014, September). When to use the Bonferroni correction. *Ophthalmic & Physiological Optics: The Journal of the British College of Ophthalmic Opticians (Optometrists)*, 34(5), 502–508. doi: 10.1111/opo.12131
- Barzilay, R., Ben-Zur, T., Bulvik, S., Melamed, E., & Offen, D. (2009, May). Lentiviral delivery of LMX1a enhances dopaminergic phenotype in differentiated human bone marrow mesenchymal stem cells. *Stem cells and development*, 18(4), 591–601. doi: 10.1089/scd.2008.0138
- Begley, C. G., & Ioannidis, J. P. A. (2015, January). Reproducibility in science: Improving the standard for basic and preclinical research. *Circulation Research*, 116(1), 116–126. doi: 10.1161/CIRCRESAHA.114.303819
- Bianco, P. (2014). "Mesenchymal" stem cells. *Annual review of cell and developmental biology*, 30, 677–704. doi: 10.1146/annurev-cellbio-100913-013132
- Bladé, J., Beksac, M., Caers, J., Jurczyszyn, A., von Lilienfeld-Toal, M., Moreau, P., ... Richardson, P. (2022, March). Extramedullary disease in multiple myeloma: A systematic literature review. *Blood Cancer Journal*, 12(3), 1–10. Retrieved 2023-03-24, from <https://www.nature.com/articles/s41408-022-00643-3> doi: 10.1038/s41408-022-00643-3
- Blonska, M., Zhu, Y., Chuang, H. H., You, M. J., Kunkalla, K., Vega, F., & Lin, X. (2015, February). Jun-regulated genes promote interaction of diffuse large B-cell lymphoma with the microenvironment. *Blood*, 125(6), 981–991. Retrieved 2023-03-01, from <https://www.ncbi.nlm.nih.gov/pmc/articles/PMC4319238/> doi: 10.1182/blood-2014-04-568188
- Bondi, A. B. (2000, September). Characteristics of scalability and their impact on performance. In *Proceedings of the 2nd international workshop on Software and performance* (pp. 195–203). New York, NY, USA: Association for Computing Machinery. Retrieved 2024-03-07, from <https://dl.acm.org/doi/10.1145/350391.350432> doi: 10.1145/350391.350432
- Boswell, D., & Foucher, T. (2011). *The Art of Readable Code: Simple and Practical Techniques for Writing Better Code*. "O'Reilly Media, Inc.".

- Brooke, J. (1996, January). SUS – a quick and dirty usability scale. In (pp. 189–194).
- Burger, R., Guenther, A., Bakker, F., Schmalzing, M., Bernand, S., Baum, W., ... Gramatzki, M. (2001). Gp130 and ras mediated signaling in human plasma cell line INA-6: A cytokine-regulated tumor model for plasmacytoma. *The Hematology Journal: The Official Journal of the European Haematology Association*, 2(1), 42–53. doi: 10.1038/sj.thj.6200075
- Burger, R., Günther, A., Bakker, F., Schmalzing, M., Bernand, S., Baum, W., ... Gramatzki, M. (2001, January). Gp130 and ras mediated signaling in human plasma cell line INA6: A cytokine-regulated tumor model for plasmacytoma. *Hematology Journal - HEMATOL J*, 2, 42–53. doi: 10.1038/sj.thj.6200075
- Bustin, S. A. (2014, December). The reproducibility of biomedical research: Sleepers awake! *Biomolecular Detection and Quantification*, 2, 35–42. Retrieved 2024-03-18, from <https://www.sciencedirect.com/science/article/pii/S2214753515000030> doi: 10.1016/j.bdq.2015.01.002
- Caplan, A. (1991). Mesenchymal stem cells. *Journal of orthopaedic research : official publication of the Orthopaedic Research Society*, 9(5), 641–50. Retrieved from <http://www.ncbi.nlm.nih.gov/pubmed/1870029> doi: 10.1002/jor.1100090504
- Caplan, A. I. (1994, July). The mesengenic process. *Clinics in plastic surgery*, 21(3), 429–435.
- Carlson, M. (2016). Org.Hs.cgi.db. *Bioconductor*. Retrieved 2023-06-09, from <http://bioconductor.org/packages/org.Hs.cgi.db/> doi: 10.18129/B9.bioc.org.Hs.cgi.db
- Chacon, S., & Straub, B. (2024, March). *Git - Book*. Retrieved 2024-03-07, from <https://git-scm.com/book/de/v2>
- Charlier, F., Weber, M., Izak, D., Harkin, E., Magnus, M., Lalli, J., ... Repplinger, S. (2022, October). *Trevismd/statannotations: V0.5*. Zenodo. Retrieved 2023-11-16, from <https://zenodo.org/record/7213391> doi: 10.5281/ZENODO.7213391
- Chatterjee, M., Hönenmann, D., Lentzsch, S., Bommert, K., Sers, C., Herrmann, P., ... Bargou, R. C. (2002, November). In the presence of bone marrow stromal cells human multiple myeloma cells become independent of the IL-6/gp130/STAT3 pathway. *Blood*, 100(9), 3311–3318. doi: 10.1182/blood-2002-01-0102
- Cooper, G. M. (2000). The Cell: A Molecular Approach. 2nd Edition. *Sinauer Associates*, Proliferation in Development and Differentiation. Retrieved from <https://www.ncbi.nlm.nih.gov/books/NBK9906/>
- da Silva Meirelles, L., Chagastelles, P. C., & Nardi, N. B. (2006, June). Mesenchymal stem cells reside in virtually all post-natal organs and tissues. *Journal of cell science*, 119(Pt 11), 2204–2213. doi: 10.1242/jcs.02932
- Dobin, A., Davis, C. A., Schlesinger, F., Drenkow, J., Zaleski, C., Jha, S., ... Gingeras, T. R. (2013, January). STAR: Ultrafast universal RNA-seq aligner. *Bioinformatics*, 29(1), 15–21. Retrieved 2023-05-27, from <https://www.ncbi.nlm.nih.gov/pmc/articles/PMC3530905/> doi: 10.1093/bioinformatics/bts635
- Dominici, M., Le Blanc, K., Mueller, I., Slaper-Cortenbach, I., Marini, F., Krause, D., ... Horwitz, E. (2006). Minimal criteria for defining multipotent mesenchymal stromal cells. The International Society for Cellular Therapy position statement. *Cytotherapy*, 8(4), 315–317. doi: 10.1080/14653240600855905
- Duvall, P., Matyas, S., & Glover, A. (2007). *Continuous integration: Improving software quality and reducing risk*. Pearson Education. Retrieved from <https://books.google.de/books?id=PV9qfEdv9L0C>
- Dziadowicz, S. A., Wang, L., Akhter, H., Aesoph, D., Sharma, T., Adjero, D. A., ... Hu, G. (2022, January). Bone Marrow Stroma-Induced Transcriptome and Regulome Signatures of Multiple Myeloma. *Cancers*, 14(4), 927. Retrieved 2022-10-25, from <https://www.mdpi.com/2072-6694/14/4/927> doi: 10.3390/cancers14040927
- Ekmekci, B., McAnany, C. E., & Mura, C. (2016, July). An Introduction to Programming for Bioscientists: A Python-Based Primer. *PLOS Computational Biology*, 12(6), e1004867. Retrieved 2024-03-10, from <https://journals.plos.org/ploscompbiol/article?id=10.1371/journal.pcbi.1004867> doi: 10.1371/journal.pcbi.1004867
- Ewels, P., Magnusson, M., Lundin, S., & Käller, M. (2016, October). MultiQC: Summarize analysis results for

- multiple tools and samples in a single report. *Bioinformatics*, 32(19), 3047–3048. Retrieved 2023-06-09, from <https://doi.org/10.1093/bioinformatics/btw354> doi: 10.1093/bioinformatics/btw354
- Fazeli, P. K., Horowitz, M. C., MacDougald, O. A., Scheller, E. L., Rodeheffer, M. S., Rosen, C. J., & Klibanski, A. (2013, March). Marrow Fat and Bone—New Perspectives. *The Journal of Clinical Endocrinology and Metabolism*, 98(3), 935–945. Retrieved 2023-12-20, from <https://www.ncbi.nlm.nih.gov/pmc/articles/PMC3590487/> doi: 10.1210/jc.2012-3634
- Fernandez-Rebollo, E., Mentrup, B., Ebert, R., Franzen, J., Abagnale, G., Sieben, T., ... Wagner, W. (2017, July). Human Platelet Lysate versus Fetal Calf Serum: These Supplements Do Not Select for Different Mesenchymal Stromal Cells. *Scientific Reports*, 7, 5132. Retrieved 2023-05-02, from <https://www.ncbi.nlm.nih.gov/pmc/articles/PMC5506010/> doi: 10.1038/s41598-017-05207-1
- Frassanito, M. A., Cusmai, A., Iodice, G., & Dammacco, F. (2001, January). Autocrine interleukin-6 production and highly malignant multiple myeloma: Relation with resistance to drug-induced apoptosis. *Blood*, 97(2), 483–489. doi: 10.1182/blood.v97.2.483
- Friedenstein, A., & Kuralesova, A. I. (1971, August). Osteogenic precursor cells of bone marrow in radiation chimeras. *Transplantation*, 12(2), 99–108.
- Friedenstein, A. J., Piatetzky-Shapiro, I. L., & Petrakova, K. V. (1966, December). Osteogenesis in transplants of bone marrow cells. *Journal of embryology and experimental morphology*, 16(3), 381–390.
- Gabr, M. M., Zakaria, M. M., Refaie, A. F., Ismail, A. M., Abou-El-Mahasen, M. A., Ashamallah, S. A., ... Ghoneim, M. A. (2013). Insulin-producing cells from adult human bone marrow mesenchymal stem cells control streptozotocin-induced diabetes in nude mice. *Cell transplantation*, 22(1), 133–145. doi: 10.3727/096368912X647162
- García-Ortiz, A., Rodríguez-García, Y., Encinas, J., Maroto-Martín, E., Castellano, E., Teixidó, J., & Martínez-López, J. (2021, January). The Role of Tumor Microenvironment in Multiple Myeloma Development and Progression. *Cancers*, 13(2). Retrieved 2021-02-02, from <https://www.ncbi.nlm.nih.gov/pmc/articles/PMC7827690/> doi: 10.3390/cancers13020217
- Gentleman. (n.d.). *Bioconductor - BiocViews*. Retrieved 2023-06-09, from <https://bioconductor.org/packages/3.17/BiocViews.html>
- Ghobrial, I. M. (2012, July). Myeloma as a model for the process of metastasis: Implications for therapy. *Blood*, 120(1), 20–30. Retrieved 2022-10-15, from <https://www.ncbi.nlm.nih.gov/pmc/articles/PMC3390959/> doi: 10.1182/blood-2012-01-379024
- Glavey, S. V., Naba, A., Manier, S., Clauser, K., Tahri, S., Park, J., ... Ghobrial, I. M. (2017, November). Proteomic characterization of human multiple myeloma bone marrow extracellular matrix. *Leukemia*, 31(11), 2426–2434. Retrieved 2023-09-05, from <https://www.nature.com/articles/leu2017102> doi: 10.1038/leu.2017.102
- Gomez-Cabrero, D., Abugessaisa, I., Maier, D., Teschendorff, A., Merkenschlager, M., Gisel, A., ... Tegnér, J. (2014, March). Data integration in the era of omics: Current and future challenges. *BMC Systems Biology*, 8(2), I1. Retrieved 2024-03-18, from <https://doi.org/10.1186/1752-0509-8-S2-I1> doi: 10.1186/1752-0509-8-S2-I1
- Gómez-López, G., Dopazo, J., Cigudosa, J. C., Valencia, A., & Al-Shahrour, F. (2019, May). Precision medicine needs pioneering clinical bioinformaticians. *Briefings in Bioinformatics*, 20(3), 752–766. doi: 10.1093/bib/bbx144
- Goodman, S. N., Fanelli, D., & Ioannidis, J. P. A. (2016, June). What does research reproducibility mean? *Science Translational Medicine*, 8(341), 341ps12-341ps12. Retrieved 2024-03-18, from <https://www.science.org/doi/10.1126/scitranslmed.aaf5027> doi: 10.1126/scitranslmed.aaf5027
- Gosselin, R.-D. (2021, February). Insufficient transparency of statistical reporting in preclinical research:

- A scoping review. *Scientific Reports*, 11(1), 3335. Retrieved 2024-03-11, from <https://www.nature.com/articles/s41598-021-83006-5> doi: 10.1038/s41598-021-83006-5
- Gramatzki, M., Burger, R., Trautman, U., Marschalek, R., Lorenz, H., Hansen-Hagge, T., ... Kalden, J. (1994). Two new interleukin-6 dependent plasma cell lines carrying a chromosomal abnormality involving the IL-6 gene locus. , 84 Suppl. 1, 173a-173a. Retrieved 2023-03-24, from <https://www.cellosaurus.org/cellpub/CLPUB00060>
- Greenstein, S., Krett, N. L., Kurosawa, Y., Ma, C., Chauhan, D., Hideshima, T., ... Rosen, S. T. (2003, April). Characterization of the MM.1 human multiple myeloma (MM) cell lines: A model system to elucidate the characteristics, behavior, and signaling of steroid-sensitive and -resistant MM cells. *Experimental Hematology*, 31(4), 271–282. doi: 10.1016/s0301-472x(03)00023-7
- Gronthos, S., Graves, S. E., Ohta, S., & Simmons, P. J. (1994, December). The STRO-1+ fraction of adult human bone marrow contains the osteogenic precursors. *Blood*, 84(12), 4164–4173.
- Harrington, D. P., & Fleming, T. R. (1982). A Class of Rank Test Procedures for Censored Survival Data. *Biometrika*, 69(3), 553–566. Retrieved 2023-08-07, from <https://www.jstor.org/stable/2335991> doi: 10.2307/2335991
- Harris, C. R., Millman, K. J., van der Walt, S. J., Gommers, R., Virtanen, P., Cournapeau, D., ... Oliphant, T. E. (2020, September). Array programming with NumPy. *Nature*, 585(7825), 357–362. Retrieved 2023-08-09, from <https://www.nature.com/articles/s41586-020-2649-2> doi: 10.1038/s41586-020-2649-2
- Hideshima, T., Mitsiades, C., Tonon, G., Richardson, P. G., & Anderson, K. C. (2007, August). Understanding multiple myeloma pathogenesis in the bone marrow to identify new therapeutic targets. *Nature Reviews Cancer*, 7(8), 585–598. Retrieved 2023-02-07, from <https://www.nature.com/articles/nrc2189> doi: 10.1038/nrc2189
- Hothorn, T., & Lausen, B. (n.d.). *Maximally Selected Rank Statistics in R*. Retrieved from <http://cran.r-project.org/web/packages/maxstat/index.html>.
- Hu, X., Villodre, E. S., Larson, R., Rahal, O. M., Wang, X., Gong, Y., ... Debeb, B. G. (2021, January). Decorin-mediated suppression of tumorigenesis, invasion, and metastasis in inflammatory breast cancer. *Communications Biology*, 4(1), 72. doi: 10.1038/s42003-020-01590-0
- Huang, S.-Y., Lin, H.-H., Yao, M., Tang, J.-L., Wu, S.-J., Hou, H.-A., ... Tien, H.-F. (2015). Higher Decorin Levels in Bone Marrow Plasma Are Associated with Superior Treatment Response to Novel Agent-Based Induction in Patients with Newly Diagnosed Myeloma - A Retrospective Study. *PLoS One*, 10(9), e0137552. doi: 10.1371/journal.pone.0137552
- Hunter, J. D. (2007, May). Matplotlib: A 2D Graphics Environment. *Computing in Science & Engineering*, 9(3), 90–95. Retrieved 2023-11-15, from <https://ieeexplore.ieee.org/document/4160265> doi: 10.1109/MCSE.2007.55
- Incerti, D., Thom, H., Baio, G., & Jansen, J. P. (2019, May). R You Still Using Excel? The Advantages of Modern Software Tools for Health Technology Assessment. *Value in Health*, 22(5), 575–579. Retrieved 2024-03-11, from <https://www.sciencedirect.com/science/article/pii/S1098301519300506> doi: 10.1016/j.jval.2019.01.003
- Jansen, B. J. H., Gilissen, C., Roelofs, H., Schaap-Oziemlak, A., Veltman, J. A., Raymakers, R. A. P., ... Adema, G. J. (2010, April). Functional differences between mesenchymal stem cell populations are reflected by their transcriptome. *Stem cells and development*, 19(4), 481–490. doi: 10.1089/scd.2009.0288
- Kaplan, E. L., & Meier, P. (1958, June). Nonparametric Estimation from Incomplete Observations. *Journal of the American Statistical Association*, 53(282), 457–481. Retrieved 2023-08-07, from <http://www.tandfonline.com/doi/abs/10.1080/01621459.1958.10501452> doi: 10.1080/01621459.1958.10501452
- Katz, B.-Z. (2010, June). Adhesion molecules—The lifelines of multiple myeloma cells. *Seminars in Can-*

- cer Biology, 20(3), 186–195. Retrieved 2021-07-04, from <https://linkinghub.elsevier.com/retrieve/pii/S1044579X10000246> doi: 10.1016/j.semancer.2010.04.003
- Kawano, M. M., Huang, N., Tanaka, H., Ishikawa, H., Sakai, A., Tanabe, O., ... Kuramoto, A. (1991, December). Homotypic cell aggregations of human myeloma cells with ICAM-1 and LFA-1 molecules. *British Journal of Haematology*, 79(4), 583–588. doi: 10.1111/j.1365-2141.1991.tb08085.x
- Kazman, R., Bianco, P., Ivers, J., & Klein, J. (2020, December). *Maintainability* (Report). Carnegie Mellon University. Retrieved 2024-03-07, from <https://kilthub.cmu.edu/articles/report/Maintainability/12954908/1> doi: 10.1184/R1/12954908.v1
- Kibler, C., Schermutzki, F., Waller, H. D., Timpl, R., Müller, C. A., & Klein, G. (1998, June). Adhesive interactions of human multiple myeloma cell lines with different extracellular matrix molecules. *Cell Adhesion and Communication*, 5(4), 307–323. doi: 10.3109/15419069809040300
- Krekel, H., Oliveira, B., Pfannschmidt, R., Bruynooghe, F., Laugher, B., & Bruhin, F. (2004). *Pytest*. Retrieved from <https://github.com/pytest-dev/pytest>
- Kuric, M., & Ebert, R. (2024, March). Plotastic: Bridging Plotting and Statistics in Python. *Journal of Open Source Software*, 9(95), 6304. Retrieved 2024-03-11, from <https://joss.theoj.org/papers/10.21105/joss.06304> doi: 10.21105/joss.06304
- Lai, T.-Y., Cao, J., Ou-Yang, P., Tsai, C.-Y., Lin, C.-W., Chen, C.-C., ... Lee, C.-Y. (2022, April). Different methods of detaching adherent cells and their effects on the cell surface expression of Fas receptor and Fas ligand. *Scientific Reports*, 12(1), 5713. Retrieved 2023-06-01, from <https://www.nature.com/articles/s41598-022-09605-y> doi: 10.1038/s41598-022-09605-y
- Li, H., Handsaker, B., Wysoker, A., Fennell, T., Ruan, J., Homer, N., ... 1000 Genome Project Data Processing Subgroup (2009, August). The Sequence Alignment/Map format and SAMtools. *Bioinformatics*, 25(16), 2078–2079. Retrieved 2023-06-09, from <https://doi.org/10.1093/bioinformatics/btp352> doi: 10.1093/bioinformatics/btp352
- McKinney, W. (2010, January). Data Structures for Statistical Computing in Python. In (pp. 56–61). doi: 10.25080/Majora-92bf1922-00a
- Moreno-Indias, I., Lahti, L., Nedyalkova, M., Elbere, I., Roshchupkin, G., Adilovic, M., ... Zomer, A. L. (2021, February). Statistical and Machine Learning Techniques in Human Microbiome Studies: Contemporary Challenges and Solutions. *Frontiers in Microbiology*, 12. Retrieved 2024-03-18, from <https://www.frontiersin.org/journals/microbiology/articles/10.3389/fmicb.2021.635781/full> doi: 10.3389/fmicb.2021.635781
- Muruganandan, S., Roman, A. A., & Sinal, C. J. (2009, January). Adipocyte differentiation of bone marrow-derived mesenchymal stem cells: Cross talk with the osteoblastogenic program. *Cellular and molecular life sciences : CMLS*, 66(2), 236–253. doi: 10.1007/s00018-008-8429-z
- Myers, G. J., Sandler, C., & Badgett, T. (2011). *The art of software testing* (3rd ed.). Wiley Publishing. Retrieved from <https://malenezi.github.io/malenezi/SE401/Books/114-the-art-of-software-testing-3-edition.pdf>
- Narzt, W., Pichler, J., Pirlbauer, K., & Zwinz, M. (1998, January). A Reusability Concept for Process Automation Software..
- Newville, M., Stensitzki, T., Allen, D. B., & Ingargiola, A. (2014, September). *LMFIT: Non-Linear Least-Square Minimization and Curve-Fitting for Python*. Zenodo. Retrieved 2023-05-30, from <https://zenodo.org/record/11813> doi: 10.5281/zenodo.11813
- Nilsson, K., Bennich, H., Johansson, S. G., & Pontén, J. (1970, October). Established immunoglobulin producing myeloma (IgE) and lymphoblastoid (IgG) cell lines from an IgE myeloma patient. *Clinical and Experimental Immunology*, 7(4), 477–489.

- Nowotschin, S., & Hadjantonakis, A.-K. (2010, August). Cellular dynamics in the early mouse embryo: From axis formation to gastrulation. *Current opinion in genetics & development*, 20(4), 420–427. doi: 10.1016/j.gde.2010.05.008
- Okuno, Y., Takahashi, T., Suzuki, A., Ichiba, S., Nakamura, K., Okada, T., ... Imura, H. (1991, February). In vitro growth pattern of myeloma cells in liquid suspension or semi-solid culture containing interleukin-6. *International Journal of Hematology*, 54(1), 41–47.
- Paszke, A., Gross, S., Massa, F., Lerer, A., Bradbury, J., Chanan, G., ... Chintala, S. (2019, December). PyTorch: An Imperative Style, High-Performance Deep Learning Library (No. arXiv:1912.01703). arXiv. Retrieved 2024-03-07, from <http://arxiv.org/abs/1912.01703> doi: 10.48550/arXiv.1912.01703
- Peng, R. D. (2011, December). Reproducible Research in Computational Science. *Science*, 334(6060), 1226–1227. Retrieved 2024-03-18, from <https://www.science.org/doi/10.1126/science.1213847> doi: 10.1126/science.1213847
- Perneger, T. V. (1998, April). What's wrong with Bonferroni adjustments. *BMJ : British Medical Journal*, 316(7139), 1236–1238. Retrieved 2021-11-24, from <https://www.ncbi.nlm.nih.gov/pmc/articles/PMC1112991/>
- Pittenger, M. F., Mackay, A. M., Beck, S. C., Jaiswal, R. K., Douglas, R., Mosca, J. D., ... Marshak, D. R. (1999). Multilineage Potential of Adult Human Mesenchymal Stem Cells. , 284(April), 143–148. doi: 10.1126/science.284.5411.143
- The Python Language Reference. (n.d.). Retrieved 2024-03-07, from <https://docs.python.org/3/reference/index.html>
- R Core Team. (2018). R: A language and environment for statistical computing [Manual]. Vienna, Austria. Retrieved from <https://www.R-project.org/>
- Radford, A., Wu, J., Child, R., Luan, D., Amodei, D., & Sutskever, I. (2019). Language Models are Unsupervised Multitask Learners.. Retrieved 2024-03-07, from <https://www.semanticscholar.org/paper/Language-Models-are-Unsupervised-Multitask-Learners-Radford-Wu/9405cc0d6169988371b2755e573cc28650d14dfe>
- Rajkumar, S. V., Dimopoulos, M. A., Palumbo, A., Blade, J., Merlini, G., Mateos, M.-V., ... Miguel, J. F. S. (2014, November). International Myeloma Working Group updated criteria for the diagnosis of multiple myeloma. *The Lancet. Oncology*, 15(12), e538-548. doi: 10.1016/S1470-2045(14)70442-5
- Rajkumar, S. V., & Kumar, S. (2020, September). Multiple myeloma current treatment algorithms. *Blood Cancer Journal*, 10(9), 94. Retrieved 2023-07-03, from <https://www.ncbi.nlm.nih.gov/pmc/articles/PMC7523011/> doi: 10.1038/s41408-020-00359-2
- Ramakers, C., Ruijter, J. M., Deprez, R. H., & Moorman, A. F. (2003, March). Assumption-free analysis of quantitative real-time polymerase chain reaction (PCR) data. *Neuroscience Letters*, 339(1), 62–66. Retrieved 2022-11-27, from <https://linkinghub.elsevier.com/retrieve/pii/S0304394002014234> doi: 10.1016/S0304-3940(02)01423-4
- Rayhan, A., & Gross, D. (2023). The Rise of Python: A Survey of Recent Research. doi: 10.13140/RG.2.2.27388.92809
- Robinson, M. D., McCarthy, D. J., & Smyth, G. K. (2010, January). edgeR: A Bioconductor package for differential expression analysis of digital gene expression data. *Bioinformatics (Oxford, England)*, 26(1), 139–140. Retrieved from <https://www.ncbi.nlm.nih.gov/pubmed/19910308> doi: 10.1093/bioinformatics/btp616
- Sacchetti, B., Funari, A., Remoli, C., Giannicola, G., Kogler, G., Liedtke, S., ... Bianco, P. (2016). No identical "mesenchymal stem cells" at different times and sites: Human committed progenitors of distinct origin and differentiation potential are incorporated as adventitial cells in microvessels. *Stem Cell Reports*, 6(6), 897–913. Retrieved from <http://dx.doi.org/10.1016/j.stemcr.2016.05.011> doi: 10.1016/j.stemcr.2016.05.011
- Sandve, G. K., Nekrutenko, A., Taylor, J., & Hovig, E. (2013, October). Ten Simple Rules for Reproducible

- Computational Research. *PLoS Computational Biology*, 9(10), e1003285. Retrieved 2024-03-07, from <https://www.ncbi.nlm.nih.gov/pmc/articles/PMC3812051/> doi: 10.1371/journal.pcbi.1003285
- Sanz-Rodríguez, F., Ruiz-Velasco, N., Pascual-Salcedo, D., & Teixidó, J. (1999, December). Characterization of VLA-4-dependent myeloma cell adhesion to fibronectin and VCAM-1: VLA-4-dependent Myeloma Cell Adhesion. *British Journal of Haematology*, 107(4), 825–834. Retrieved 2023-04-02, from <http://doi.wiley.com/10.1046/j.1365-2141.1999.01762.x> doi: 10.1046/j.1365-2141.1999.01762.x
- Seabold, S., & Perktold, J. (2010). Statsmodels: Econometric and Statistical Modeling with Python. In *Python in Science Conference* (pp. 92–96). Austin, Texas. Retrieved 2023-05-29, from <https://conference.scipy.org/proceedings/scipy2010/seabold.html> doi: 10.25080/Majora-92bf1922-011
- Seckinger, A., Delgado, J. A., Moser, S., Moreno, L., Neuber, B., Grab, A., ... Vu, M. D. (2017, March). Target Expression, Generation, Preclinical Activity, and Pharmacokinetics of the BCMA-T Cell Bispecific Antibody EM801 for Multiple Myeloma Treatment. *Cancer Cell*, 31(3), 396–410. Retrieved 2023-07-21, from [https://www.cell.com/cancer-cell/abstract/S1535-6108\(17\)30016-8](https://www.cell.com/cancer-cell/abstract/S1535-6108(17)30016-8) doi: 10.1016/j.ccr.2017.02.002
- Seckinger, A., Hillengass, J., Emde, M., Beck, S., Kimmich, C., Dittrich, T., ... Hose, D. (2018). CD38 as Immunotherapeutic Target in Light Chain Amyloidosis and Multiple Myeloma-Association With Molecular Entities, Risk, Survival, and Mechanisms of Upfront Resistance. *Frontiers in Immunology*, 9, 1676. doi: 10.3389/fimmu.2018.01676
- Shenghui, H., Nakada, D., & Morrison, S. J. (2009). Mechanisms of Stem Cell Self-Renewal. *Annual Review of Cell and Developmental Biology*, 25(1), 377–406. Retrieved from <https://doi.org/10.1146/annurev.cellbio.042308.113248> doi: 10.1146/annurev.cellbio.042308.113248
- Smith, A. M., Niemeyer, K. E., Katz, D. S., Barba, L. A., Githinji, G., Gymrek, M., ... Vanderplas, J. T. (2018). Journal of Open Source Software (JOSS): Design and first-year review. *PeerJ Preprints*, 4, e147. doi: 10.7717/peerj.cs.147
- Solimando, A. G., Malerba, E., Leone, P., Prete, M., Terragna, C., Cavo, M., & Racanelli, V. (2022, September). Drug resistance in multiple myeloma: Soldiers and weapons in the bone marrow niche. *Frontiers in Oncology*, 12, 973836. Retrieved 2022-10-23, from <https://www.ncbi.nlm.nih.gov/pmc/articles/PMC9533079/> doi: 10.3389/fonc.2022.973836
- Stock, P., Bruckner, S., Winkler, S., Dollinger, M. M., & Christ, B. (2014, April). Human bone marrow mesenchymal stem cell-derived hepatocytes improve the mouse liver after acute acetaminophen intoxication by preventing progress of injury. *International journal of molecular sciences*, 15(4), 7004–7028. doi: 10.3390/ijms15047004
- Tai, Y.-T., Li, X.-F., Breitkreutz, I., Song, W., Neri, P., Catley, L., ... Anderson, K. C. (2006, July). Role of B-cell-activating factor in adhesion and growth of human multiple myeloma cells in the bone marrow microenvironment. *Cancer Research*, 66(13), 6675–6682. doi: 10.1158/0008-5472.CAN-06-0190
- Tam, P. P., & Beddington, R. S. (1987, January). The formation of mesodermal tissues in the mouse embryo during gastrulation and early organogenesis. *Development (Cambridge, England)*, 99(1), 109–126.
- Tanavalee, C., Luksanapruksa, P., & Singhathanadighe, W. (2016, June). Limitations of Using Microsoft Excel Version 2016 (MS Excel 2016) for Statistical Analysis for Medical Research. *Clinical Spine Surgery*, 29(5), 203. Retrieved 2024-03-11, from https://journals.lww.com/jspinaldisorders/fulltext/2016/06000/limitations_of_using_microsoft_excel_version_2016.5.aspx doi: 10.1097/BSD.0000000000000382
- Team, T. P. D. (2020, February). *Pandas-dev/pandas: Pandas*. Zenodo. Retrieved from <https://doi.org/10.5281/zenodo.3509134> doi: 10.5281/zenodo.3509134
- Terpos, E., Ntanasis-Stathopoulos, I., Gavriatopoulou, M., & Dimopoulos, M. A. (2018, January). Pathogenesis of bone disease in multiple myeloma: From bench to bedside. *Blood Cancer Journal*, 8(1), 7. doi: 10.1038/s41408-017-0037-4

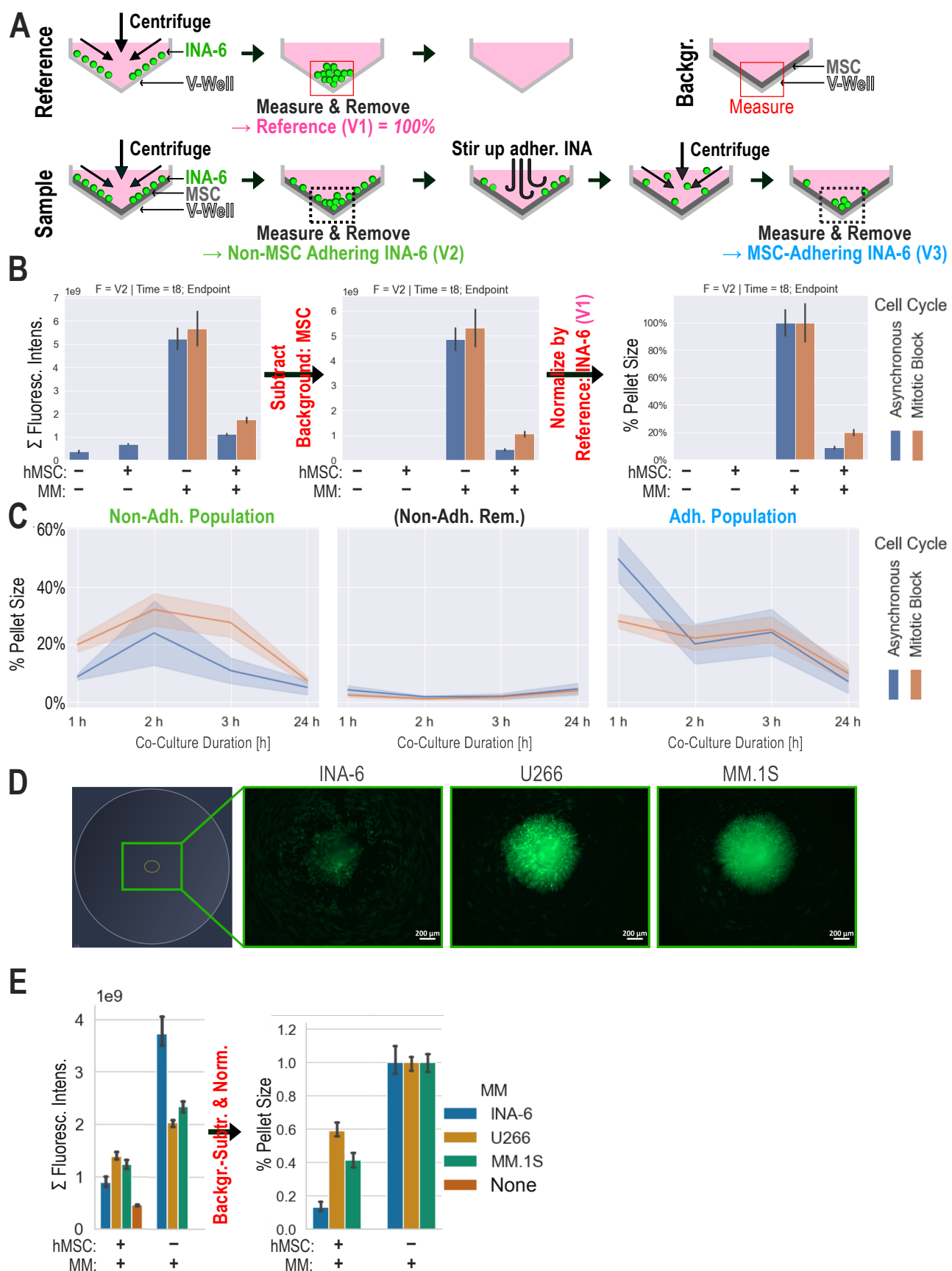
- Ullah, I., Subbarao, R. B., & Rho, G. J. (2015). Human mesenchymal stem cells - current trends and future prospective Bioscience Reports.
doi: 10.1042/BSR20150025
- Urashima, M., Chauhan, D., Uchiyama, H., Freeman, G., & Anderson, K. (1995, April). CD40 ligand triggered interleukin-6 secretion in multiple myeloma. *Blood*, 85(7), 1903–1912. Retrieved 2021-02-01, from <https://ashpublications.org/blood/article/85/7/1903/123565/CD40-ligand-triggered-interleukin6-secretion-in> doi: 10.1182/blood.V85.7.1903.bloodjournal8571903
- Vallat, R. (2018, November). Pingouin: Statistics in Python. *Journal of Open Source Software*, 3(31), 1026. Retrieved 2023-05-29, from <https://joss.theoj.org/papers/10.21105/joss.01026> doi: 10.21105/joss.01026
- van Rossum, G., Lehtosalo, J., & Langa, L. (2014). PEP 484 – Type Hints / peps.python.org. Retrieved 2024-03-08, from <https://peps.python.org/pep-0484/>
- Viguet-Carrin, S., Garnero, P., & Delmas, P. D. (2006, March). The role of collagen in bone strength. *Osteoporosis International*, 17(3), 319–336. Retrieved 2023-12-20, from <https://doi.org/10.1007/s00198-005-2035-9> doi: 10.1007/s00198-005-2035-9
- Waskom, M. L. (2021, April). Seaborn: Statistical data visualization. *Journal of Open Source Software*, 6(60), 3021. Retrieved 2023-03-26, from <https://joss.theoj.org/papers/10.21105/joss.03021> doi: 10.21105/joss.03021
- Weetall, M., Hugo, R., Maida, S., West, S., Wattanasin, S., Bouhel, R., ... Friedman, C. (2001, June). A Homogeneous Fluorometric Assay for Measuring Cell Adhesion to Immobilized Ligand Using V-Well Microtiter Plates. *Analytical Biochemistry*, 293(2), 277–287. Retrieved 2022-09-25, from <https://linkinghub.elsevier.com/retrieve/pii/S0003269701951401> doi: 10.1006/abio.2001.5140
- Wickham, H. (2014, September). Tidy Data. *Journal of Statistical Software*, 59, 1–23. Retrieved 2023-11-15, from <https://doi.org/10.18637/jss.v059.i10> doi: 10.18637/jss.v059.i10
- Wilkins, A., Kemp, K., Ginty, M., Hares, K., Mallam, E., & Scolding, N. (2009, July). Human bone marrow-derived mesenchymal stem cells secrete brain-derived neurotrophic factor which promotes neuronal survival in vitro. *Stem cell research*, 3(1), 63–70. doi: 10.1016/j.scr.2009.02.006
- Wilkinson, M. D., Dumontier, M., Aalbersberg, I. J., Appleton, G., Axton, M., Baak, A., ... Mons, B. (2016, March). The FAIR Guiding Principles for scientific data management and stewardship. *Scientific Data*, 3(1), 160018. Retrieved 2024-03-18, from <https://www.nature.com/articles/sdata201618> doi: 10.1038/sdata.2016.18
- Xu, W., Zhang, X., Qian, H., Zhu, W., Sun, X., Hu, J., ... Chen, Y. (2004, July). Mesenchymal stem cells from adult human bone marrow differentiate into a cardiomyocyte phenotype in vitro. *Experimental biology and medicine (Maywood, N.J.)*, 229(7), 623–631.
- Yang, A., Troup, M., & Ho, J. W. (2017, July). Scalability and Validation of Big Data Bioinformatics Software. *Computational and Structural Biotechnology Journal*, 15, 379–386. Retrieved 2024-03-07, from <https://www.ncbi.nlm.nih.gov/pmc/articles/PMC5537105/> doi: 10.1016/j.csbj.2017.07.002
- Zeissig, M. N., Zannettino, A. C. W., & Vandyke, K. (2020, December). Tumour Dissemination in Multiple Myeloma Disease Progression and Relapse: A Potential Therapeutic Target in High-Risk Myeloma. *Cancers*, 12(12). Retrieved 2021-02-03, from <https://www.ncbi.nlm.nih.gov/pmc/articles/PMC7761917/> doi: 10.3390/cancers12123643
- Zerbino, D. R., Achuthan, P., Akanni, W., Amode, M. R., Barrell, D., Bhai, J., ... Flicek, P. (2018, January). Ensembl 2018. *Nucleic Acids Research*, 46(D1), D754-D761. Retrieved 2023-05-27, from <https://doi.org/10.1093/nar/gkx1098> doi: 10.1093/nar/gkx1098
- Zhou, Y., Zhou, B., Pache, L., Chang, M., Khodabakhshi, A. H., Tanaseichuk, O., ... Chanda, S. K. (2019, April). Metascape provides a biologist-oriented resource for the analysis of systems-level datasets. *Nature*

Communications, 10(1), 1523. Retrieved 2023-02-09, from <https://www.nature.com/articles/s41467-019-09234-6> doi: 10.1038/s41467-019-09234-6

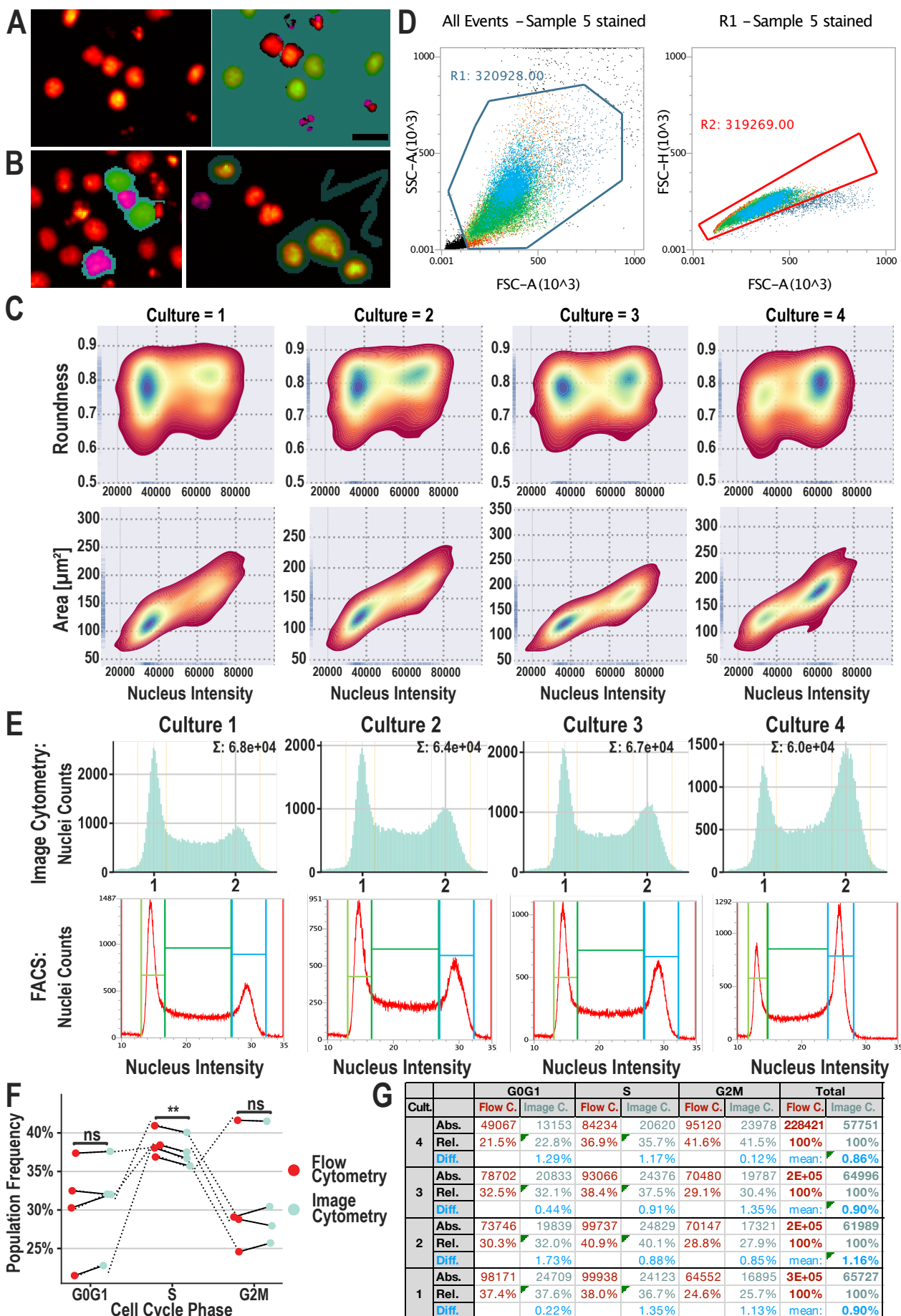
Appendices

A Supplementary Data & Methods

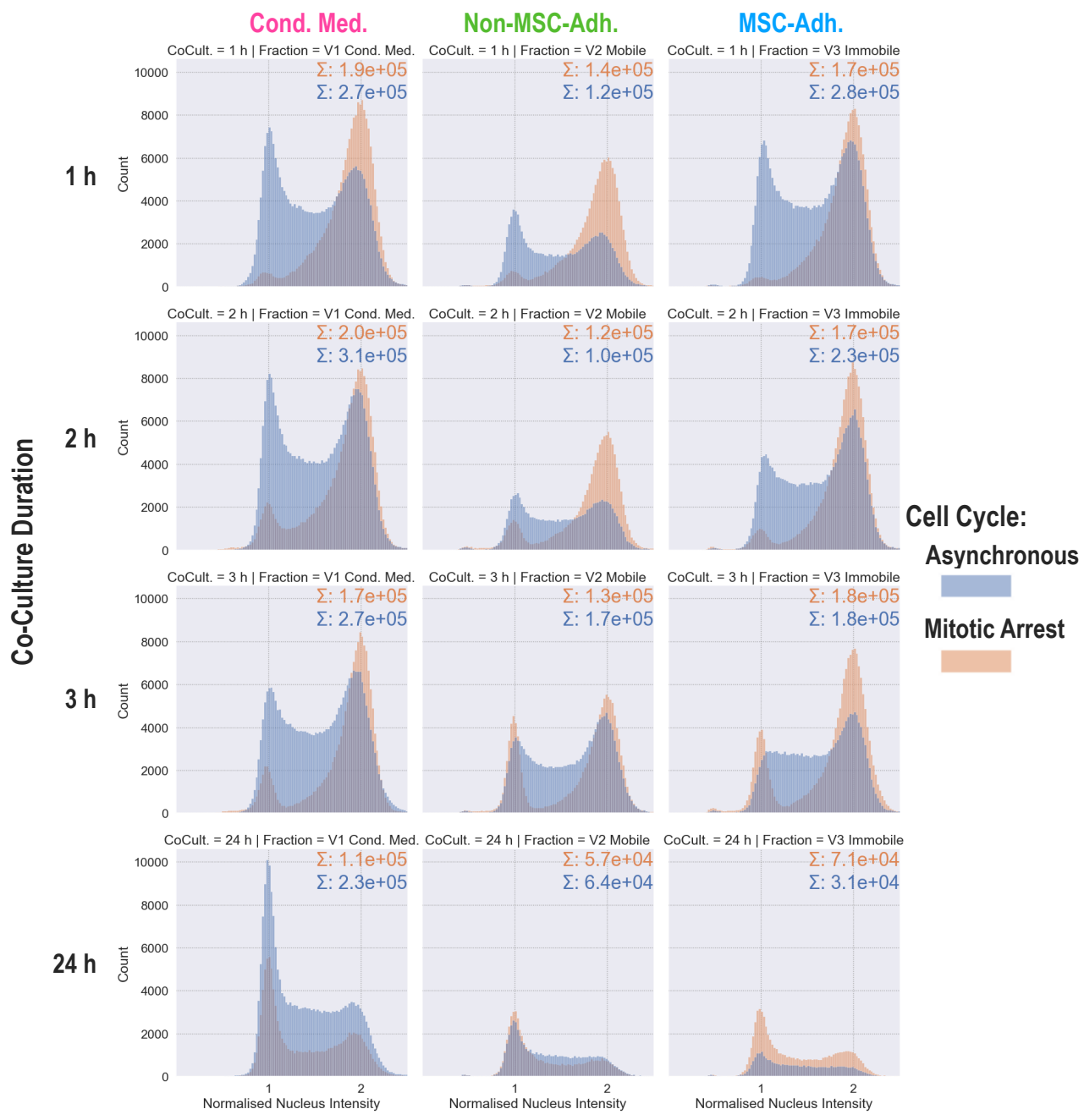
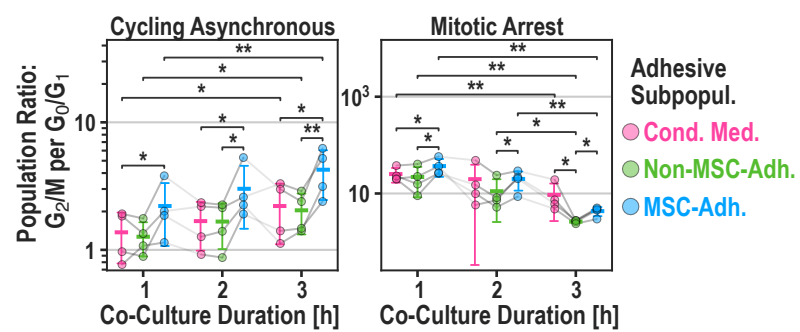
A.1 Figures



Appendix A Figure 1: Principle and quantification of the V-well adhesion assay of fluorescently labeled myeloma cells adapted by Weetall et al. (2001). **A:** Sample: Subsequent rounds of centrifugation and removal of cell pellet yielded the size of adhesive subpopulations. Fluorescently stained INA-6 cells were added to an hMSC monolayer. Non-adherent INA-6 cells (V2) were pelleted in the well-tip. Pellets were quantified by fluorescence brightness and isolated by pipetting. Immobile INA-6 cells (V3) were manually detached by forceful pipetting. Reference: Omitting adhesive hMSC-layer yielded 100% non-adherent cells (V1) after the first centrifugation step; Background: hMSC monolayer was used as background signal. **B:** Calculation of the population size relative to total cells starting with pellet intensity. The shown example is the pellet gained by centrifuging mobile subpopulation (V2) after 1 h of co-culture. (see Figure 3 for context): Intensity values from pellet images were summarized. After subtracting the unlabeled hMSC signal and normalization by a full-size pellet (reference), the resulting values represented the fraction of the adhesive subpopulation. **C:** One of three biological replicates summarized in Figure 3. Line range shows the standard deviation of four technical replicates. Non.Adh. Rem.: Fluorescence signal after removal of V2. **D:** Example images of myeloma cell lines (INA-6, U266, MM.1S) pelleted in the tip of V-wells. The leftmost image shows the recorded area in a complete V-well. Scale bar = 200 µm. **E:** Results from (D) comparing adhesion strength of three myeloma cell lines to hMSC. Error bars represent technical deviation. MM: Multiple Myeloma.



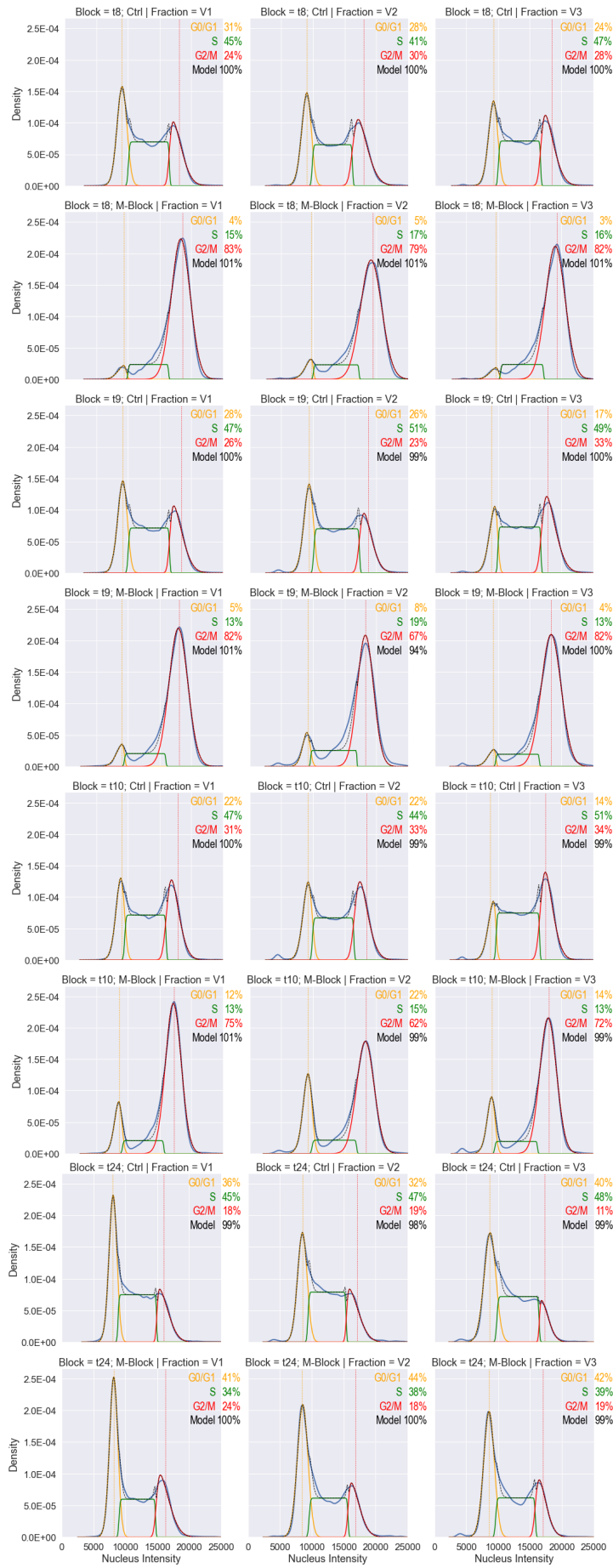
Appendix A Figure 2: Validation of image cytometric analysis of cell cycle in four INA-6 cultures. **A:** Left: Example image cytometric scan: INA-6 cells were stained with Hoechst33342 and scanned by automated fluorescence microscopy. Right: The image was segmented using a convolutional neural network (ZEISS ZEN intellesis) trained to discern healthy nuclei (green) from fragmented ones (magenta). Doublets are excluded by setting an area- and roundness threshold. Scale bar: 20 μm . **B:** Two example images from the training set. **C:** Quality of image cytometric data was ensured by plotting the distribution of nuclei brightnesses vs. the distribution of both nuclei-roundnesses and nuclei-areas. Nuclei with double fluorescence intensity have the same roundness while their area increases, as expected from a cell in G2 phase. **D:** The same samples from (C) were also measured with flow cytometry. Representative example of gating strategy: Left: Dead cells were excluded by setting a minimum threshold for side-scattering (SSC-A). Right: Doublets were excluded by setting a maximum threshold for forward scatter area (FSC-A) (sample "5" represents culture "4" in this figure). **E:** Cell cycle profiles of four independent INA-6 cultures were measured by both image cytometry (top) and flow cytometry (bottom). For both methods, frequencies of G0/G1, S, and G2M were summed up by setting fluorescence intensity thresholds. **F:** Image cytometry yields the same frequencies for G0/G1, S, and G2M when compared to flow cytometry. RM-ANOVA showed that the method has no significant effect on the frequencies of cell cycle populations [$F(1, 3) = 1.421, p\text{-unc} = .32$]. **G:** Results from (F) in tabular form. On average, frequencies for G0/G1, S, and G2M measured by Image cytometry differ by 0.95 percent points compared to flow cytometry measurement. Cult.: Culture; C.: Image cytometry; Abs.: Absolute cell count; Rel.: Relative cell count; Diff.: Difference between relative cell counts determined by flow cytometry and image cytometry.

A**B**

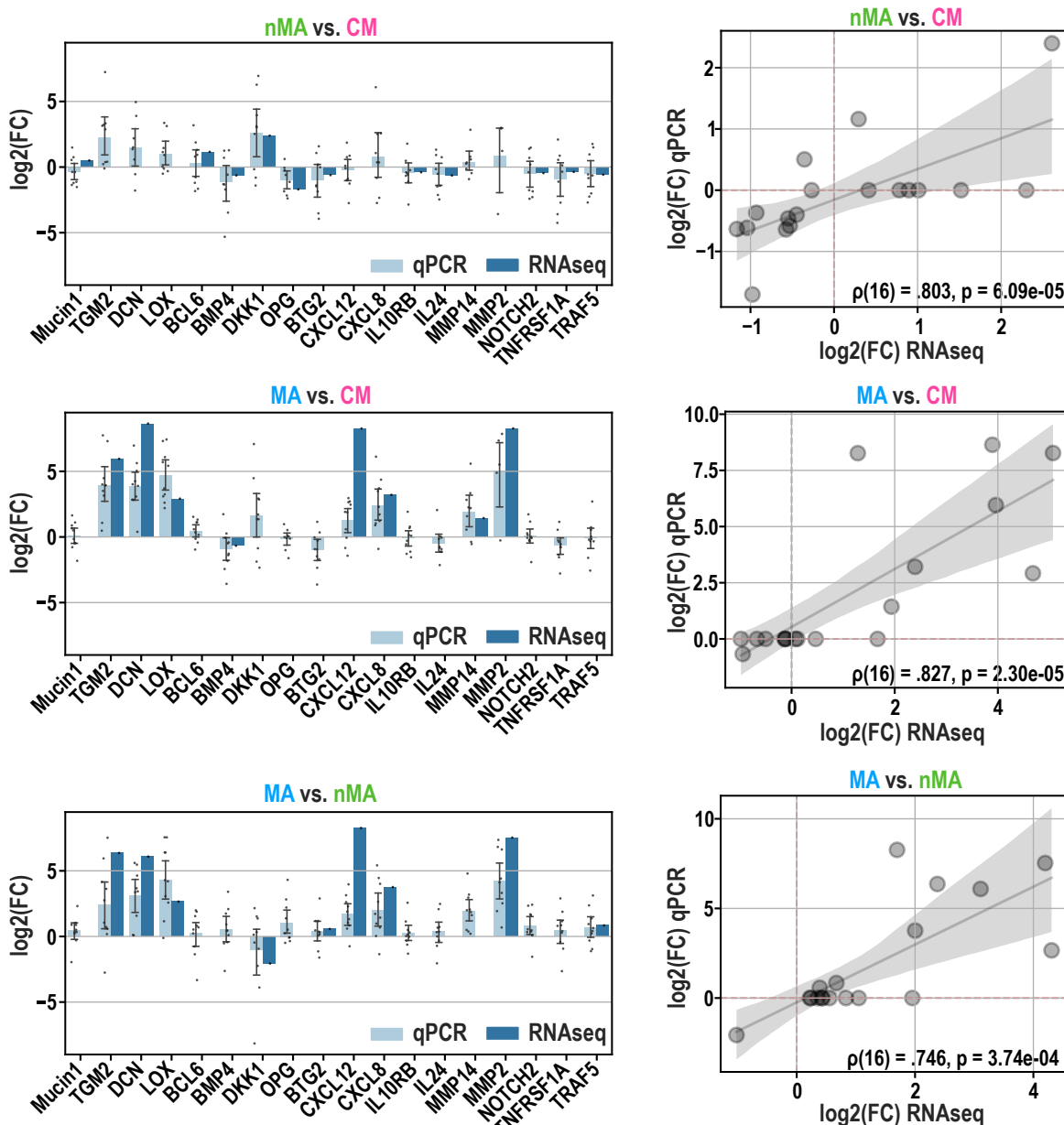
Appendix A Figure 3: Cell cycle analysis of INA-6 pellets gained from V-Well Adhesion assay (Figure 3).

A: Cell cycle profiles of MSC-adhering subpopulations. INA-6 cells were synchronized by double thymidine block followed by nocodazole. Cell cycle was released directly before addition to hMSCs. Histograms were normalized and summed up across all biological replicates ($n = 4$). Technical replicates (3) were pooled prior to cell cycle profiling. CoCult. = Co-culture duration. Fraction = Adhesion subpopulations.

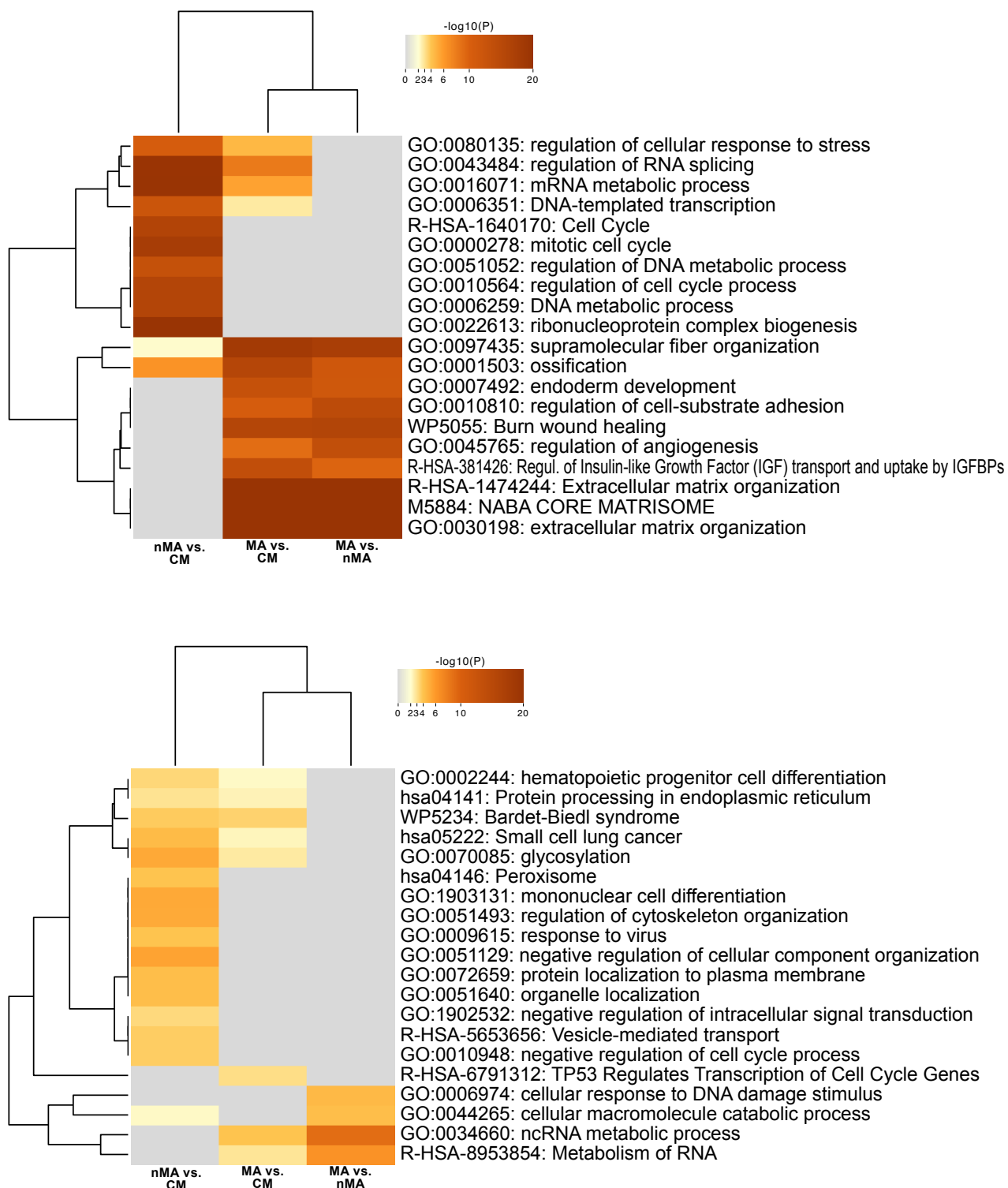
B: Similar figure to Fig. 3C displaying ratio of INA-6 populations (G2/M to G0/G1). **Statistics::** Paired t-test (B).



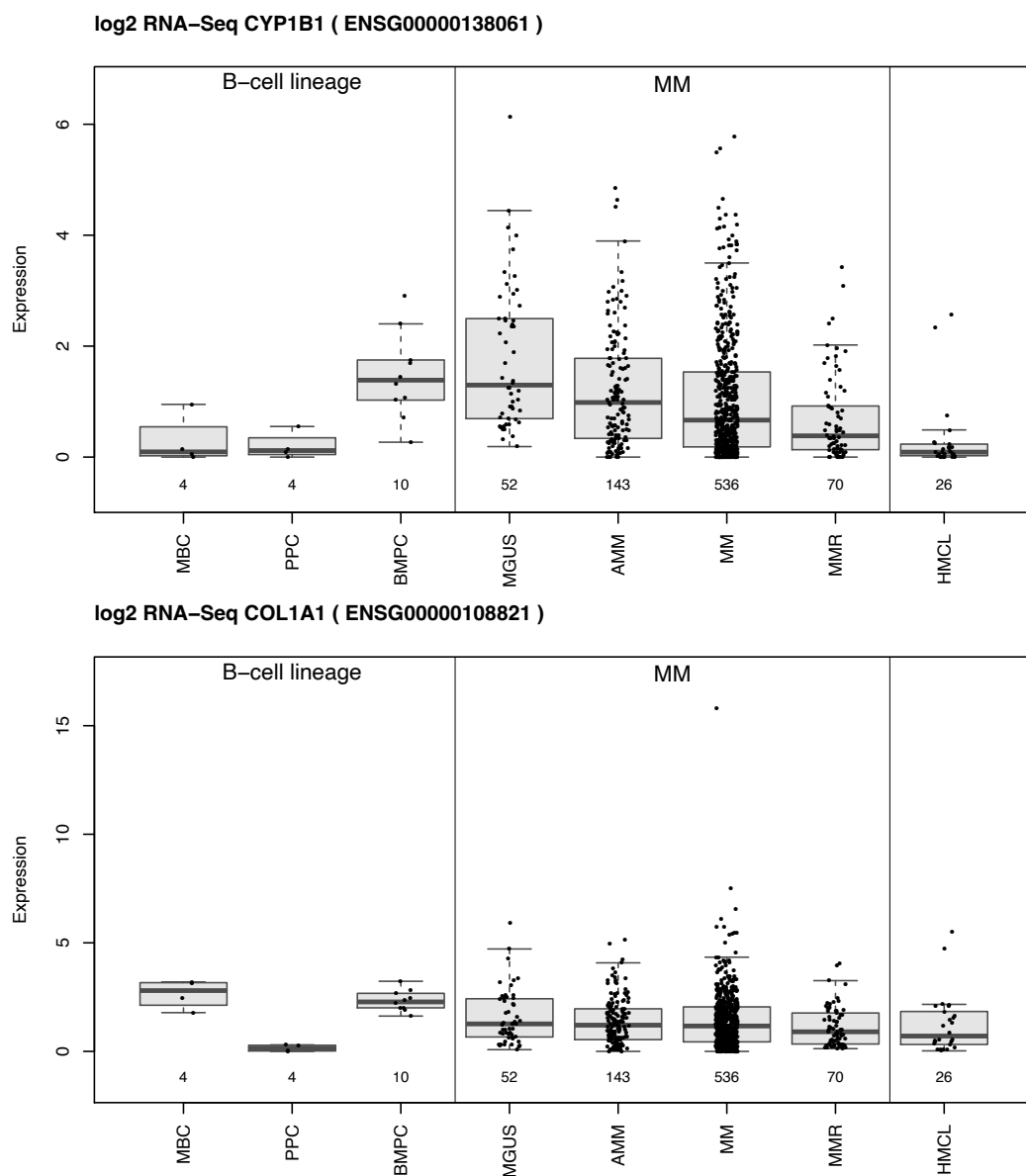
Appendix A Figure 4: Representative (one of the four independent sample sets as seen in Appendix A: Figure 3) curve fitting analysis of cell cycle profiles generated by Image Cytometry. t8, t9, t10, and t24 refer to 1, 2, 3, and 24 hours after the addition of INA-6 cells to hMSCs.



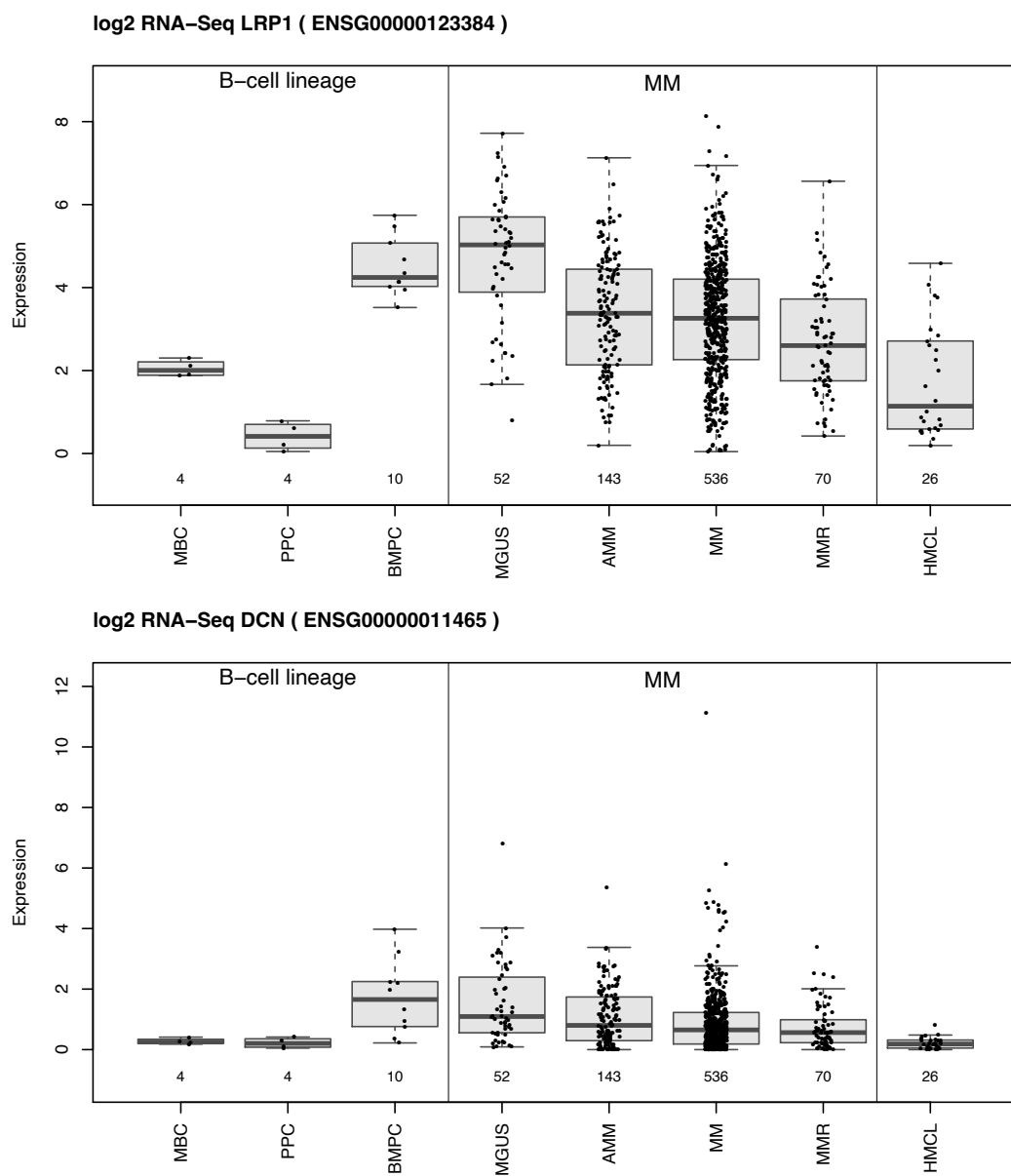
Appendix A Figure 5: Correlation of RNAseq with qPCR Left: Validation of RNAseq results (Figure 4) with qPCR showing the \log_2 (foldchange expression) of 18 genes. For qPCR, Datapoints each represent one biological replicate ($n = 10$), which is the mean of technical replicates ($n = 3$). Bar height represents mean of biological replicates, error bars show standard deviation of biological replicates. Right: Correlation between qPCR and RNAseq in terms of \log_2 (mean foldchange expression per gene). Each dot represents one gene shown in the barplot to the left. Genes measured with qPCR that showed no differential expression in RNAseq were set to have a $-\log_2(FC) = 0$. Shaded area shows the confidence interval of linear regression. Correlation coefficient was calculated using Spearman's rank. $N = 18$ genes. FC : Fold change expression.

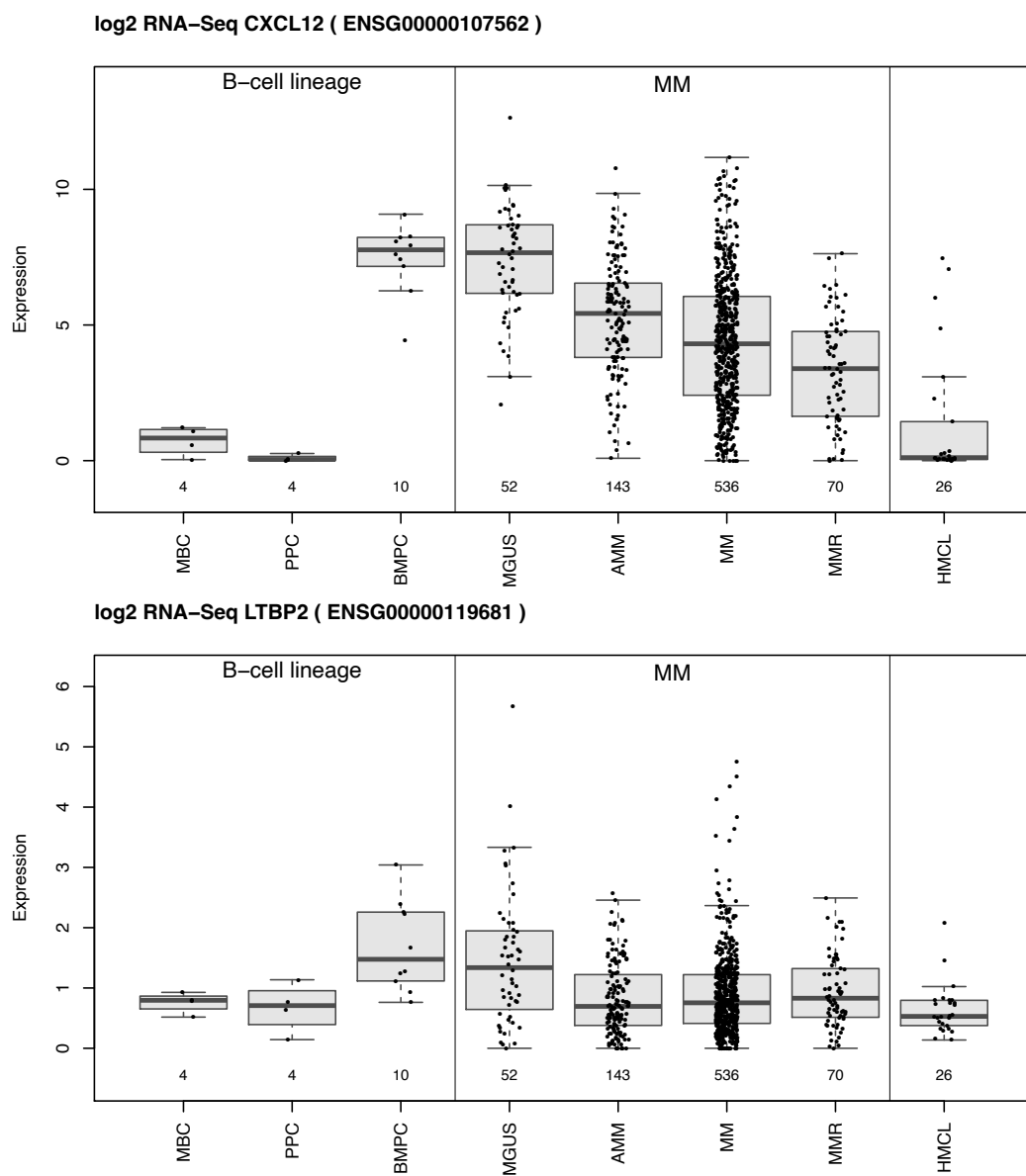


Appendix A Figure 6: Functional enrichment analysis by Metascape using genes that are differentially expressed between MSC-interacting subpopulations. Top: Upregulated genes. Bottom: Downregulated genes.

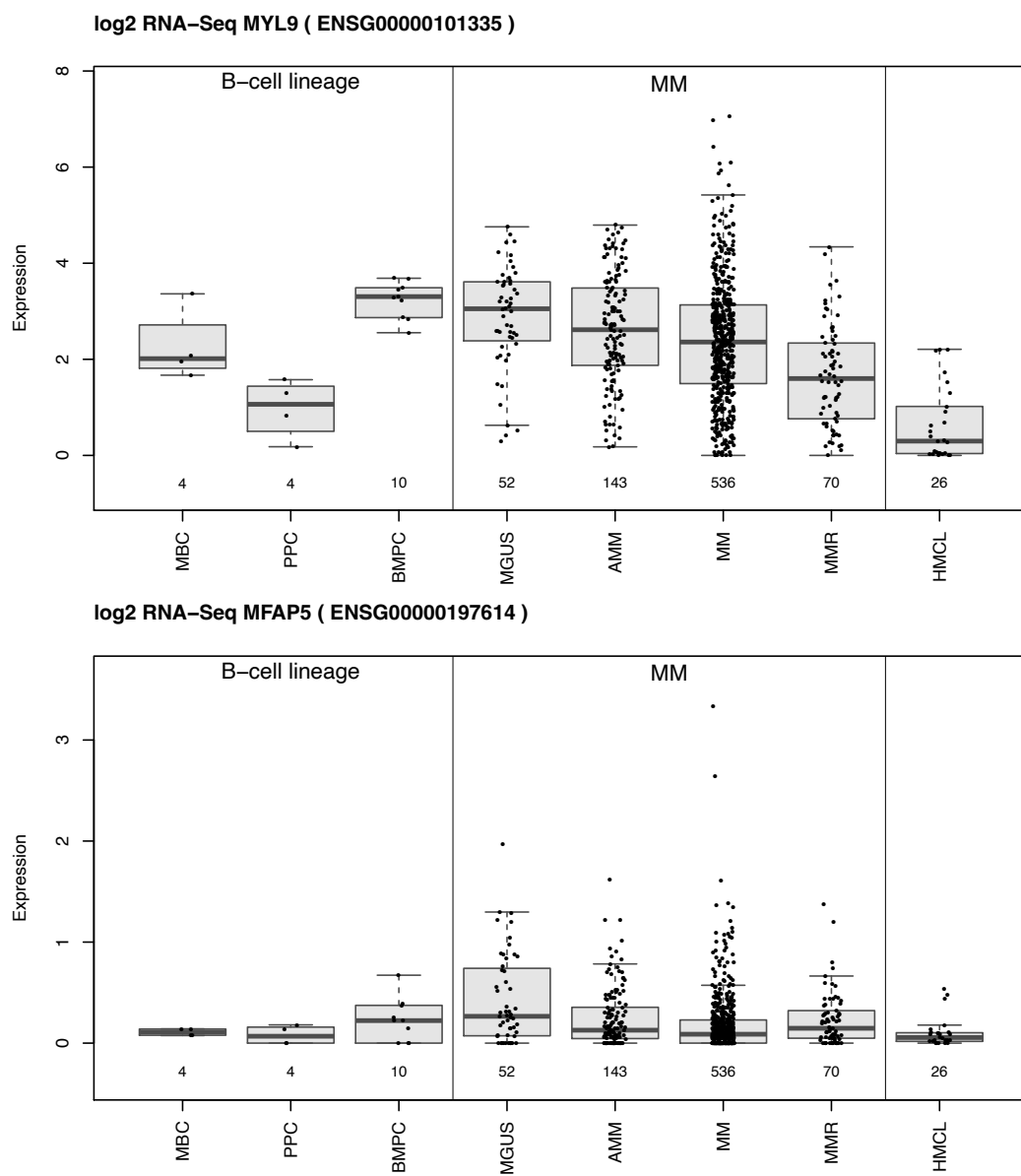


Appendix A Figure 7: Expression levels of adhesion genes that are downregulated and associated with survival ($p < 0.01$). Bone Marrow Plasma Cell (BMPC), Monoclonal Gammopathy of Undetermined Significance (MGUS), Smoldering Multiple Myeloma (sMM), Multiple Myeloma (MM), Multiple Myeloma Relapse (MMR).

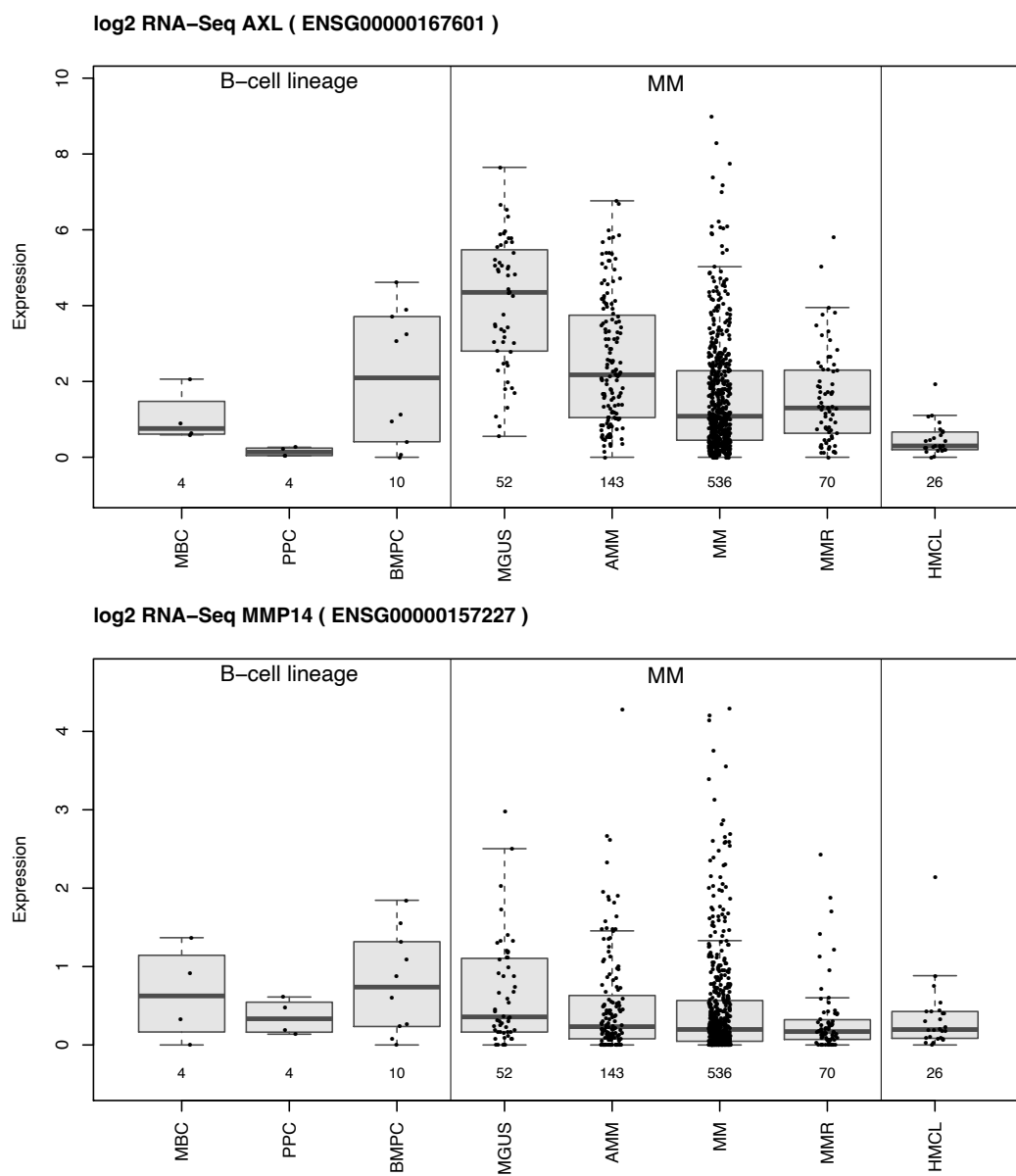
**Appendix A Figure 7:** continued from previous page

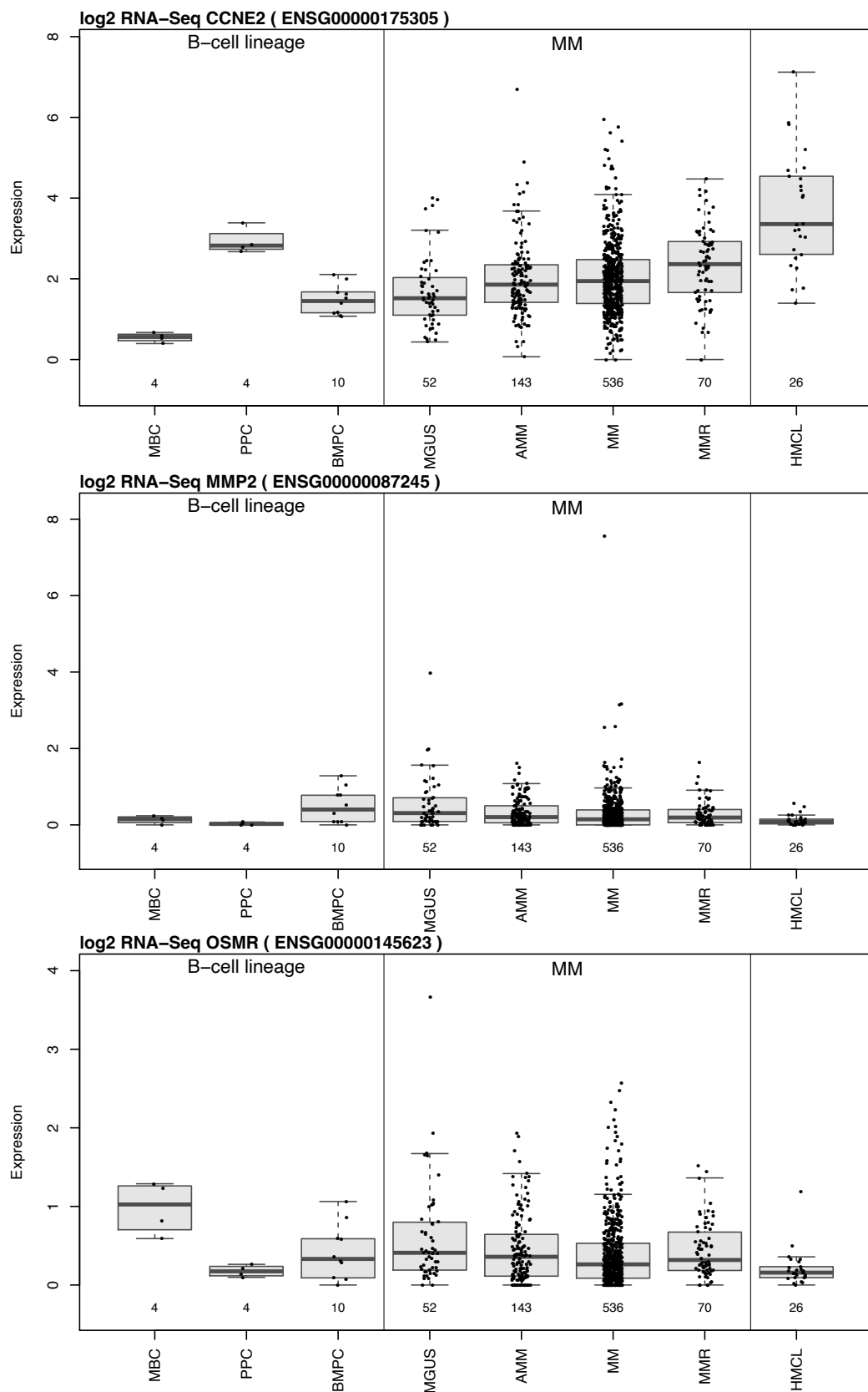


Appendix A Figure 7: continued from previous page



Appendix A Figure 7: continued from previous page

**Appendix A Figure 7:** continued from previous page



Appendix A Figure 8: Expression levels of adhesion genes that are not downregulated and associated with survival ($p < 0.01$). Bone Marrow Plasma Cell (BMPC), Monoclonal Gammopathy of Undetermined Significance (MGUS), Smoldering Multiple Myeloma (sMM), Multiple Myeloma (MM), Multiple Myeloma Relapse (MMR).

A.2 Tables

Appendix A Table 1: List of hMSC donors, myeloma cell lines, and their mycoplasma test status. If no unique donors were available, hMSC donors were used twice for the same experiment at different passages. WPSC: Well plate sandwich centrifugation.

Cell Type	Donor / Line	Donor Ages	Donor Sex	Date of negative Mycoplasma test	Experiment(s)	Figures
Myeloma Cell Line	INA-6	80	m	09.02.22	All	All
	U266			10.10.22	- Validation of V-Well Adhesion Assay	S1E
	MM1.S			24.02.22		
hMSC	1639	49	m	not tested	- Validation of V-Well Adhesion Assay - Time-lapse: INA-6 on dispersed hMSC	S1E 1D; 2[A-E]
	1571	72	m	not tested	- Saturation of hMSCs	1[A-B]
	1573	47	m	not tested		
	1578	82	m	not tested		
	1842	63	m	not tested	- INA-6 Viability dependent on time and hMSC adhesion surface (INA not washed off)	1E right
	1843	60	m	not tested		
	1537	77	f	not tested		
	1794	82	m	not tested	- INA-6 Viability dependent on time and hMSC adhesion surface (INA washed off)	1[C, E left]
	1779	61	m	not tested		
	1849	69	m	not tested		
	1854	80	f	not tested	- Time-lapse: INA-6 on dispersed hMSC	1D; 2[A-E]
	1605	71	f	not tested		
	1650	57	m	not tested		
	1859	64	f	not tested	- Time-lapse: INA-6 on confluent hMSC	2[G-I]
	1863	79	f	not tested		
	1861	52	f	not tested		
	1818	81	f	not tested	- Cell Cycle Profiling after V-well assay	3C
	1824	82	f	not tested	(Donor measured twice, different passages) - V-well adhesion assay of mitotically blocked INA-6 followed by Cell Cycle Profiling after V-well assay - V-well adhesion assay of mitotically blocked INA-6 followed by Cell Cycle Profiling after V-well assay	3[B,C]
	1827	56	m	not tested		

continued on next page

Appendix A Table 1 – continued from previous page

hMSC	1501	59	m	not tested	- INA-6 AI-assisted count during WPSC (INA-6 stained with celltracker green)	4B
	1643	75	f	not tested		
	1718	67	m	not tested		
	1720	58	m	not tested		
	1653	65	m	not tested		
	1591	78	m	not tested	- WPSC (MACS) followed by RNaseq, Metascape analysis, and qPCR validation	4[A,C,D,E]; 5[A-C]
					- WPSC (Wash) followed by qPCR-Validation and Luminescent Viability assays	4[C-E], 4F
	1654	74	m	not tested	- WPSC (MACS) followed by RNaseq, Metascape analysis, and qPCR validation	4[A,C,D,E]; 5[A-C]
					- WPSC (Wash) followed by qPCR-Validation and Luminescent Viability assays	4[C-E], 4F
	1655	78	f	not tested	- WPSC (MACS) followed by RNaseq, Metascape analysis, and qPCR validation	4[A,C,D,E]; 5[A-C]
	1668	80	f	not tested		
	1670	66	f	not tested		
	1701	81	m	not tested	- WPSC (Wash) followed by qPCR-Validation and Luminescent Viability assays	4[C-E], 4F
	1702	79	f	not tested		
	1600	77	m	not tested		
	1681	56	m	not tested	- WPSC (Wash) followed by Luminescent Viability assays	4F
	1672	65	m	not tested	- WPSC (Wash) followed by qPCR-Validation	4[C-E]

Appendix A Table 2: Adhesion genes (from Figure 6A) categorized by a continuous downregulation across disease progression. Bone Marrow Plasma Cell (BMPC), Monoclonal Gammopathy of Undetermined Significance (MGUS), Smoldering Multiple Myeloma (sMM), Multiple Myeloma (MM), Multiple Myeloma Relapse (MMR). p-adj. = adjusted p-values (Benj.-Hoch.).

Regulation during disease progression	Gene	Ensemble ID	Progression Free / Overall Survival	Better Prognosis with high/low expression	Association of expression with survival	
					[p-unc]	[p-adj]
False	ADAMTS1	ENSG00000154734	Prog. Free	low	0.031875	0.084719
			Overall	low	0.048755	0.120104
	ADAMTS2	ENSG0000087116	Prog. Free	high	0.63795	0.767059
			Overall	high	0.811174	0.890528
	BGN	ENSG00000182492	Prog. Free	high	0.38065	0.533967
			Overall	high	0.279004	0.426961
	CAVIN1	ENSG00000177469	Prog. Free	high	0.407479	0.548739
			Overall	high	0.210903	0.3492
	CCDC80	ENSG0000091986	Prog. Free	high	0.002038	0.015833
			Overall	high	0.023743	0.077356
	CCN1	ENSG00000142871	Prog. Free	high	0.285568	0.443729
			Overall	low	0.931563	0.961309
	CCN2	ENSG00000118523	Prog. Free	high	0.030562	0.083425
			Overall	high	0.002889	0.024263
	CCNE2	ENSG00000175305	Prog. Free	low	0.012138	0.046195
			Overall	low	0.000534	0.008638
	CDH11	ENSG00000140937	Prog. Free	high	0.413948	0.550115
			Overall	high	0.044627	0.117163
	CEMIP	ENSG00000103888	Prog. Free	high	0.798984	0.877146
			Overall	low	0.287022	0.428378
	COL12A1	ENSG00000111799	Prog. Free	high	0.340978	0.491983
			Overall	low	0.829338	0.900679
	COL16A1	ENSG0000084636	Prog. Free	low	0.281112	0.443629
			Overall	low	0.162895	0.293792
	COL4A1	ENSG00000187498	Prog. Free	high	0.040286	0.098969
			Overall	high	0.009472	0.039863
	COL4A2	ENSG00000134871	Prog. Free	high	0.0124	0.046195
			Overall	high	0.175895	0.3063
	COL5A1	ENSG00000130635	Prog. Free	high	0.368403	0.524066
			Overall	low	0.860512	0.914414
	COL6A3	ENSG00000163359	Prog. Free	low	0.103315	0.208697
			Overall	low	0.197836	0.336625
	COL8A1	ENSG00000144810	Prog. Free	high	0.680745	0.807636
			Overall	high	0.289334	0.428378
	CREB3L1	ENSG00000157613	Prog. Free	low	0.165978	0.310441
			Overall	low	0.047989	0.120104
	EDIL3	ENSG00000164176	Prog. Free	high	0.863476	0.899083
			Overall	low	0.496663	0.611744
	F3	ENSG00000117525	Prog. Free	high	0.091858	0.197397
			Overall	high	0.009177	0.039863
	FBN1	ENSG00000166147	Prog. Free	high	0.472247	0.603376
			Overall	low	0.401546	0.533633
	FLNC	ENSG00000128591	Prog. Free	high	0.18539	0.329735
			Overall	low	0.474071	0.598515
	FN1	ENSG00000115414	Prog. Free	high	0.843432	0.896701
			Overall	low	0.421268	0.552573
	FBN1	ENSG00000166147	Prog. Free	high	0.472247	0.603376
			Overall	low	0.401546	0.533633
	FLNC	ENSG00000128591	Prog. Free	high	0.18539	0.329735
			Overall	low	0.474071	0.598515
	FN1	ENSG00000115414	Prog. Free	high	0.843432	0.896701

continued on next page

Appendix A Table 2 – continued from previous page

False			Overall	low	0.421268	0.552573
	FOSB	ENSG00000125740	Prog. Free	low	0.585138	0.712035
			Overall	high	0.942273	0.961309
	GJA1	ENSG00000152661	Prog. Free	high	0.333512	0.491983
			Overall	low	0.34262	0.467631
	GREM1	ENSG00000166923	Prog. Free	high	0.457976	0.59302
			Overall	low	0.591104	0.685623
	HBEGF	ENSG00000113070	Prog. Free	low	0.145103	0.281656
			Overall	low	0.051592	0.124067
	HTRA1	ENSG00000166033	Prog. Free	high	0.01203	0.046195
			Overall	high	0.040407	0.116603
	IGFBP3	ENSG00000146674	Prog. Free	high	0.248011	0.410641
			Overall	low	0.841566	0.904236
	IGFBP7	ENSG00000163453	Prog. Free	low	0.009533	0.043766
			Overall	low	0.024942	0.078722
	ITGA11	ENSG00000137809	Prog. Free	high	0.97438	0.97438
			Overall	low	0.966513	0.976178
	KLF11	ENSG00000172059	Prog. Free	low	0.229416	0.39273
			Overall	low	0.060892	0.133697
	LAMB1	ENSG00000091136	Prog. Free	high	0.477921	0.603376
			Overall	high	0.604163	0.685623
	LOX	ENSG00000113083	Prog. Free	low	0.748901	0.840433
			Overall	low	0.035028	0.104055
	MMP2	ENSG00000087245	Prog. Free	high	2.29E-05	0.002316
			Overall	high	0.044615	0.117163
	NFKBIZ	ENSG00000144802	Prog. Free	high	0.725256	0.832396
			Overall	high	0.310216	0.441293
	NR4A1	ENSG00000123358	Prog. Free	high	0.0214	0.065497
			Overall	high	0.060042	0.133697
	NR4A2	ENSG00000153234	Prog. Free	high	0.275313	0.441375
			Overall	high	0.11176	0.217072
	OSMR	ENSG00000145623	Prog. Free	high	0.000567	0.007153
			Overall	high	0.01287	0.046422
	PDGFRB	ENSG00000113721	Prog. Free	high	0.691005	0.807636
			Overall	high	0.599357	0.685623
	POSTN	ENSG00000133110	Prog. Free	low	0.858041	0.899083
			Overall	low	0.496348	0.611744
	PTX3	ENSG00000163661	Prog. Free	high	0.020943	0.065497
			Overall	high	0.045241	0.117163
	PXDN	ENSG00000130508	Prog. Free	low	0.403966	0.548739
			Overall	low	0.172495	0.305648
	SERPINE1	ENSG00000106366	Prog. Free	low	0.543711	0.669693
			Overall	high	0.869146	0.914414
	SERPINH1	ENSG00000149257	Prog. Free	low	0.001825	0.015833
			Overall	low	0.004399	0.026138
	SIX1	ENSG00000126778	Prog. Free	high	0.784446	0.870649
			Overall	high	0.592089	0.685623
	SMAD3	ENSG00000166949	Prog. Free	low	0.027411	0.0791
			Overall	low	0.016437	0.055338
	SPARC	ENSG00000113140	Prog. Free	high	0.073989	0.162455
			Overall	high	0.244069	0.391285
	SPOCK1	ENSG00000152377	Prog. Free	low	0.531524	0.662765
			Overall	low	0.303273	0.437579
	SULF1	ENSG00000137573	Prog. Free	high	0.190403	0.331564
			Overall	high	0.388706	0.523458
	THBS2	ENSG00000186340	Prog. Free	low	0.318676	0.480392
			Overall	high	0.292654	0.428378
	VPS37B	ENSG00000139722	Prog. Free	low	0.1478	0.281656
			Overall	low	0.199975	0.336625

continued on next page

Appendix A Table 2 – continued from previous page

True	ACTN1	ENSG0000072110	Prog. Free	high	0.170661	0.313396
			Overall	high	0.007728	0.035478
ADAM12		ENSG00000148848	Prog. Free	high	0.019179	0.062487
			Overall	high	0.081847	0.168704
AEBP1		ENSG00000106624	Prog. Free	high	0.010829	0.046195
			Overall	high	0.057228	0.133697
AXL		ENSG00000167601	Prog. Free	high	0.001496	0.015105
			Overall	high	3.64E-05	0.00184
CD99		ENSG00000002586	Prog. Free	low	0.916833	0.941333
			Overall	low	0.083964	0.169607
COL1A1		ENSG00000108821	Prog. Free	high	0.000303	0.004367
			Overall	high	0.000593	0.008638
COL1A2		ENSG00000164692	Prog. Free	high	0.298023	0.456066
			Overall	high	0.566636	0.673297
COL3A1		ENSG00000168542	Prog. Free	high	0.025985	0.07719
			Overall	high	0.010794	0.042917
COL5A2		ENSG00000204262	Prog. Free	low	0.74501	0.840433
			Overall	low	0.99967	0.99967
COL6A1		ENSG00000142156	Prog. Free	high	0.011972	0.046195
			Overall	high	0.011048	0.042917
COL6A2		ENSG00000142173	Prog. Free	high	0.261528	0.426037
			Overall	high	0.3235	0.447582
CXCL12		ENSG00000107562	Prog. Free	high	0.000116	0.002927
			Overall	high	0.000648	0.008638
CXCL8		ENSG00000169429	Prog. Free	low	0.839416	0.896701
			Overall	high	0.224913	0.366391
CYP1B1		ENSG00000138061	Prog. Free	high	0.008641	0.041735
			Overall	high	0.000684	0.008638
DCN		ENSG0000011465	Prog. Free	high	0.004827	0.030473
			Overall	high	0.000247	0.008327
DUSP1		ENSG00000120129	Prog. Free	high	0.695686	0.807636
			Overall	high	0.454061	0.583718
FBLN1		ENSG0000077942	Prog. Free	high	0.002676	0.019305
			Overall	high	0.003734	0.026138
GNB3		ENSG00000111664	Prog. Free	high	0.003748	0.025234
			Overall	high	0.005734	0.03048
GSTP1		ENSG0000084207	Prog. Free	high	0.972219	0.97438
			Overall	low	0.668091	0.749746
IGFBP4		ENSG00000141753	Prog. Free	high	0.008677	0.041735
			Overall	high	0.007089	0.034093
IL1R1		ENSG00000115594	Prog. Free	high	0.126318	0.250159
			Overall	high	0.256501	0.398563
ITGA5		ENSG00000161638	Prog. Free	high	0.094893	0.19967
			Overall	high	0.159113	0.29219
ITGAX		ENSG00000140678	Prog. Free	high	0.006717	0.036021
			Overall	high	0.003123	0.024263
ITGB5		ENSG0000082781	Prog. Free	low	0.436018	0.57192
			Overall	high	0.539497	0.648681
LAMA4		ENSG00000112769	Prog. Free	high	0.018518	0.062345
			Overall	high	0.104178	0.206314
LAMB2		ENSG00000172037	Prog. Free	high	0.015472	0.053885
			Overall	high	0.001354	0.013865
LOXL2		ENSG00000134013	Prog. Free	high	0.808671	0.878235
			Overall	low	0.933264	0.961309
LRP1		ENSG00000123384	Prog. Free	high	0.006458	0.036021
			Overall	high	0.000434	0.008638
LTBP2		ENSG00000119681	Prog. Free	high	9.03E-05	0.002927
			Overall	high	0.011656	0.043603
LUM		ENSG00000139329	Prog. Free	high	0.05158	0.118399
			Overall	high	0.065084	0.139862

continued on next page

Appendix A Table 2 – continued from previous page

True	MAP3K8	ENSG00000107968	Prog. Free	high	0.000958	0.010755
		Overall	high	0.01617	0.055338	
	MAP4K4	ENSG0000071054	Prog. Free	high	0.041155	0.098969
			Overall	high	0.31743	0.445284
	MFAP5	ENSG00000197614	Prog. Free	high	0.000243	0.004094
			Overall	high	0.004269	0.026138
	MMP14	ENSG00000157227	Prog. Free	high	6.93E-05	0.002927
			Overall	high	0.006691	0.033787
	MXRA5	ENSG00000101825	Prog. Free	high	0.034865	0.088035
			Overall	high	0.033819	0.103505
	MYL9	ENSG00000101335	Prog. Free	high	0.000146	0.00295
			Overall	high	1.56E-05	0.001572
	NRP1	ENSG00000099250	Prog. Free	high	0.001888	0.015833
			Overall	high	0.002212	0.020312
	PAPLN	ENSG00000100767	Prog. Free	high	0.034256	0.088035
			Overall	high	0.159113	0.29219
	TEX14	ENSG00000121101	Prog. Free	high	0.237488	0.399771
			Overall	low	0.518581	0.631044
	TGFBI	ENSG00000120708	Prog. Free	high	0.102621	0.208697
			Overall	high	0.004299	0.026138
	TGM2	ENSG00000198959	Prog. Free	high	0.058634	0.131601
			Overall	high	0.119621	0.227958
	THBS1	ENSG00000137801	Prog. Free	high	0.39286	0.543545
			Overall	high	0.456572	0.583718
	TNC	ENSG00000041982	Prog. Free	high	0.012806	0.046195
			Overall	high	0.004752	0.026663
	TNS1	ENSG00000079308	Prog. Free	high	0.338737	0.491983
			Overall	high	0.757617	0.840872
	TPM1	ENSG00000140416	Prog. Free	high	0.029263	0.0821
			Overall	high	0.001373	0.013865
	TUBA1A	ENSG00000167552	Prog. Free	low	0.006776	0.036021
			Overall	low	0.042929	0.117163
	TUBB6	ENSG00000176014	Prog. Free	low	0.186088	0.329735
			Overall	low	0.060071	0.133697
	VCAN	ENSG0000038427	Prog. Free	high	0.042782	0.100487
			Overall	high	0.080757	0.168704
	ZFP36L1	ENSG00000185650	Prog. Free	high	0.922693	0.941333
			Overall	high	0.24957	0.393852

Appendix A Table 3: List of primers. Some primers required a melting step to be performed before fluorescent readout to remove byproducts.

Primer	Sequence 5' - 3'	base pairs [bp]	annealing temp. [°C]
36B4_s	tgcattcgtacccattctatcat	122	60
36B4_as	aggcagatggatcagccaaga		
BCL6_s	tagagcccataaaacggtcctcat	221	55 + Melting Step at 77 °C
BCL6_as	cgc当地attgagccgagatgtgt		
BMP4_s	tacatgcggatcttaccg	132	58
BMP4_as	atgttcttcgtggtggaagc		
BTG2_s	gtattcttgttaggccgacactaa	264	60 + Melting Step at 78 °C
BTG2_as	tcttaaggtattcggtttggaa		
CXCL8_s	actgagagtgattgagagtggacc	251	55 + Melting Step at 77 °C
CXCL8_as	ccctacaacagacccacacaatac		
CXCL12_s	gattctcgaaagccatgttgcga	119	56
CXCL12_as	caatgcacacttgtctgttgttgc		
DCN_s	caacaacaagcttaccagagtacct	160	57
DCN_as	tgaaaagactcacacccgaaataaga		
DKK1_s	gcactgatgagtaactgcgcgttag	129	56
DKK1_as	ttttgcagtaattcccgcccc		
IL10RB_s	gagtgaggctgtctgtgagcaa	139	55
IL10RB_as	cttgc当地aacgcaccacagcaag		
IL24_s	caaacagttggacgtagaagcagc	149	55
IL24_as	tgaaatgacacagggaaacaaacca		
LOX_s	ctgctc当地agattccccaaag	125	57
LOX_as	tggcatcaagcaggctcatag		
MMP2_s	ttgtatgtatggcatgcgtcaga	155	56
MMP2_as	cgtataccgc当地atctttccg		
MMP14_s	cgacaagattgatgctgctc	140	57
MMP14_as	tccctccc当地agactttgatg		
MUC1_s	gcagccctctcgatataacctg	200	58
MUC1_as	gtaggtaggggtactcgctca		
NOTCH2_s	gtgc当地gttgaacacttgtgcc	185	55
NOTCH2_as	cactcgcatctgtatccaccaatg		
OPG_s	no sequence available (Proprietary primers from Qiagen: QT00014294 TNFRSF11B_1_SG)		60
OPG_as			
PRICKLE1_s	cagaggtaatacatgaaggacggc	102	56
PRICKLE1_as	gtccacaccaataatgttccccac		
TGM2_s	caacccttctcatcgagtaattccg	100	58
TGM2_as	tcatccacgactccacccag		
TNFRSF1A_s	ctc当地ttcaccgcttc当地aaaaacc	153	55
TNFRSF1A_as	ttcactccaataatgccc当地tactg		
TRAF5_s	tgc当地ctgttagataaagaggctcatca	177	56
TRAF5_as	aacactgc当地acaggtt当地gaaataagc		

A.3 Materials & Methods

Isolation and Culturing of Primary Human Bone Marrow-Derived Mesenchymal Stromal Cells

Primary human Mesenchymal Stromal Cells (MSCs) were obtained from the femoral head of patients (Appendix A: Table 1) undergoing elective hip arthroplasty. Material was collected with written informed consent of all patients and the procedure was approved by the local Ethics Committee of the University of Würzburg (186/18). In brief, bone marrow was washed with MSC-medium (Dulbecco's modified Eagle's medium (DMEM/F12, Thermo Fisher Scientific, Darmstadt, Germany) supplemented with 10 % Fetal Calf Serum (FCS, Bio&Sell GmbH, Feucht, Germany, Fernandez-Rebollo et al. (2017)), 100 U/ml penicillin, 0.1 mg/ml streptomycin (Thermo Fisher Scientific), 50 µg/ml ascorbate and 100 nmol/l sodium selenite (both Sigma-Aldrich GmbH, Munich, Germany)) and centrifuged at 250 g for 5 min. The pellet was washed four times with MSC-medium and resulting supernatants containing released cells were collected. Cells were pelleted and cultured at a density of 1×10^9 cells per 175 cm² culture flask. After two days non-attached cells were washed away and adherent ones were cultivated in MSC-medium until confluence. Then, they were either frozen in liquid nitrogen or directly utilized for experiments. hMSC cultures were sustained for a maximum of two passages. All cells were cultured at 37 °C and at 5 % CO₂.

Culturing of Myeloma Cell Lines

The plasmacytoma cell line INA-6 [[RRID:CVCL_5209](#); DSMZ, Braunschweig, Germany, authenticated by DSMZ in 2014 (Burger, Guenther, et al., 2001; Gramatzki et al., 1994)] was cultivated in RPMI1640 medium (Thermo Fisher Scientific) supplemented with 20 % (v/v) FCS, 100 µg/ml gentamicin, 2 mmol/l L-glutamine (both Thermo Fisher Scientific), 1 mmol/l sodium pyruvate, 100 nmol/l sodium selenite (both Sigma Aldrich GmbH) and 2 ng/ml recombinant human interleukin-6 (IL-6; Miltenyi Biotec, Bergisch Gladbach, Germany). INA-6 were passaged three times per week by diluting them to 1×10^5 cells/ml, 2×10^5 cells/ml, or 4×10^5 cells/ml for 3, 2, and 1 days of culturing, respectively. MM.1S [[RRID:CVCL_8792](#)] (Greenstein et al., 2003), and U266 cells [[CVCL_0566](#)] (Nilsson et al., 1970) were propagated and cultivated in RPMI1640 medium comprising 10 % (v/v) FCS, 100 U/ml penicillin, 100 µg/ml streptomycin, 2 mmol/l L-glutamine, and 1 mmol/l sodium pyruvate. All cells were cultured at 37 °C and at 5 % CO₂.

Co-Culturing of Primary hMSCs and INA-6 and MSC-Conditioning of Medium

For each co-culture, hMSCs were seeded out 24 h prior to INA-6 addition to generate MSC-conditioned medium (CM). CM from different donors was collected separately and used immediately when adding INA-6. To ensure that CM was free of hMSCs, it was strained (40 µm)

and centrifuged for 15 min at 250 g. INA-6 cells were washed with PBS (5 min, 1200 rpm), re-suspended in MSC-medium and added to hMSCs such that co-culture comprised 33 % (v/v) of CM gathered directly from the respective hMSC-donor. Co-cultures did not contain IL-6 (Chatterjee et al., 2002).

Collagen I Coating

Collagen I solution (isolated from rat tail, Corning, NY, USA) was diluted 1:2 (75 ng/mL) in acetic acid (0.02 N), applied to 96-well plates (30 μ L in each well) and incubated for 2 h at room temperature. Acetic acid was removed and wells were washed once with 100 μ L of PBS. Coated plates were stored dry at 4 °C.

Fluorescent Staining of Cells

For each live staining, cells were strained (70 μ m) to remove clumps and washed (5 min, 250 g) once with the respective media (without FCS) and then resuspended in staining reagents. For *CellTracker™Green CMFDA Dye* and *CellTracker™Deep Red Dye* (Thermo Fisher Scientific) staining, 1 mL staining solution for a maximum of 1×10^6 cells was prepared. Staining was done at room temperature (RT) for 15 min using 5 μ M CMFDA (5-Chlormethyl-fluoresceindiacetat) and 5 min of 1–2 μ M DeepRed. To reduce background, stained cells were pelleted, resuspended in cell medium (containing FCS), incubated for 30 min (37 °C, 5 % CO₂), washed in cell medium, resuspended in 100–1000 μ L and counted.

For PKH26 staining (Sigma Aldrich GmbH), a maximum of 1×10^4 cells was resuspended in 500 μ L diluent C before swiftly adding 500 μ L of staining solution (1 μ L diluted in 500 μ L diluent C) and incubating cells for 5 min at RT. The staining reaction was stopped by adding 1 mL of FCS-containing medium and adding 3 mL of FCS-free medium. Cells were washed with 10 mL of FCS-containing medium, resuspended in 100–1000 μ L cell medium, and counted.

For Calcein-AM (Calcein-O,O -diacetat-tetrakis-(acetoxymethyl)-ester) (Thermo Fisher Scientific) staining, end concentrations of 0.5 μ M were used. 12.5 μ L of diluted stock solution (2.5 μ M) was carefully added to 50 μ L of the co-culture and incubated for 10 min at 37 °C.

For Hoechst 33342 staining, cells were washed once with PBS, resuspended in a maximum of 500 μ L of PBS, and fixed with 5 mL of ice-cold ethanol (70 % v/v) by vigorously pipetting up and down to dissociate aggregates. Cells were washed once with PBS and stained with 2.5 μ g/mL Hoechst 33342 (Thermo Fisher Scientific) diluted in PBS for 1 hour at 37 °C.

Automated Fluorescence Microscopy

To remove clumps for microscopic applications, we cultured cells in 40 μ m strained medium containing FCS. To reduce background fluorescence and phototoxicity, we used phenol-red free versions of the respective medium, if available.

All microscopy equipment was acquired from ZEISS. The microscope was an *Axio Observer 7* with confocal *ApoTome.2* equipped with a motorized reflector revolver and motorized scanning table (130×100 mm). The microscope was mounted on an Antivibrations-Set (Axio Observer (D)) with two antivibration carrier plates, each equipped with two vibration dampening feet. The light source was a *microLED 2* for transmission light and (for fluorescence) *Colibri 7* (R[G/Y]B-UV) for five channels of incident light (385 nm, 475 nm, 555 nm, 590 nm and 630 nm). For excitation (EX) and emission (EM) light filtering and beam splitting (BS) we used the following reflectors: *96 HE BFP shift free* (E) (EX: 390 / 40 nm, BS: 420 nm, EM: 450 / 40 nm), *43 HE Cy 3 shift free* (E) (EX: 550 / 25 nm, BS: 570 nm, EM: 605 / 70 nm), *38 HE eGFP shift free* (E) (EX: 470 / 40 nm, BS: 495 nm, EM: 525 / 50 nm) and *90 HE LED* (E) (EX: 385 + 475 + 555 + 630 nm, BS: 405 + 493 + 575 + 653 nm, EM: 425/30 + 514/30 + 592/30 + 709/100 nm). We used the black and white camera *Axiocam 506 mono* (D) and if not stated otherwise, 2×2 binning was used for fluorescence imaging. For mosaic acquisitions (“tiles”) we used a tiling overlap of 8–10 % and image tiles were not stitched. Images were magnified 5x and 10x (*Fluar 5x/0.25 M27* and *EC Plan-Neofluar 10x/0.3 Ph1 M27*).

Cell Viability and Apoptosis Assay

To examine cell viability and apoptosis, cells were seeded in a 96-well plate (1×10^4 cells per well) to be measured inside culture wells after respective incubation time immediately. ATP-amount and Caspase 3/7 activity were used as a proxy for viability and apoptosis rates, respectively. They were assessed using the *CellTiter-Glo Luminescent Cell Viability Assay* and the *Caspase-Glo 3/7 Assay*, respectively (Promega GmbH, Mannheim, Germany), according to the manufacturer’s instructions. Luminescence was measured with an Orion II Luminometer (Berthold Detection Systems, Pforzheim, Germany).

Microscopic Characterization of hMSC Saturation

For saturating hMSC with INA-6, hMSCs were stained with *CellTracker Green*, plated out on 384-well plates (Greiner Bio-One GmbH, Frickenhausen, Germany) at 5×10^3 hMSC/cm² and cultured for 24 h. INA-6 cells were stained with *CellTracker DeepRed*, resuspended in MSC-medium, added to adhering hMSCs in different amounts (5×10^3 INA6/cm², 1×10^3 INA6/cm², 2×10^3 INA6/cm²) and co-cultured for 24 h and 48 h. The complete co-culture was scanned and the number of INA-6 cells adhering to one hMSC was counted manually for 100 MSCs for each technical replicate. Fluorescent images were digitally re-stained (INA-6 green, hMSC inverse black).

Analysis of INA-6 Survival and Aggregation Depending on hMSC Confluence

To describe aggregate growth and survival of INA-6 depending on hMSC density, unstained hMSCs were seeded out into 96-well plates (white, clear bottom, Greiner) at different densities (see Seeding Table). To ensure nutrient supply, we used lower cell densities for longer co-culturing durations while maintaining constant ratios of INA-6 to adhesion surface provided by hMSCs. Those plates that were to be assessed after 72 h of co-culturing received an additional 100 µL of fresh MSC-medium after 24 h of co-culturing (total volume of 300 µL), and after 48 h of co-culturing, 100 µL was gently removed from the co-culture and carefully replaced with fresh MSC-medium without disturbing the co-culture on the bottom.

To describe aggregate growth, complete wells were scanned using 10x magnification, phase contrast, 2 × 2 binning, and autofocus focusing on each tile both before and after harvesting. Afterwards, INA-6 cells were harvested for measuring viability and apoptosis.

Seeding Table: Seeding densities for describing growth and survival of INA-6 depending on hMSC density.

Co-cult. dur.: Co culturing duration; MSC-adh. surface: adhesion surface provided by hMSCs; vol.: volume.

Co-cult. dur. [h]	hMSC density [1000 hMSC/cm ²]	INA-6 density [1000 INA6/cm ²]	Ratios INA : MSC (adh. surface)	Seeding vol. [µL]	End vol. [µL]
24	2, 10, 40	10	1:0.2, 1:1, 1:confluent	200	200
48	1, 5, 40	5	1:0.2, 1:1, 1:confluent	200	200
72	1, 5, 40	5	1:0.2, 1:1, 1:confluent	200	300 [after 24 h: +100], [after 48 h: exchange 100]

For luminescent assessment of cell survival, INA-6 cells were harvested by removing co-culture medium, adding 150 µL of MSC-medium, and then stirred by strongly pipetting up and down twice while aiming the pipette tip at the upper corner, lower left, and lower right of the well bottom ('Mercedes star'). Washing and stirring was repeated once before washing wells again with 150 µL MSC-medium. Harvested INA-6 cells were strained (40 µm filter), pelleted, and resuspended in 200 µL MSC-medium. Cells were counted using Neubauer chambers, re-distributed into 96-well plates (white, clear bottom) with 1×10^5 INA-6 cells per well, and then subjected to viability and apoptosis assays.

To minimize the loss of sensitive apoptotic cells, another approach was used to measure viability and apoptosis without harvesting INA-6 cells. hMSCs and INA-6 were seeded out individually in parallel to the co-cultures. Prior to measuring viability and apoptosis, culture volume was adjusted to 150 µL by removing 50 µL or 150 µL for the timepoints 48 h or 72 h, respectively (carefully not to stir up culture on bottom). 100 µL of luminescent reagents were then added directly to 150 µL of co-culture. The fold change of viability or apoptosis that is due to MSC interaction ($FC_{MSC\ interaction}$) was then calculated using the following formula, with L being the

mean of four technical replicates measured in relative luminescent units per seconds [RLU/s], and $L_{\text{Co Culture}}$, L_{MSC} , L_{INA6} the luminescence measured in the co-culture, hMSCs alone, and INA-6 alone, respectively.

$$FC_{\text{MSC Interaction}} = \frac{L_{\text{Co Culture}}}{L_{\text{MSC}} + L_{\text{INA-6}}}$$

Time-Lapse Characterization of INA-6 Aggregation, Detachment and Division

In order to record the aggregation and detachment of INA-6 in contact with hMSCs, hMSCs (5×10^3 cells/cm 2) were fluorescently stained with PKH26 and plated onto 8-well μ -Slides (ibidi, Gräfelfing, Germany). hMSCs were incubated for 24 h before being placed into an ibidi Stage Top Incubation System and were equilibrated to the incubation system for a minimum of 3 h (80 % humidity and 5 % CO₂). INA-6 cells (2×10^4 cells/cm 2) were washed and resuspended in 33 % (v/v) MSC-conditioned medium before adding them directly before acquisition start in a small volume (10 μ L). Brightfield and fluorescence images of 13 mm 2 of co-culture were acquired every 15 minutes for 63 h. Movement speed of the motorized table was adjusted to the lowest setting that allows acquisition of the complete region within 15 minutes.

Respective events of interest were analyzed manually and categorized into defined event parameters. Events were binned across the time axis using these boundaries: [0.0, 12.85, 25.7, 38.55, 51.4, 64.25]. We collected a minimum of events per recording and analysis so that each time bin contained at least 5 values, except when analyzing detachment events, since these did not appear before 20 h of incubation for some replicates. For each recording and event parameter, the event count was normalized by dividing by the total number of events per time bin.

We determined the frequency and the cause of aggregation by looking for two interacting INA-6 cells and went backward in time to see if they were two daughter cells or if two independent INA-6 cells had collided. We determined the frequency of aggregates with detaching cells by tracing their growth across the complete time-lapse and looking for detachment events. We picked random 100 aggregates by including aggregates from both the border and center of the well.

We characterized detachment events by noting multiple parameters manually: Time point of detachment, aggregate size (at the time of detachment), the last interaction partner, and the number of detaching INA-6 cells.

For characterizing cell division events, we recorded a new set of time-lapse videos using unstained hMSCs that were grown to confluence for 24 h (4×10^4 hMSCs/cm 2) to provide for unlimited adhesion surface. We categorized daughter cells in terms of their mobility (mobility being the speed of putative movements or “rolling”). The mobility criteria were met if one INA-6 daughter cell moved farther than half a cell radius within one frame (15 min) relative to the MSC-adherent INA-6 cell which was required to stand still in-between respective frames. We measured the “rolling” duration by subtracting the time point of the last perceived movement from the time

point of division. We excluded those division events from the measurement of rolling duration if INA-6 cells underwent apoptosis shortly after division.

Cell Cycle Synchronization at M-Phase

INA-6 cells were arrested at mitosis by double thymidine (2 mM) treatments followed by 5 h of nocodazole (500 ng/mL) incubation. In detail: 3×10^5 cells/mL INA-6 in 4 mL were treated with 2 mM thymidine (Sigma Aldrich GmbH) for 16.5 h. Cells were released by washing them in INA-6 medium once and allowed to cycle for 9 h before treating them with 2 mM thymidine for 18 h a second time. Afterwards, cells were released and allowed to cycle for 2 h before treating them with 100 ng/mL nocodazole (Sigma Aldrich GmbH) for 5 h. Arrested INA-6 were released by washing them once and resuspending them in MSC-medium with 33 % MSC-conditioned medium. Cell cycle profile was checked using image cytometry (Appendix A: Figure 2).

V-Well Adhesion Assay

This assay was modified from (Weetall et al., 2001). 96 v-well plates were coated with collagen I (rat tail, Corning). Collagen coating ensures that confluent hMSCs withstand centrifugation even after hMSCs in the well tip were removed. hMSCs (4×10^4 cells/cm²) were seeded out and grown to confluence for 24 h in collagen-coated v-well plates. To ensure that only INA-6 are pelleted in the v-well tip, hMSCs were removed from the well-tip by touching the well-ground with a 10 µL pipette and roughly pipetting hMSCs away.

Arrested INA-6 (1×10^4 cells/cm²) were released by washing them once in PBS and resuspending them in 33 % (v/v) MSC-conditioned medium before adding them on top of confluent hMSCs. INA-6 adhered for 1, 2, 3, and 24 h before the complete co-culture was stained with 0.5 µM Calcein-AM (10 min at 37 °C). Non-adherent INA-6 were pelleted by centrifugation using a Hettich 1460 rotor ($r = 124$ mm) at 2000 rpm (555 g) for 10 min.

The well tip was imaged by fluorescence microscopy with 5x magnification, 96 HE emission filter, autofocus configured for maximum signal intensity, 2 × 2 binning and 14 bit grayscale depth. Pellet brightness was analyzed in ZEN 2.6 (Zeiss) by summing up pixel brightnesses across the complete pellet image. Background brightness was acquired from a cell culture with only hMSCs. Reference brightness was acquired from a cell culture with only INA-6, defining 100 % pellet brightness without adhesion. Background intensity was subtracted before normalizing by reference. Outliers were removed from technical replicates ($n = 4$) if their z-score was larger than 1.5σ technical variation.

After measuring pellet brightnesses, the cell pellet was removed by pipetting 10 µL from the well tip. Pellets of the same technical replicates were pooled, washed in PBS, resuspended in 200 µL PBS, added to 1.8 mL ice-cold 70 % ethanol, and stored at -20 °C. Remaining non-MSC-adhering INA-6 cells were removed by replacing culture medium with 100 µL of medium.

MSC-adherent INA-6 were manually detached by rapid pipetting and equally pelleted, analyzed, and isolated.

Cell Cycle Profiling

INA-6 cells were fixed in 70 % ice-cold ethanol, washed, resuspended in PBS, distributed in 96-well plates, and stained with Hoechst 33342 (2.5 µg/mL in PBS) for 1 h at 37 °C. For image cytometric cell cycle profiling, plates were scanned completely using automated fluorescence microscopy with 5x magnification, 96 HE emission filter, 1 × 1 binning, 14 bit depth, and an illumination time that fills 70 % of the grayscale range. The autofocus was configured to re-adjust every second tile. A pre-trained convolutional neural network (“DeepFeatures 2 reduced”, *Intellessis*, Zeiss) was fine-tuned to segment scans into background, single nuclei, and fragmented nuclei. Nuclei were filtered to exclude fragmented nuclei and those nuclei with extreme size (within the range of 50–500 µm²) and roundness (within the range of 0.4–1.0). Cell cycle profiles were normalized by the mode of the nucleus intensities within the G0/G1 peak. To retrieve frequencies of cells cycling in G0/G1, S, and G2 phase, the brightness distribution of all single nuclei was fitted to the sum of three Gaussian curves (“Skewed Gaussian Model” for G0G1 and G2 phase, and “Rectangle Model” for S phase) using the python package LMFIT (Newville et al., 2014) (Appendix A: Figure 4). The Gaussian curves were used to calculate the cell frequencies for each cell cycle phase by integration using the composite trapezoidal rule implemented by numpy.trapz (Harris et al., 2020).

For validation of image cytometry, 5 mL of INA-6 stock culture was removed and ethanol fixed as described above. Flow cytometry analyses were performed using an *Attune Nxt Flow Cytometer* (Thermo Fisher Scientific). Data analyses were performed using FlowJo V10 software (TreeStar, USA).

Protocol: Well Plate Sandwich Centrifugation (WPSC)

96-well plates (flat bottom, clear) were coated with collagen I (rat tail, Corning) to ensure that confluent hMSCs withstand centrifugation and repeated washing. hMSCs (2×10^4 cells/cm²) were seeded out and grown to confluence for 72 hours in collagen-coated 96-well plates. To remove aggregates from the medium and prevent clogging of magnetic columns, any FCS-containing fluid was strained with a 40 µm cell strainer.

- **Collect MSC-Conditioned Medium and Add INA-6:**

1. Collect hMSC-conditioned medium (CM) from the well plates and replace it with 100 µL of fresh hMSC medium. Collect CM from different donors separately.
2. Strain CM (40 µm) and centrifuge for 15 minutes at 250 g to ensure that CM does not contain hMSCs.

3. Dilute CM by mixing 2 parts of CM with 1 part of MSC-medium (dilute 1.5 fold).
4. Count INA-6 cells and retrieve enough cells to fill all 96 wells with 2×10^4 INA6/cm² (6.8×10^4 cells per well, covering approximately 65 % of the well bottom).
5. Centrifuge INA-6 (5 minutes, 250 g) and resuspend them in a volume of diluted CM to reach a concentration of 6.8×10^5 INA6/mL.
6. Add 100 µL INA-6 suspension to hMSCs (end volume: 200 µL; end concentration: 33 % (v/v) hMSC-conditioned medium).
7. Incubate for 24 hours at 37 °C and 5 % CO₂.

- **Prepare CM-INA6 Reference:**

8. Add 100 µL of fresh MSC-medium into each well of an empty 96-well plate (not coated).
9. Add 100 µL of INA-6 suspension (6.8×10^5 INA-6/mL in diluted CM).
10. Incubate for 24 hours at 37 °C and 5 % CO₂.

- **Collect CM-INA6 and nMA-INA6:**

11. Pre-warm well plate centrifuge to 37 °C.
12. Prepare a counter-weight by filling 200 µL of water into all wells of an empty 96-well plate.
13. Prepare well-plate sandwiches:
 - a. Turn an empty 96-well plate (“catching plate”) upside down and place one on top of the co-culture-plate, the CM-INA6 reference plate, and the counter-weight so that all well openings align.
 - b. Fix well plates using tape with reusable adhesive (e.g., *Leukofix*).
14. Turn both plates around. Medium will spill from the co-culture plate into the catching plate.
15. Centrifuge plate for 40 seconds at 1000 rpm with the catching plate facing the ground.
16. Remove the adhesive tape and the co-culture plate.
17. Turn the co-culture plate around and add 30 µL of washing medium (MSC-medium 0% FCS, 3 mM EDTA) gently by touching the wall of each well and pressing the pipette slowly.
 - a. Work quickly to ensure that co-culture does not dry. We recommend using a multipette (Eppendorf).

- b. Many nMA-INA6 are removed by physical force applied by adding 30 μ L of medium and not just by centrifugation. Hence, it is critical to apply the same dispensing technique across all replicates. We recommend using a multipette (Eppendorf) that can apply 30 μ L with controllable pressure, since its push-button retains a long pushing path even for dispensing small volumes, unlike push-buttons from the usual 100 μ L pipettes that reduce the pushing-path for smaller volumes.
- c. Centrifugation minimizes technical variability by replacing one step of manual pipetting. Also, it ensures that confluent MSCs remain unharmed. Manual pipetting on the other hand would require touching the well-bottom to remove all fluids which damages the adhesive hMSC layer.
18. Turn the co-culture plate upside down, place it onto the catching plate and re-apply adhesive tape to fix the well plate sandwich.
 19. Repeat steps 14-18 two more times until the catching plate contains 290 μ L of medium in each well.
 20. Pool CM-INA6 from the catching plate that was fixed to the reference plate.
 21. Pool nMA-INA6 from the catching plate that was fixed to the co-culture plate.
 22. Collect remaining INA-6 by adding 100 μ L of PBS into each well of the catching plates, collect and pool with CM-INA6 or nMA-INA6.
 23. Strain CM-INA6 and nMA-INA6 using 40 μ m cell strainer.
 24. Isolate MA-INA6 by continuing with either accutase dissociation or rough pipetting.
- **Collect MA-INA6 by Accutase Dissociation Followed by MAC Sorting:**
25. Block 2 mL tubes with sorting buffer (PBS, 2 mM EDTA, 1% BSA) for 1 hour at 4 °C.
 26. Dilute accutase (Sigma Aldrich GmbH) (400 to 600 units/mL) 4-fold in cold PBS. Always keep accutase on ice, since accutase loses activity at room temperature.
 27. Add 50 μ L of cold accutase (directly after the last centrifugation step) and incubate co-culture plate for 5 minutes at 37 °C.
 28. Place a co-culture plate onto a shaker and shake for 1 minute at 300 rpm.
 29. Collect cell suspension from wells and stop the reaction by adding 500 μ L of FCS to pooled cell suspension.
 30. Evaluate presence of adherent INA-6 cells and the integrity of confluent hMSCs under the microscope.

31. Repeat steps 27-30 until all INA-6 cells have dissociated or until confluent hMSCs start to tear.
32. Strain cell suspension ($30\text{ }\mu\text{m}$). This yields MA-INA6.
33. Pellet MA-INA6, nMA-INA6, and CM-INA6 (1200 rpm, 10 minutes).
34. Resuspend MA-INA6 in $86\text{ }\mu\text{L}$ sorting buffer (PBS, 2 mM EDTA, 1 percent BSA).
35. Resuspend CM-INA6 and nMA-INA6 in $300\text{ }\mu\text{L}$ cold diluted accutase and incubate for 3 minutes at 37°C to ensure equal treatment for all samples.
36. Stop accutase by adding $200\text{ }\mu\text{L}$ of FCS (100 percent).
37. Pellet CM-INA6 and nMA-INA6 (1200 rpm, 10 minutes) and resuspend in $86\text{ }\mu\text{L}$ sorting buffer (PBS, 2 mM EDTA, 1 percent BSA).
38. Transfer samples into 2 mL tubes that were blocked with sorting buffer.
39. Add $10\text{ }\mu\text{L}$ of CD45 coated magnetic beads (Miltenyi Biotec B.V. & Co. KG, Bergisch Gladbach).
40. Place tubes into rotator and incubate for 15 minutes at 4°C .
41. Continue with MAC sorting according to the manual. Use an MS column and wash 3 times.
42. Improve purity of eluted MA-INA6 by straining eluate ($30\text{ }\mu\text{m}$) (wash strainer using 1 mL of sorting buffer) and applying it onto an MS column a second time. Wash three times.
43. Collect $20\text{ }\mu\text{L}$ per eluate and apply it onto a 96 well plate to evaluate purity.
 - a. Incubate plate for 24 hours.
 - b. Count the number of adherent cells (hMSCs) per INA-6 using phase contrast microscopy.
 - c. We reached a mean purity of $3.2 \times 10^{-4} (\pm 2.2 \times 10^{-4})$ hMSCs per MA-INA6.
 - d. hMSC contamination did not have an impact on RNAseq, since those genes that are highly expressed in hMSCs (VCAM1, ALPL, FGF5, FGFR2), did not appear as differentially expressed in MA-INA6 (data not shown). RNAseq detected 0.44 ± 0.16 CPM-normalized counts of VCAM1 transcripts in MA-INA6, however, it was excluded like all genes with less than 1 count in at least 2 of 5 replicates.
44. Count cells using a Neubauer chamber.
45. Pellet samples (250 g for 5 minutes).
46. Resuspend in respective medium or lysis buffer (e.g., RA1 for RNA extraction).

- **Collect MA-INA6 by Rough Pipetting (No MAC Sorting):**

47. After the last centrifugation step, add hMSC-medium to each well of the co-culture plate to reach a volume of 150 µL.
- a. Since the yield of MA-INA6 was large, we dissociated MA-INA6 cells from hMSCs by vigorous pipetting (for further samples after RNAseq, see Supplementary Table 1). Since no enzymatic digestion is used, we reckoned that there would be no need for MAC sorting. Confluent hMSCs withstand this procedure and don't dissociate as single cells, which can be removed by straining cells (30 µm). We reached similar purities as for MAC-sorting (data not shown).
48. Using a multi-channel pipette (100 µL), gently raise 90 µL into the tips.
49. Lean pipette tip on the upper well-border and roughly pipette up and down once.
50. Repeat step 48 at the lower right and lower left well border (Total of 3 pipetting steps “Mercedes Star”).
51. Attach a catching plate onto the co-culture and centrifuge for 40 seconds at 500 rpm (28 g).
52. Repeat steps 46-50 until a sufficient amount of MA-INA6 is removed.
53. Control purity of MA-INA6 by placing out aliquot onto an empty 96 well plate.
54. Collect MA-INA6 from catching plate.
55. Remove hMSCs by straining cell suspension (30 µm).
56. Count cells using a Neubauer chamber.
57. Pellet MA-INA6 (250 g for 5 minutes).
58. Resuspend in respective medium or lysis buffer.

Centrifugal Force: We used a Hettich 1460 rotor ($r = 124$ mm) (Hettich GmbH & Co. KG, Tuttlingen, Germany). For calculating the centrifugal force that acts onto the co-culture within well plate sandwiches, we subtracted the height of the catching plate (14.4 mm, Greiner 96-well plate) and the depth of each well (10.9 mm). This yields a radius of 98.7 mm, which translates to the following centrifugal forces: 500 rpm: 28 g; 1000 rpm: 110 g; 2000 rpm: 441 g.

Washing medium containing EDTA: Washing medium containing EDTA: EDTA removes calcium from integrins, which are required for adhesion. It is not strong enough to dissociate INA-6 from hMSCs, but could help with removing INA-6 from other INA-6. For generating samples for RNAseq, we added 3 mM of EDTA to the washing medium. For further samples, we did not add EDTA to the washing medium, since we found that it does not increase yield for all biological replicates consistently (data not shown). We suspect that integrin-mediated

adhesion depends on hMSC donor or internal variance of INA-6. We recommend using 3 mM of EDTA, however, this requires further optimizations like including an incubation time at 37 °C after the addition of washing medium to account for biological variance. However, this could take long incubation times of up to 60 minutes (Lai et al., 2022).

Track Cell Number During WPSC

To track the cell count during WPSC, INA-6 cells were stained with *CellTracker green*, and both co-culturing and catching plates were scanned after each centrifugation step. For each round of centrifugation, an empty catching plate was used. A pre-trained convolutional neural network (*Intellesis*, Zeiss) was fine-tuned to segment the scans into background, cells, and cell borders. Single cells were counted, and the cumulative sum for each catching plate was calculated.

Sub-Culturing After WPSC of MSC-Interacting INA-6 Subpopulations

After CM-INA6, nMA-INA6, and MA-INA6 were isolated, they were counted with a Neubauer chamber using all nine quadrants and diluted to 1×10^5 cells/mL in MSC-medium (10% FCS, no IL-6 except for control). 100 µL of cell suspension was applied to 96-well plates, incubated for 48 hours at 37 °C and 5 % CO₂, and then subjected to viability and apoptosis assays.

RNA Isolation

Total RNA was isolated from INA-6 cells using the *NucleoSpin RNA II Purification Kit* (Macherey-Nagel, Düren, Germany) according to the manufacturer's instructions.

RNAseq, Differential Expression and Functional Enrichment Analysis of INA-6 cells

FASTQ files were merged to the respective sample. The quality of FASTQ files was assessed with FastQC (Andrews, 2010) and a joint report was created with MultiQC (Ewels et al., 2016). FASTQ files were aligned with STAR (Dobin et al., 2013) to the GRCh38 reference genome build (Zerbino et al., 2018). Quality and alignment statistics of final BAM files were assessed with samtools stats (Li et al., 2009), and a joint report with FastQC reports by MultiQC was generated.

Raw read counts were generated with HTSeq (Anders et al., 2015) using the union method. HTSeq runs internally in STAR. Differential gene expression analysis was performed with edgeR (Robinson et al., 2010) in R 3.6.3 (R Core Team, 2018), according to the edgeR manual.

Counts were merged and genes with zero counts in all samples were removed (number of genes: 36380). The whole count table was annotated with R Bioconductor (Gentleman, n.d.) human annotation data package org.Hs.eg.db (Carlson, 2016). A DGEList Element was created with

the raw counts, gene information, i.e., Ensembl GeneIDs, HUGO Symbol, Genename, and ENTREZ GeneIDs and a sample grouping metadata table.

```
1 y <- DGEList(counts=ct2[, -1:4], group=meta.data$group, genes=ct2[, 1:4])
```

Counts were filtered to keep only those genes which have at least 1 read per million in at least 2 samples (number of genes: 14136). Afterwards, normalization factors were recalculated.

```
1 keep <- rowSums(cpm(y)>1) >= 2
2 y <- y[keep, , keep.lib.size=FALSE]
3 y1 <- calcNormFactors(y)
```

A design matrix was created with the grouping factor by treatment condition (group=F1, F2, F3, which are abbreviations for CM-INA6, nMA-INA6, MA-INA6, respectively)

```
1 design = model.matrix(~0+group)
```

Dispersion was estimated, the resulting coefficient of biological variation (BCV) is 0.135, i.e., BCV expression values vary up and down by 13.5% between samples.

```
1 y1.1 <- estimateDisp(y1, design)
2 BCV <- sqrt(model.F$y1.1$common.dispersion)
```

A generalized linear model (`glmQLFit` function) was fitted.

```
1 fit <- glmQLFit(y1.1, design)
```

and pairwise comparisons were made, e.g.

```
1 F1vsF2 <- glmQLFTest(fit, contrast=makeContrasts(groupF1 - groupF2, levels=design))
2 DE.F1vsF2 <- topTags(F1vsF2, n=nrow(F1vsF2), p.value=0.05)
```

Afterwards, gene list of differentially expressed genes were used for functional enrichment analysis with Metascape (Zhou et al., 2019).

RT-qPCR

For cDNA synthesis, 1 µg of total RNA was reverse transcribed with Oligo(dT)15 primers and Random Primers (both Promega GmbH) and *Superscript IV* reverse transcriptase (Thermo Fisher Scientific) according to the manufacturer's instructions. For quantitative PCR, the cDNA was diluted 1:10, and qPCR was performed in 20 µL using 2 µL of cDNA, 10 µL of *GoTaq qPCR Master Mix* (Promega GmbH), and 5 pmol of sequence-specific primers obtained from biomers.net GmbH (Ulm, Germany) or Qiagen GmbH (Hilden, Germany) (see Supplementary Table 3 for primer sequences and PCR conditions). qPCR conditions were as follows: 95 °C for 3 minutes; 40 cycles: 95 °C for 10 seconds; respective annealing temperature for 10 seconds; 72 °C for 10 seconds; followed by melting curve analysis for the specificity of qPCR products using an *TOptical Gradient 96 PCR Thermal Cycler* (Analytik Jena AG, Jena, Germany). Samples that showed unspecific byproducts were discarded. Ct values were measured in three technical replicates (triplicates). Non-detects were discarded. One of three technical replicates was treated

as an outlier and excluded if its z-score crossed 1.5σ technical variation. We normalized expression by the housekeeping gene *36B4*. Efficiencies were determined in each reaction by linear regression of log-transformed amplification curves (Ramakers et al., 2003). Differential expression was calculated based on a modified $\Delta\Delta Ct$ formula that separated exponents to apply individual efficiencies to each *Ct* value:

$$\begin{aligned} \text{Fold Change} &= \frac{E_{\text{tar}}^{\Delta Ct_{\text{tar}(co - treated)}}}{E_{\text{ref}}^{\Delta Ct_{\text{ref}(co - treated)}}} \\ &= \frac{E_{\text{tar},\text{co}}^{Ct_{\text{tar},\text{co}}} \div E_{\text{tar},\text{treated}}^{Ct_{\text{tar},\text{treated}}}}{E_{\text{ref},\text{co}}^{Ct_{\text{ref},\text{co}}} \div E_{\text{ref},\text{treated}}^{Ct_{\text{ref},\text{treated}}}} \end{aligned}$$

- $E_{\text{tar},\text{co}}$ = Efficiency of the target gene measured in the control sample
- $Ct_{\text{tar},\text{co}}$ = Ct value of the target gene measured in the control sample
- *tar* = Target Gene
- *ref* = Reference Gene
- *treated* = Treated sample
- *co* = Control Sample

Fold change expression was normalized by the median of CM-INA6 (and not sample-wise, as commonly used in $\Delta\Delta Ct$) since some genes were not expressed without direct hMSC contact (e.g., *MMP2*), and also in order to display variation of CM-INA6 next to nMA-INA6 and MA-INA6.

Statistics

For molecular analyses, each data point represents one biological replicate, defined as the mean of all technical replicates of co-cultures seeded from the same batch of hMSCs and/or INA-6 cells on the same day. For analyses of time-lapse recordings, each data point represents the normalized event count from one co-culture recording. Unique hMSCs were prioritized for each biological replicate or recording (see Appendix A: Table 1). Bars and lines represent the mean, and error bars represent the standard deviation of all hMSC donors or recordings (= all biological replicates).

Metric, normally distributed, dependent data were analyzed using factorial RM-ANOVA and paired Student's t-tests. Results of RM-ANOVA are reported as follows

$$[F(df_1, df_2) = F; p = p\text{-value}],$$

where df_1 is the degrees of freedom of the observed effect, df_2 is the degrees of freedom of the error, and F is the F-statistic (Vallat, 2018). If sphericity was met, p -values were not corrected using the Greenhouse-Geisser method ($p\text{-unc}$).

$$df_1 = k - 1$$

(k = number of groups)

$$df_2 = (k - 1)(n - 1)$$

(n = number of samples in each group)

$$F = \frac{SS_{\text{Effect}}/df_1}{SS_{\text{Error}}/df_2}$$

(SS = Sums of squares for effect or error)

If data points within dependent sample pairs were missing, such pairs were excluded from paired t-tests while others from the same subject remained.

Metric non-normal distributed, independent data was analyzed using the Kruskal-Wallis H-test and Mann-Whitney U tests. Results of the Kruskal-Wallis H-test are reported as

$$H(df) = H$$

, with df being the degrees of freedom and H being the Kruskal-Wallis H statistic, corrected for ties (Vallat, 2018).

Metric bivariate non-normal distributed data was correlated using Spearman's rank correlation and reported as:

$$\rho(df) = \rho, p = p\text{-value}$$

, where ρ is Spearman's rank correlation coefficient. df is calculated as

$$df = n - 2 \quad (n = \text{number of observations})$$

These tests were applied using Python (3.10) packages `pingouin` (0.5.1) and `statsmodels` (0.14.0) (Seabold & Perktold, 2010; Vallat, 2018). Data was plotted using `seaborn` (Waskom, 2021) and `plotastic` (Kuric & Ebert, 2024). Sphericity was ensured by Mauchly's test. Normality was checked with the Shapiro-Wilk test for $n > 3$.

Data points were log10 transformed to convert the scale from multiplicative ("fold change") to additive, or to fulfill sphericity requirements. P -values derived from patient survival data were corrected using the Benjamini-Hochberg procedure. For other post-hoc analyses, p -values were not adjusted for family-wise error rate in order to minimize type I errors. To prevent type II errors, the same conclusions were validated by different experimental setups and through varying hMSCs donors across experiments (see Appendix A: Table 1).

Significant p -values from pairwise tests were annotated as stars between data groups

$$p\text{-value} = 0.05 > * > 0.01 > ** > 10^{-3} > *** > 10^{-4} > ****.$$

If too many significant pairs were detected, only those pairs of interest were annotated.

No power calculation was performed to determine sample size since samples were limited by availability of primary hMSC donors. Experiments were repeated until a minimum of three biological replicates were gathered.

Patient Cohort, Analysis of Survival and Expression

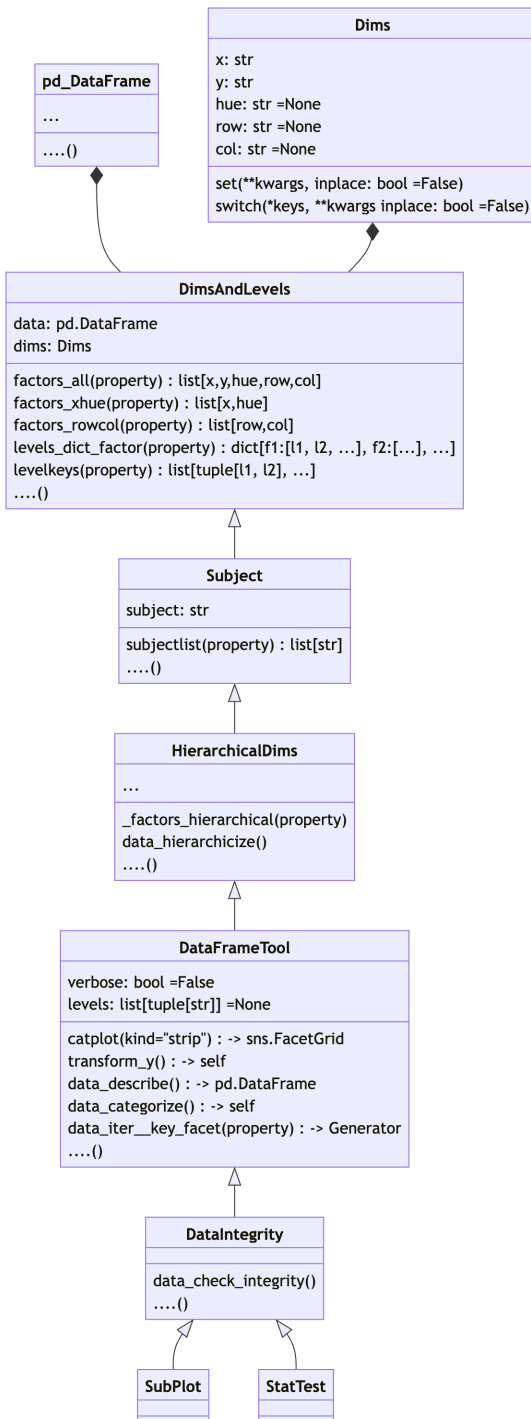
Patient samples ($n = 873$) were collected at the University Hospital Heidelberg and processed as described (Seckinger et al., 2017, 2018), and are available at the European Nucleotide Archive

(ENA) via accession numbers PRJEB36223 and PRJEB37100. Consecutive patients with monoclonal gammopathy of unknown significance (MGUS) ($n = 62$), asymptomatic ($n = 259$), symptomatic, therapy-requiring ($n = 764$), and relapsed/refractory myeloma ($n = 90$), as well as healthy donors ($n = 19$) as comparators were included in the study approved by the ethics committee (#229/2003, #S-152/2010) after written informed consent.

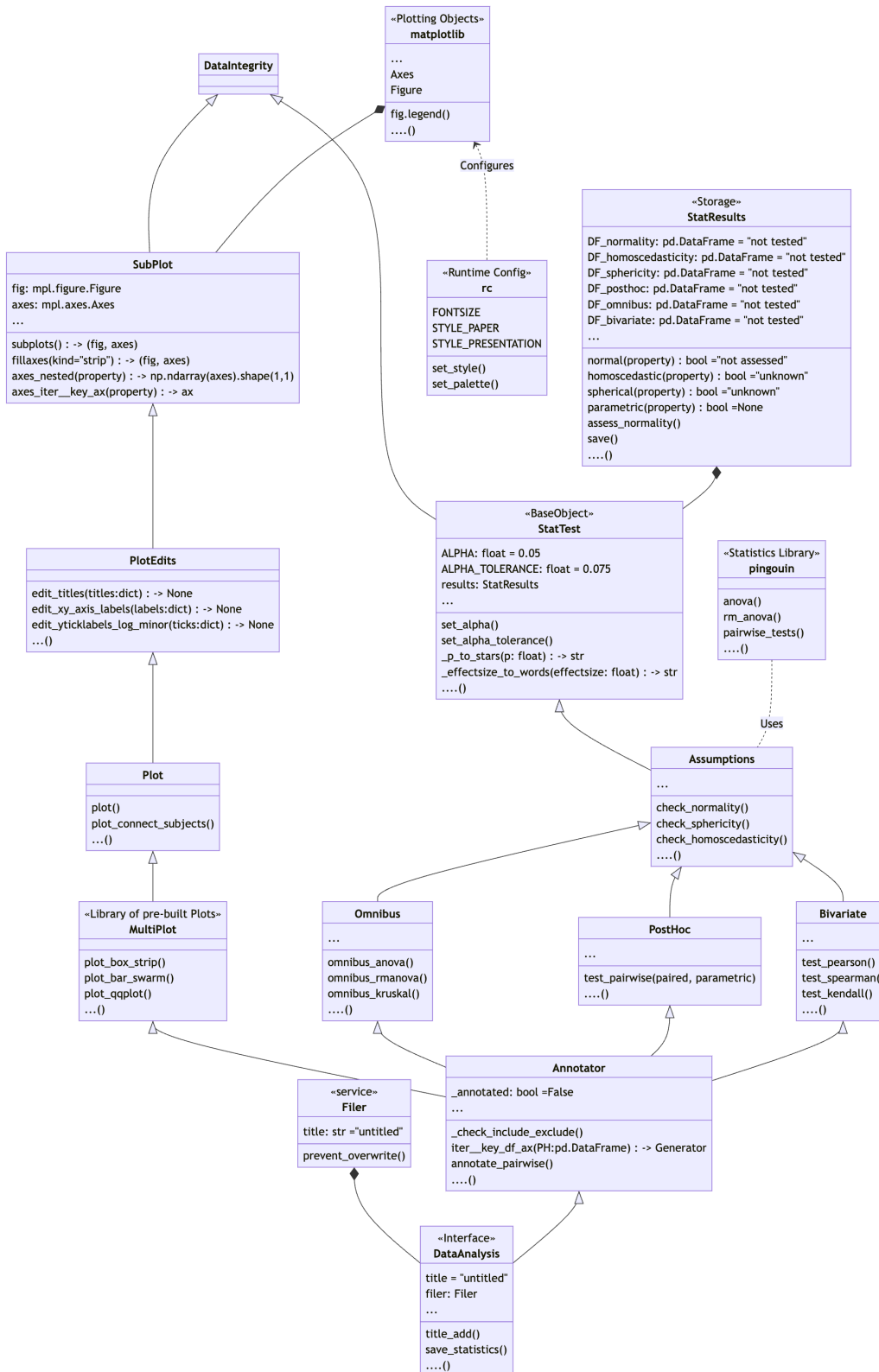
Gene expression was measured by RNA sequencing as previously described (Seckinger et al., 2018). Gene expression is defined as the \log_2 transformed value of normalized counts + 1 (as pseudocount). Progression-free (PFS) and overall survival (OS) were analyzed for the subset of previously untreated symptomatic myeloma patients. For delineating “high” and “low” expression of target adhesion ($n = 101$) and cell cycle ($n = 173$) genes, thresholds per gene were calculated with maximally selected rank statistics by the maxstat package in R (Hothorn & Lausen, n.d.). PFS and OS were analyzed for high vs. low expression with the Kaplan-Meier method (Kaplan & Meier, 1958). Significant differences between the curves were analyzed with log-rank tests (Harrington & Fleming, 1982). P -values were corrected for multiple testing by the Benjamini-Hochberg method. Analyses were performed with R version 3.6.3 (R Core Team, 2018).

B Documentation of `plotastic`

B.1 Class Diagram



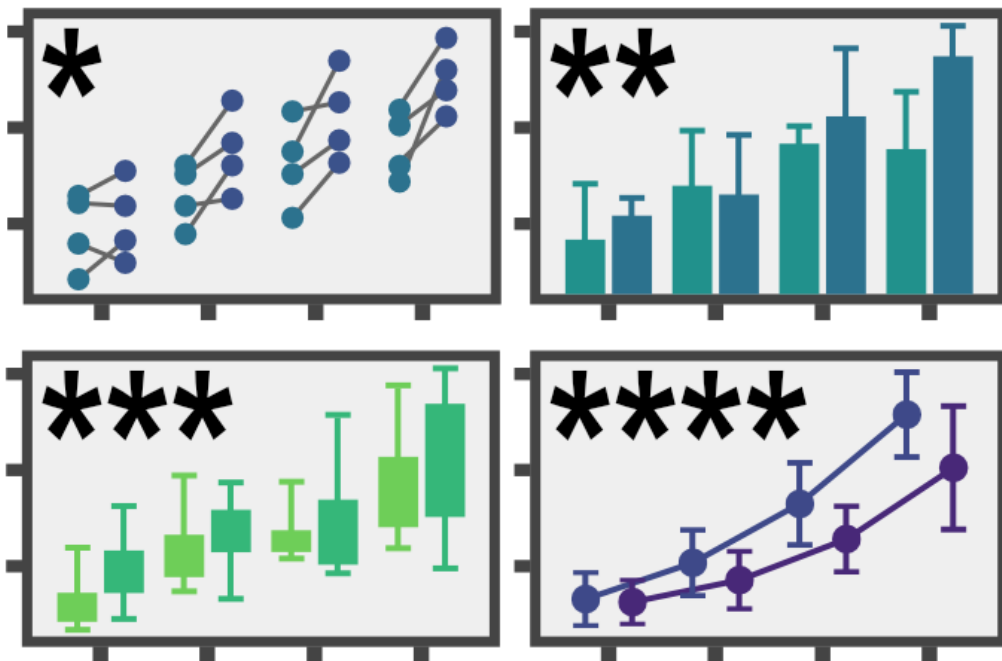
Appendix B Figure 1: Class diagram of plotastic (upper part): The architecture of plotastic begins with classes that are related to handling a pandas.DataFrame object which stores the data, and defining dimensions to group the data (y, x, hue, col, row). This diagram ends with the classes SubPlot and StatTest and is continued on the next page. Arrow shapes follow the UML (unified modeling language): A hollow triangle indicates inheritance (“is a”) and a filled diamond indicates composition (“has a”).



Appendix B Figure 1: continued from previous page The architecture of plotastic continues after the class `DataIntegrity` with classes for plotting (`SubPlot`) and statistical testing (`StatTest`) and ends with the class `DataAnalysis`, which serves as the main user interface. Arrow shapes follow the UML (unified modeling language): A hollow triangle indicates inheritance ("is a") and a filled diamond indicates composition ("has a").

B.2 Readme

The following pages are the README.md of `plotastic` found in the Python Package Index (PyPi) (pypi.org/project/plotastic), and on GitHub (github.com/markur4/plotastic).



code style black codecov 79% JOSS 10.21105/joss.06304

plotastic: Bridging Plotting and Statistics

Installation

Install from PyPi:

```
pip install plotastic
```

Install from GitHub: (experimental, check CHANGELOG.md)

```
pip install git+https://github.com/markur4/plotastic.git
```

Requirements

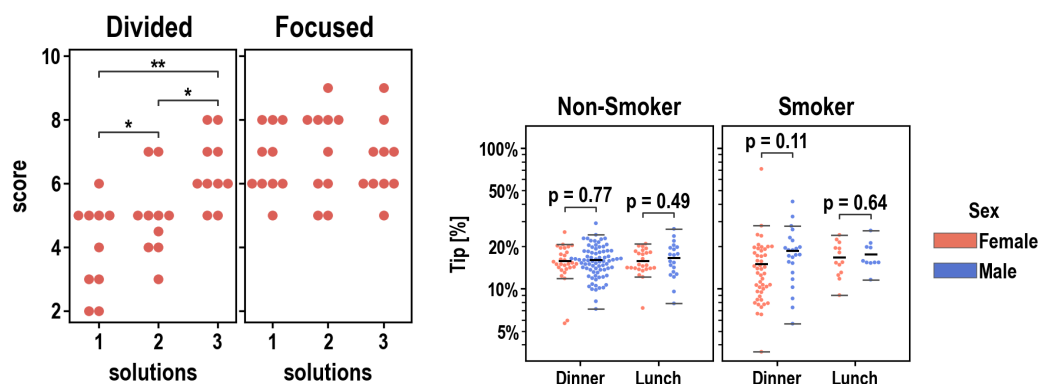
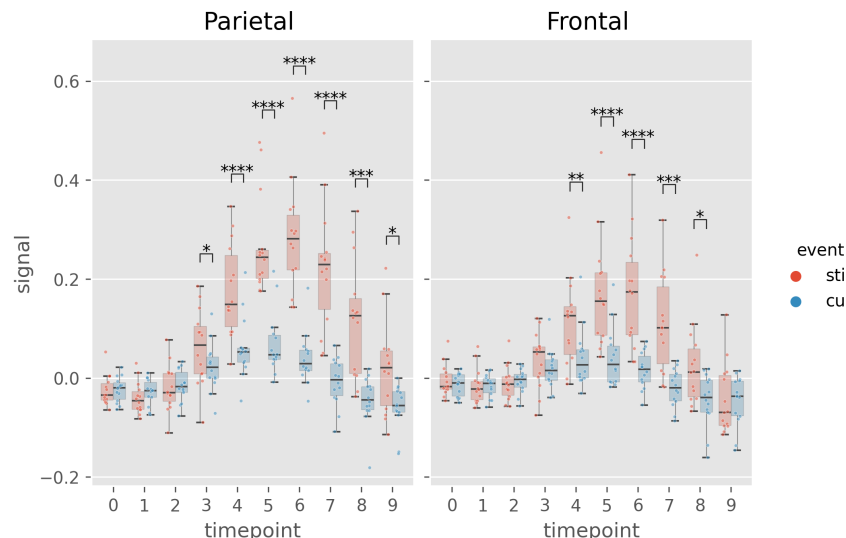
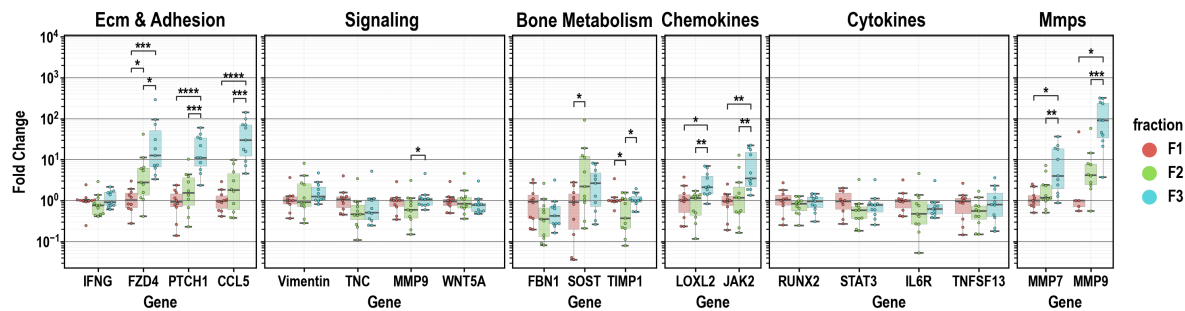
- Python >= 3.11 (*not tested with earlier versions*)

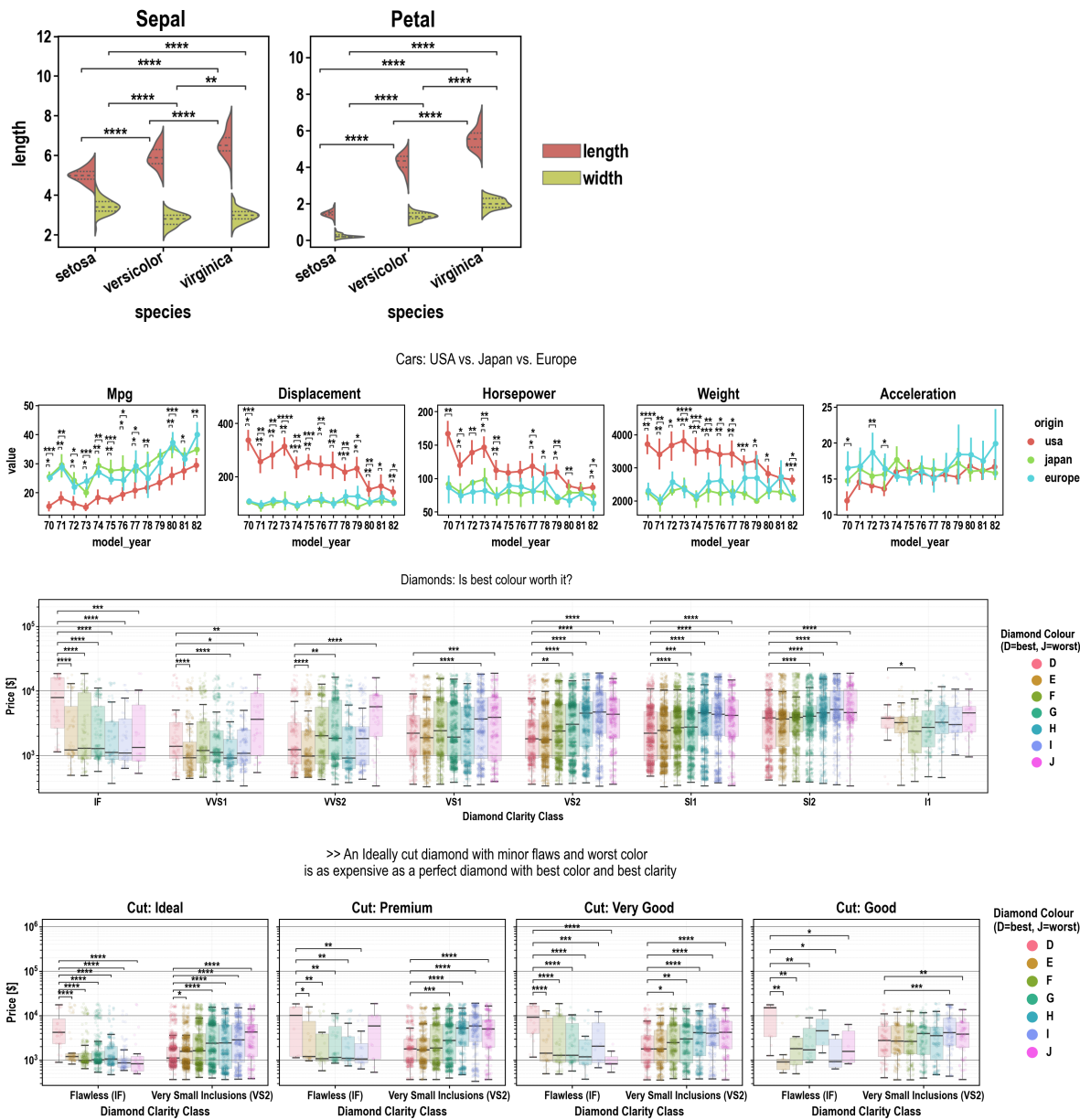
- pandas == 1.5.3 (*pingouin needs this*)
- seaborn <= 0.12.2 (*later versions reworked hue*)

Example Gallery

► (click to unfold)

(Mouse) Click on Images for Code! (Mouse)





>About plotastic

▶ 🧑 Summary

plotastic addresses the challenges of transitioning from exploratory data analysis to hypothesis testing in Python's data science ecosystem. Bridging the gap between **seaborn** and **pingouin**, this library offers a unified environment for plotting and statistical analysis. It simplifies the workflow with a user-friendly syntax and seamless integration with familiar **seaborn** parameters (`y`, `x`, `hue`, `row`, `col`). Inspired by **seaborn**'s consistency, **plotastic** utilizes a **DataAnalysis** object to intelligently pass parameters to **pingouin** statistical functions. The library systematically groups the data according to the needs of statistical tests and plots, conducts visualisation, analyses and supports extensive customization options. In essence, **plotastic** establishes a protocol for configuring statical analyses through plotting parameters.

This approach streamlines the process, translating `seaborn` parameters into statistical terms, providing researchers and data scientists with a cohesive and user-friendly solution in python.!

Workflow:

1. Import & Prepare your pandas DataFrame

- o We require a long-format pandas dataframe with categorical columns
- o If it works with seaborn, it works with plotastic!

2. Make a DataAnalysis Object

- o `DataAnalysis(DataFrame, dims={x, y, hue, row, col})`
- o Check for empty data groups, differing samplesizes, NaN-count, etc. automatically

3. Explore Data

- o Check Data integrity, unequal samplesizes, empty groups, etc.
- o Quick preliminary plotting with e.g. `DataAnalysis.catplot()`

4. Adapt Data

- o Categorize multiple columns at once
- o Transform dependent variable
- o Each step warns you, if you introduced NaNs without knowledge!
- o etc.

5. Perform Statistical Tests

- o Check Normality, Homoscedasticity, Sphericity
- o Perform Omnibus tests (ANOVA, RMANOVA, Kruskal-Wallis, Friedman)
- o Perform PostHoc tests (Tukey, Dunn, Wilcoxon, etc.) based on `pg.pairwise_tests()`

6. Plot figure

- o Use pre-defined and optimized multi-layered plots with one line (e.g. strip over box)!
- o Annotate statistical results (p-values as *, **, ***, etc.) with full control over which data to include or exclude!

7. Save all results at once!

- o One DataAnalysis object holds:
 - One DataFrame in `self.data`
 - One Figure in `self.fig, self.axes`
 - Multiple statistical results: `self.results`
- o Use `DataAnalysis.save_statistics()` to save all results to different sheets collected in one .xlsx filesheet per test

► Translating Plots into Statistics!

In Principle:

- Categorical data is separable into `seaborn`'s categorization parameters: `x, y, hue, row, col`. We call those "*dimensions*".
- These dimensions are assigned to statistical terms:
 - o `y` is the **dependent variable (DV)**
 - o `x` and `hue` are **independent variables (IV)** and are treated as **within/between factors** (categorical variables)
 - o `row` and `col` are **grouping variables** (categorical variables)
 - o A `subject` may be specified for within/paired study designs (categorical variable)

- For each level of **row** or **col** (or for each combination of **row-** and **col** levels), statistical tests will be performed with regards to the two-factors **x** and **hue**

Example with ANOVA:

- Imagine this example data:
 - Each day you measure the tip of a group of people.
 - For each tip, you note down the **day**, **gender**, **age-group** and whether they **smoke** or not.
 - Hence, this data has 4 categorical dimensions, each with 2 or more *levels*:
 - **day**: 4 levels (*monday, tuesday, wednesday, Thursday*)
 - **gender**: 2 levels (*male, female*)
 - **smoker**: 2 levels (*yes, no*)
 - **age-group**: 2 levels (*young, old*)
- Each category is assigned to a place of a plot, and when calling statistical tests, we assign them to statistical terms (in comments):

```

◦ # dims is short for dimensions
dims = dict(           # STATISTICAL TERM:
    y = "tip",         # y-axis, dependent variable
    x = "day",          # x-axis, independent variable (within-
    subject factor)
    hue = "gender",     # color, independent variable (within-
    subject factor)
    col = "smoker",     # axes, grouping variable
    row = "age-group"   # axes, grouping variable
)

```

- We perform statistical testing groupwise:
 - For each level-combinations of **smoker** and **age-group**, a two-way ANOVA will be performed (with **day** and **gender** as **between** factors for each datagroup):
 - 1st ANOVA assesses datapoints where **smoker=yes** AND **age-group=young**
 - 2nd ANOVA assesses datapoints where **smoker=yes** AND **age-group=old**
 - 3rd ANOVA assesses datapoints where **smoker=no** AND **age-group=young**
 - 4th ANOVA assesses datapoints where **smoker=no** AND **age-group=old**
 - Three-way ANOVAs are not possible (yet), since that would require setting e.g. **col** as the third factor, or implementing another dimension (e.g. **hue2**).

► ! Disclaimer about Statistics

This software was inspired by ...

- ... ***Intuitive Biostatistics*** - Fourth Edition (2017); Harvey Motulsky
- ... ***Introduction to Statistical Learning with applications in Python*** - First Edition (2023); Gareth James, Daniela Witten, Trevor Hastie, Robert Tibshirani, Jonathan Taylor
- ... talking to other scientists struggling with statistics

 **plotastic** can help you with...

- ... gaining some practical experience when learning statistics
- ... quickly gain statistical implications about your data without switching to another software
- ... making first steps towards a full statistical analysis
- ... plotting publication grade figures (check statistics results with other software)
- ... publication grade statistical analysis **IF** you really know what you're doing OR you have back-checked your results by a professional statistician
- ... quickly test data transformations (log)

🚫 **plotastic** can NOT ...

- ... replace a professional statistician
- ... teach you statistics, you need some basic knowledge (but is awesome for practicing!)
- ... test for multicollinearity (Absence of multicollinearity is required by ANOVA!)
- ... perform stringent correction for multiple testing (e.g. bonferroni), as statistical tests are applied to sub-facets of the whole dataframe for each axes, which depends on the definition of x, hue, col, etc. Hence, corrected p-values might over-estimate the significance of your results.

🟡 Be critical and responsible with your statistical analysis!

- **Expect Errors:** Don't trust automated systems like this one!
- **Document your work in ridiculous detail:**
 - Include the applied tests, the number of technical replicates and the number of biological/independent in each figure legend
 - State explicitly what each datapoint represents:
 - 1 datapoint = 1 Technical replicate?
 - 1 datapoint = The mean of all technical replicate per independent replicate/subject?
 - State explicitly what the error-bars mean: Standard deviation? Confidence interval?
 - (Don't mix technical with biological/independent variance)
 - Report if/how you removed outliers
 - Report if you did or did not apply correction methods (multiple comparisons, Greenhouse Geyser, etc.) and what your rationale is (exploratory vs. confirmatory study? Validation through other methods to reduce Type I error?)
- **Check results with professionals:**
 - "Here is my data, here is my question, here is my analysis, here is my interpretation. What do you think?"

► ✅ Feature List

- ✅ : Complete and tested
- 👍 : Complete
- 📅 : Planned or unfinished (no date)
- 🧑‍💨 : Maybe..? (Rather not...)
- 🚫 : Not planned, don't want
- 😢 : Help Please..?

▼ Plotting

- 👍 Make and Edit Plots: Implemented ✅

- All (non-facetgrid) seaborn plots should work, not tested
- QQ-Plot
- Kaplan-Meyer-Plot
- Interactive Plots (where you click stuff and adjust scale etc.)
 - That's gonna be a lot of work!
- Support for `seaborn.FacetGrid`
 - Why not? - `plotastic` uses `matplotlib` figures and fills its axes with `seaborn` plot functions. In my opinion, that's the best solution that offers the best adaptability of every plot detail while being easy to maintain
- Support for `seaborn.objects` (same as Facetgrid)
 - Why not? - I don't see the need to refactor the code
- NEED HELP WITH: The hidden state of `matplotlib` figures/plots/stuff that gets drawn:
 - I want to save the figure in `DataAnalysis.fig` attribute. As simple as that sounds, `matplotlib` does weird stuff, not applying changes after editing the plot.
 - It'd be cool if I could control the changes to a `DataAnalysis` object better (e.g. using `inplace=True` like with `pd.DataFrame`). But I never figured out how to control `matplotlib` figure generation, even with re-drawing the figure with `canvas`. It's a mess and I wasted so much time already.

▼ Multi-Layered Plotting

- Box-plot + swarm
- Box-plot + strip
- Violin + swarm/strip

▼ Statistics

- Assumption testing
 - Normality (e.g. Shapiro-Wilk)
 - Homoscedasticity (e.g. Levene)
 - Sphericity (e.g. Mauchly)
- Omnibus tests
 - ANOVA, RMANOVA, Kruskal-Wallis, Friedman
 - Mixed ANOVA
 - Annotate Results into Plot
- PostHoc
 - `pg.pairwise_tests()`
 - Works with all primary options. That includes all parametric, non-parametric, paired, unpaired, etc. tests (*t-test*, paired *t-test*, *MWU*, *Wilcoxon*, etc.)
 - Annotate Stars into plots (*, **, etc.)
 - Specific pairs can be included/excluded from annotation
 - Make correction for multiple testing go over complete DataFrame and not Facet-wise:
- Bivariate
 - Find and Implement system to switch between numerical and categorical x-axis
 - Function to convert numerical data into categorical data by binning?
 - Pearson, Spearman, Kendall

▼ Analysis Pipelines

Idea: Put all those statistical tests into one line. I might work on this only after everything's implemented and working confidently and well!

- 🐦 `between_samples(parametric=True)`: ANOVA + Tukey (if Normality & Homoscedasticity are given)
- 🐦 `between_samples(parametric=False)`: Kruskal-Wallis + Dunn
- 🐦 `within_samples(parametric=True)`: RM-ANOVA + multiple paired t-tests (if Normality & Sphericity are given)
- 🐦 `within_samples(parametric=False)`: Friedman + multiple Wilcoxon



How To Use

Documentations

1. Example Gallery

1. Quick Example: FMRI
2. qPCR (paired, parametric)
3. Cars (unpaired, non-parametric)
4. Diamonds (unpaired, non-parametric)
5. Attention (paired/mixed, parametric)
6. Iris (unpaired, parametric)
7. Tips (unpaired, parametric)

2. Data

1. Set/Switch Dimensions

3. Plotting

1. Quick & Simple: MultiPlots
2. Constructing Plots
3. Legends
4. Styles

Quick Example

Import plotastic and example Data

```
import matplotlib.pyplot as plt
import plotastic as plst

# Import Example Data (Long-Format)
DF, _dims = plst.load_dataset("fmri", verbose = False)
DF.head()
```

Assign each column to a dimension (y, x, hue, col, row):

```

dims = dict(
    y = "signal",      # y-axis, dependent variable
    x = "timepoint",  # x-axis, independent variable & within-subject
                      # factor
    hue = "event",    # color, grouping variable & within-subject factor
    col = "region"   # axes, grouping variable
)

```

Initialize DataAnalysis Object

```

DA = plst.DataAnalysis(
    data=DF,           # Dataframe, long format
    dims=dims,         # Dictionary with y, x, hue, col, row
    subject="subject", # Datapoints are paired by subject (optional)
    verbose=False,     # Print out info about the Data (optional)
)

```

Perform Statistics

No arguments need to be passed, although `**kwargs`, are passed to respective `pingouin` functions.

```

DA.check_normality() # Normal Distribution?
DA.check_sphericity() # Sphericity?
DA.omnibus_rm_anova() # Repeated Measures ANOVA
DA.test_pairwise() # Post-hoc tests

```

Save Results:

Output is one excel file containing results of all performed tests (normality, anova, t-tests, etc.) in different sheets

```
DA.save_statistics("example.xlsx")
```

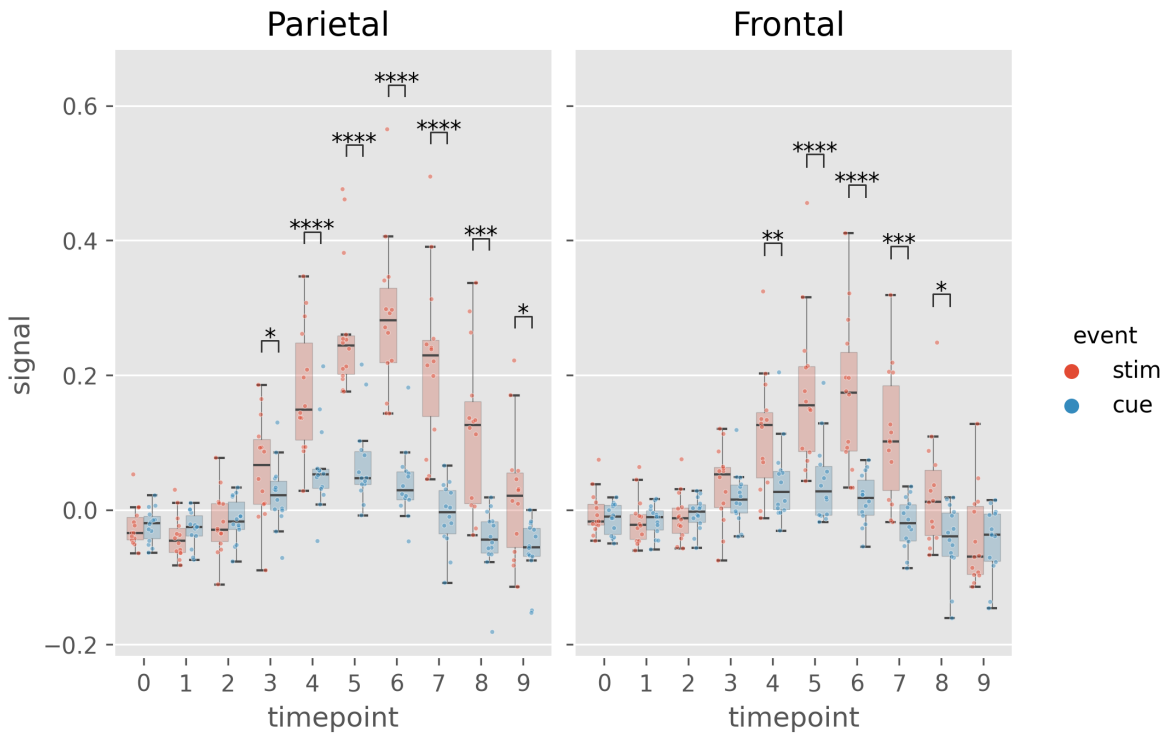
Annotate post-hoc results into plot:

```

(DA
    .plot_box_strip() # Pre-built plotting function initializes plot
    .annotate_pairwise( # Annotate results from DA.test_pairwise()
        include="__HUE" # Use only significant pairs across each hue
    )
)

```

```
# Saving the plot like matplotlib!
plt.savefig("example.png", dpi=200, bbox_inches="tight")
```



🧪 Testing

▶ (click to unfold)

- Download/Clone repository
- Install development tools `pip install .[dev]`
- Run tests
 - Run `pytest ./tests`
 - To include a coverage report run `pytest ./tests -cov--cov-report=html` and open `./htmlcov/index.html` with your browser.

🤝 Community Guidelines

▶ (click to unfold)

When interacting with the community, you must adhere to the [Code of Conduct](#)

Contribute

I am grateful for [pull requests!](#)

- Make sure to understand the code (e.g. see Class diagram in this Readme)
- Run tests before submitting a pull request

Reporting Issues & Problems

If you need help, please open an [issue](#) on this repository.

- Please provide a minimal example to reproduce the problem.

Support

If you need help, please open an [issue](#) on this repository.

✍ Cite These!

► **(click to unfold)**

Kuric et al., (2024). plotastic: Bridging Plotting and Statistics in Python. *Journal of Open Source Software*, 9(95), 6304, <https://doi.org/10.21105/joss.06304>

Vallat, R. (2018). Pingouin: statistics in Python. *Journal of Open Source Software*, 3(31), 1026, <https://doi.org/10.21105/joss.01026>

Waskom, M. L., (2021). seaborn: statistical data visualization. *Journal of Open Source Software*, 6(60), 3021, <https://doi.org/10.21105/joss.03021>.

```
@article{Kuric2024,
  doi = {10.21105/joss.06304},
  url = {https://doi.org/10.21105/joss.06304},
  year = {2024}, publisher = {The Open Journal},
  volume = {9},
  number = {95},
  pages = {6304},
  author = {Martin Kuric and Regina Ebert},
  title = {plotastic: Bridging Plotting and Statistics in Python},
  journal = {Journal of Open Source Software}
}

@article{Waskom2021,
  doi = {10.21105/joss.03021},
  url = {https://doi.org/10.21105/joss.03021},
  year = {2021},
  publisher = {The Open Journal},
  volume = {6},
  number = {60},
  pages = {3021},
  author = {Michael L. Waskom},
  title = {seaborn: statistical data visualization},
  journal = {Journal of Open Source Software}
}

@article{Vallat2018,
  title = "Pingouin: statistics in Python",
  author = "Vallat, Raphael",
  journal = "The Journal of Open Source Software",
  volume = 3,
```

```
number    = 31,  
pages     = "1026",  
month     = nov,  
year      = 2018  
}
```

B.3 Example Analysis “qpcr”

The following pages are a jupyter notebook from an example analysis using `plotastic`. This notebook and further analyses examples are found on GitHub (github.com/markur4/plotastic). The qPCR dataset was derived from the experiments described in Chapter 1 Figure 4 and was changed into a public test dataset by exchanging the original gene names with random ones while preserving gene classes and quantitative fold changes.

qPCR

April 9, 2024

```
[ ]: import plotastic as plst
import matplotlib.pyplot as plt
import seaborn as sns
import pandas as pd

[ ]: # Set Plot Style
plst.set_style("paper")
# plst.set_palette("hls", verbose=True)
plst.set_palette(["#db5f57", "#91db57", "#57d3db"])

#! You chose this color palette: ['#db5f57', '#91db57', '#57d3db', '#db5f57',
'#91db57', '#57d3db', '#db5f57', '#91db57']

['#db5f57',
 '#91db57',
 '#57d3db',
 '#db5f57',
 '#91db57',
 '#57d3db',
 '#db5f57',
 '#91db57']
```

1 Example Analysis: qPCR

Raw Data: https://github.com/markur4/plotastic/tree/main/src/plotastic/example_data/data

Original Source: (unpublished)

```
[ ]: # Import Example Data
DF, _dims = plst.load_dataset("qpcr", verbose=False)
dims = dict(
    y="fc",
    x="gene",
    hue="fraction",
    # col= 'method',
    row="class",
)
DA = plst.DataAnalysis(DF, dims, subject="subject", verbose=False)
```

```
[ ]: DA.transform_y("log10", inplace=True) # Log transform
DA.check_normality() # -> Only few groups are not normal -> parametric
```

[]:

				W	pval	normal	n
	class	gene	fraction				
Bone Metabolism		F1	FBN1	0.936873	0.518768	True	10
			SOST	0.880395	0.131862	True	10
			TIMP1	0.745494	0.004807	False	9
		F2	FBN1	0.954764	0.705148	True	11
			SOST	0.967810	0.863610	True	11
			TIMP1	0.914325	0.274168	True	11
		F3	FBN1	0.915247	0.281020	True	11
			SOST	0.923112	0.345415	True	11
			TIMP1	0.937230	0.488505	True	11
Chemokines		F1	LOXL2	0.930358	0.451421	True	10
			JAK2	0.897331	0.204749	True	10
		F2	LOXL2	0.874630	0.088876	True	11
			JAK2	0.960025	0.772006	True	11
		F3	LOXL2	0.943678	0.564652	True	11
			JAK2	0.878406	0.099301	True	11
Cytokines		F1	RUNX2	0.947142	0.634825	True	10
			STAT3	0.933422	0.482382	True	10
			IL6R	0.927258	0.421472	True	10
			TNFSF13	0.907481	0.264130	True	10
		F2	RUNX2	0.915611	0.283765	True	11
			STAT3	0.907354	0.226836	True	11
			IL6R	0.985709	0.989621	True	11
			TNFSF13	0.958855	0.757330	True	11
		F3	RUNX2	0.924060	0.353917	True	11
			STAT3	0.932663	0.438418	True	11
			IL6R	0.826181	0.020798	False	11
			TNFSF13	0.970421	0.890746	True	11
ECM & Adhesion		F1	IFNG	0.715267	0.001349	False	10
			FZD4	0.981633	0.973303	True	10
			PTCH1	0.911578	0.292008	True	10
			CCL5	0.969121	0.882582	True	10
		F2	IFNG	0.899109	0.180269	True	11
			FZD4	0.979590	0.963841	True	11
			PTCH1	0.986610	0.990734	True	10
			CCL5	0.925780	0.407685	True	10
		F3	IFNG	0.905665	0.216509	True	11
			FZD4	0.923819	0.351743	True	11
			PTCH1	0.957827	0.744318	True	11
			CCL5	0.940093	0.521596	True	11
MMPs		F1	MMP7	0.955749	0.752957	True	9
			MMP9	0.675286	0.005186	False	5
		F2	MMP7	0.926078	0.372552	True	11

		MMP9	0.971128	0.901100	True	10
	F3	MMP7	0.924886	0.361455	True	11
		MMP9	0.913554	0.268549	True	11
Signaling	F1	Vimentin	0.919696	0.354424	True	10
		TNC	0.928589	0.434161	True	10
		NOTCH1	0.922084	0.374662	True	10
		WNT5A	0.903581	0.239742	True	10
	F2	Vimentin	0.957763	0.743507	True	11
		TNC	0.959813	0.769352	True	11
		NOTCH1	0.977556	0.951045	True	11
		WNT5A	0.937156	0.487661	True	11
	F3	Vimentin	0.910924	0.250109	True	11
		TNC	0.884194	0.117578	True	11
		NOTCH1	0.779982	0.005132	False	11
		WNT5A	0.812114	0.013581	False	11

[]: DA.check_sphericity()

		spher	W	chi2	dof	pval	\
class	fraction						
Bone Metabolism	F1	0	True	0.592922	3.658847	2	0.160506
	F2	0	True	0.703252	3.168356	2	0.205116
	F3	0	True	0.832864	1.645964	2	0.439120
Chemokines	F1	0	True	NaN	NaN	1	1.000000
	F2	0	True	NaN	NaN	1	1.000000
	F3	0	True	NaN	NaN	1	1.000000
Cytokines	F1	0	True	0.629185	3.577934	5	0.614197
	F2	0	False	0.262747	11.657816	5	0.040987
	F3	0	False	0.210032	13.610980	5	0.019012
ECM & Adhesion	F1	0	True	0.486690	5.560987	5	0.354712
	F2	0	True	0.295164	8.202615	5	0.149255
	F3	0	True	0.297080	10.586623	5	0.061736
MMPs	F1	0	True	NaN	NaN	1	1.000000
	F2	0	True	NaN	NaN	1	1.000000
	F3	0	True	NaN	NaN	1	1.000000
Signaling	F1	0	True	0.536227	4.812474	5	0.442437
	F2	0	True	0.554009	5.151113	5	0.400336
	F3	0	False	0.117602	18.669462	5	0.002375
		group	count	n per group			
class	fraction						
Bone Metabolism	F1	0	3	[10, 10, 9]			
	F2	0	3	[11, 11, 11]			
	F3	0	3	[11, 11, 11]			
Chemokines	F1	0	2	[10, 10]			
	F2	0	2	[11, 11]			
	F3	0	2	[11, 11]			

Cytokines	F1	0	4	[10, 10, 10, 10]
	F2	0	4	[11, 11, 11, 11]
	F3	0	4	[11, 11, 11, 11]
ECM & Adhesion	F1	0	4	[10, 10, 10, 10]
	F2	0	4	[10, 11, 11, 10]
	F3	0	4	[11, 11, 11, 11]
MMPs	F1	0	2	[9, 5]
	F2	0	2	[11, 10]
	F3	0	2	[11, 11]
Signaling	F1	0	4	[10, 10, 10, 10]
	F2	0	4	[11, 11, 11, 11]
	F3	0	4	[11, 11, 11, 11]

```
[ ]: # Default is (paired) t-test, and since DA has subject: paired=True
DA.test_pairwise()
```

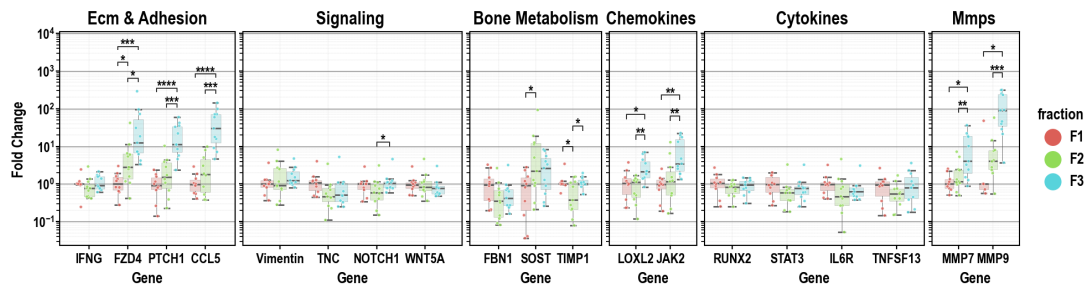
			gene	A	B	mean(A)	\
	class	fraction Contrast					
ECM & Adhesion	-	gene	-	CCL5	FZD4	0.591713	
		gene	-	CCL5	IFNG	0.591713	
		gene	-	CCL5	PTCH1	0.591713	
		gene	-	FZD4	IFNG	0.622994	
		gene	-	FZD4	PTCH1	0.622994	
..			
MMPs	NaN	gene * fraction	MMP9	F1	F3	0.256111	
		gene * fraction	MMP9	F2	F3	0.677357	
	F1	fraction * gene	NaN	MMP7	MMP9	0.032549	
	F2	fraction * gene	NaN	MMP7	MMP9	0.185211	
	F3	fraction * gene	NaN	MMP7	MMP9	0.742060	
			std(A)	mean(B)	std(B)	Paired	\
	class	fraction Contrast					
ECM & Adhesion	-	gene	0.253752	0.622994	0.266747	True	
		gene	0.253752	-0.026656	0.149430	True	
		gene	0.253752	0.469495	0.330886	True	
		gene	0.266747	-0.026656	0.149430	True	
		gene	0.266747	0.469495	0.330886	True	
..			
MMPs	NaN	gene * fraction	0.802159	1.845550	0.600687	True	
		gene * fraction	0.546148	1.845550	0.600687	True	
	F1	fraction * gene	0.228544	0.256111	0.802159	True	
	F2	fraction * gene	0.361750	0.677357	0.546148	True	
	F3	fraction * gene	0.567249	1.845550	0.600687	True	
			Parametric		T	dof	\
	class	fraction Contrast					
ECM & Adhesion	-	gene	True	-0.327586	10.0		

		gene	True	7.882620	10.0	
		gene	True	1.320783	10.0	
		gene	True	7.532512	10.0	
		gene	True	2.105924	10.0	
..			
MMPs	NaN	gene * fraction	True	-3.513968	4.0	
		gene * fraction	True	-5.680475	9.0	
	F1	fraction * gene	True	-0.543884	4.0	
	F2	fraction * gene	True	-3.811156	9.0	
	F3	fraction * gene	True	-15.767066	10.0	
			alternative		p-unc	BF10 \
class		fraction Contrast				
ECM & Adhesion -		gene	two-sided	7.499799e-01		0.312
		gene	two-sided	1.339935e-05		1643.947
		gene	two-sided	2.160003e-01		0.598
		gene	two-sided	1.987311e-05		1165.781
		gene	two-sided	6.146203e-02		1.461
..			
MMPs	NaN	gene * fraction	two-sided	2.458360e-02		3.686
		gene * fraction	two-sided	3.016844e-04		111.751
	F1	fraction * gene	two-sided	6.154168e-01		0.448
	F2	fraction * gene	two-sided	4.145762e-03		12.636
	F3	fraction * gene	two-sided	2.163081e-08		4.845e+05
			hedges	**p-unc	Sign.	\
class		fraction Contrast				
ECM & Adhesion -		gene	-0.115597	ns	False	
		gene	2.856874	****	signif.	
		gene	0.398765	ns	False	
		gene	2.890772	****	signif.	
		gene	0.491362	0.061	toler.	
..			
MMPs	NaN	gene * fraction	-2.179426	*	signif.	
		gene * fraction	-2.024511	***	signif.	
	F1	fraction * gene	-0.255634	ns	False	
	F2	fraction * gene	-0.939861	**	signif.	
	F3	fraction * gene	-1.817138	****	signif.	
				pairs	cross	
class		fraction Contrast				
ECM & Adhesion -		gene		(CCL5, FZD4)	x	
		gene		(CCL5, IFNG)	x	
		gene		(CCL5, PTCH1)	x	
		gene		(FZD4, IFNG)	x	
		gene		(FZD4, PTCH1)	x	
..				

MMPs	NaN	gene * fraction	((MMP9, F3), (MMP9, F1))	hue
		gene * fraction	((MMP9, F3), (MMP9, F2))	hue
	F1	fraction * gene	((MMP9, F1), (MMP7, F1))	x
	F2	fraction * gene	((MMP9, F2), (MMP7, F2))	x
	F3	fraction * gene	((MMP9, F3), (MMP7, F3))	x

[167 rows x 19 columns]

```
[ ]: # Plot
(
  DA.switch("row", "col", verbose=False)
  .set(y="fc", inplace=False) # set y back to fc to display non-log values
  .plot_box_strip(
    subplot_kws=dict(
      figsize=(10, 2.5),
      width_ratios=[4, 5, 3, 2, 5, 2],
    ),
    strip_kws=dict(alpha=0.8),
  )
  .edit_grid()
  .edit_y_scale_log(10)
  .edit_xy_axis_labels(y_leftmost_col="Fold Change", x="Gene")
  .annotate_pairwise(include="__HUE")
)
plt.savefig("qpcr1.png", dpi=300, bbox_inches="tight")
```



C Submission Forms & Documents

C.1 Author Contributions



Statement of individual author contributions and of legal second publication rights to manuscripts included in the dissertation

Manuscript 1: Research Article (submitted, under revision)

Martin Kuric (MK), Susanne Beck, Doris Schneider, Wyonna Rindt, Marietheres Evers, Jutta Meißner-Weigl, Sabine Zeck, Melanie Krug, Marietta Herrmann, Tanja Nicole Hartmann, Ellen Leich, Maximilian Rudert, Denitsa Docheva, Anja Seckinger, Dirk Hose, Franziska Jundt, Regina Ebert (RE) (2024): Keep it Together: Describing Myeloma Dissemination *in vitro* with hMSC-Interacting Subpopulations and their Aggregation/Detachment Dynamics, **Cancer Research Communications**

Participated in	Author Initials, Responsibility decreasing from left to right				
Study Design	<u>MK</u>	Regina Ebert	Wyonna Rindt		
Methods Development	<u>MK</u>	Doris Schneider			
Data Collection	<u>MK</u>	Doris Schneider			
Data Analysis and Interpretation	<u>MK</u>	Susanne Beck	Regina Ebert		
Manuscript Writing Writing of Introduction Writing of Materials & Methods Writing of Discussion Writing of First Draft	<u>MK</u>	Regina Ebert			

Explanations: The content of this publication exceeds the usual scope (~29 pages Supplemental). It includes not only research findings but also survival data and protocols of new, established methods and their validations. The contribution of Martin Kuric was pivotal and predominant in all aspects of this work. Doris Schneider assisted in the experimental procedures. Susanne Beck analyzed the raw data from RNAseq and survival data, which were interpreted, depicted, and summarized by Martin Kuric.

Manuscript 2: Data Analysis Software (submitted, passed peer-review, under revision)

Martin Kuric (MK), Regina Ebert (2024): plotastic: Bridging Plotting and Statistics in Python, **Journal of Open Source Software**

Participated in	Author Initials, Responsibility decreasing from left to right				
Idea, Architectural Design	<u>MK</u>				
Software Development Feature Implementation Testing	<u>MK</u>				
Distribution of Software Documentation Version Control (GitHub) Deployment (PyPi)	<u>MK</u>				
Manuscript Writing Writing of Statement of Need Writing of Example Writing of Overview	<u>MK</u>	Regina Ebert			

Explanations: The software was entirely created by Martin Kuric, comprising more than 8000 total lines (including ~2000 testable lines) and is comparable in size to a typical web application. The release of this software involved version control using GitHub, packaging and deployment on PyPi. Regina Ebert gave feedback on submitted manuscript.

Manuscript 3: Research Letter (published)					
Daniela Simone Maichl, Julius Arthur Kirner, Susanne Beck, Wen-Hui Cheng, Melanie Krug, <u>Martin Kuric (MK)</u> , Carsten Patrick Ade, Thorsten Bischler, Franz Jakob, Dirk Hose, Anja Seckinger, Regina Ebert & Franziska Jundt (2023): Identification of NOTCH-driven matrisome-associated genes as prognostic indicators of multiple myeloma patient survival, Blood Cancer Journal 13:134					
Participated in	Author Initials , Responsibility decreasing from left to right				
Study Design Methods Development	Daniela Simone		Franziska Jundt		
Data Collection	Daniela Simone		Franziska Jundt		
Data Analysis and Interpretation	Daniela Simone	Susanne Beck	Franziska Jundt	<u>MK</u>	
Manuscript Writing Writing of Introduction Writing of Materials & Methods Writing of Discussion Writing of First Draft	Daniela Simone		Franziska Jundt	<u>MK</u>	

Explanations: This co-authorship is not a chapter in this dissertation. Martin Kuric produced figures of processed but complex-to-visualize data and gave feedback on submitted manuscript.

Manuscript 4: Research Paper (under peer-review)					
Wyonna Rindt, Melanie Krug, Shuntaro Yamada, Franziska Sennefelder, Louisa Belz, Wen-Hui Cheng, Azeem Muhammad, <u>Martin Kuric (MK)</u> , Marietheres Evers, Ellen Leich, Tanja Nicole Hartmann, Ana Rita Pereira, Marietta Herrmann, Jan Hansmann, Mohammed Ahmed Yassin, Kamal Mustafa, Regina Ebert, and Franziska Jundt (2024): A 3D bioreactor model to study osteocyte differentiation and mechanobiology under perfusion and compressive mechanical loading, Acta Biomaterialia					
Participated in	Author Initials , Responsibility decreasing from left to right				
Study Design Methods Development	Wyonna Rindt	Franziska Jundt		<u>MK</u>	
Data Collection	Wyonna Rindt	Franziska Jundt		<u>MK</u>	
Data Analysis and Interpretation	Wyonna Rindt	Franziska Jundt		<u>MK</u>	
Manuscript Writing Writing of Introduction Writing of Materials & Methods Writing of Discussion Writing of First Draft	Wyonna Rindt	Franziska Jundt		<u>MK</u>	

Explanations: This co-authorship is not a chapter in this dissertation. Martin Kuric contributed by counseling during weekly meetings in tight collaboration with Franziska Jundt's group, assisting Wyonna Rindt during laboratory experiments, image analysis and giving feedback on submitted manuscript.

Manuscript 5: Research Paper (under revision)					
Marietta Herrmann, Jutta Schneidereit, Susanne Wiesner, <u>Martin Kuric (MK)</u> , Maximilian Rudert, Martin Lüdemann, Mugdha Srivastava, Norbert Schütze, Regina Ebert, Denitsa Docheva, Franz Jakob (2024): Peripheral blood cells enriched by adhesion to CYR61 are heterogenous myeloid modulators of tissue regeneration with early endothelial progenitor characteristics, European Cells and Materials					
Participated in	Author Initials , Responsibility decreasing from left to right				
Study Design Methods Development	Marietta Herrmann				
Data Collection	Marietta Herrmann			<u>MK</u>	

Data Analysis and Interpretation	Marietta Herrmann				
Manuscript Writing Writing of Introduction Writing of Materials & Methods Writing of Discussion Writing of First Draft	Marietta Herrmann			<u>MK</u>	

Explanations: This co-authorship is not a chapter in this dissertation. Martin Kuric contributed by establishing and measuring large automated microscopy scans of stained cells for quantifying osteogenic differentiation and giving feedback on submitted manuscript.

Manuscript 6: Research Letter (published)					
Participated in	Author Initials, Responsibility decreasing from left to right				
Study Design Methods Development	Marietheres Evers				
Data Collection	Marietheres Evers				
Data Analysis and Interpretation	Marietheres Evers			<u>MK</u>	
Manuscript Writing Writing of Introduction Writing of Materials & Methods Writing of Discussion Writing of First Draft	Marietheres Evers			<u>MK</u>	

Explanations: This co-authorship is not a chapter in this dissertation. Martin Kuric contributed by counseling during regular meetings with Ellen Leich's group and giving feedback on submitted manuscript.

If applicable, the doctoral researcher confirms that she/he has obtained permission from both the publishers (copyright) and the co-authors for legal second publication.

The doctoral researcher and the primary supervisor confirm the correctness of the above mentioned assessment.

Würzburg

Doctoral Researcher's Name	Date	Place	Signature
----------------------------	------	-------	-----------

Würzburg

Primary Supervisor's Name	Date	Place	Signature
---------------------------	------	-------	-----------



Statement of individual author contributions to figures/tables of manuscripts included in the dissertation

Manuscript 1: Research Article (submitted, under revision)

Martin Kuric (MK), Susanne Beck, Doris Schneider, Wyonna Rindt, Marietheres Evers, Jutta Meißner-Weigl, Sabine Zeck, Melanie Krug, Marietta Herrmann, Tanja Nicole Hartmann, Ellen Leich, Maximilian Rudert, Denitsa Docheva, Anja Seckinger, Dirk Hose, Franziska Jundt, Regina Ebert1 (2024): Keep it Together: Describing Myeloma Dissemination *in vitro* with hMSC-Interacting Subpopulations and their Aggregation/Detachment Dynamics, **Cancer Research Communications**

Figure	Author Initials , Responsibility decreasing from left to right				
1	<u>MK</u>	Doris Schneider			
2	<u>MK</u>	Doris Schneider			
3	<u>MK</u>	Doris Schneider	Sabine Zeck	Wyonna Rindt	Melanie Krug
4	<u>MK</u>	Doris Schneider	Susanne Beck		
5	<u>MK</u>	Susanne Beck			
6	<u>MK</u>	Susanne Beck			
7	<u>MK</u>				
S1	<u>MK</u>	Doris Schneider	Sabine Zeck	Wyonna Rindt	Melanie Krug
S2	<u>MK</u>	Doris Schneider	Marietta Herrmann		
S3	<u>MK</u>	Doris Schneider	Sabine Zeck		
S4	<u>MK</u>				
S5	<u>MK</u>				
S6	<u>MK</u>	Susanne Beck			
Table	Author Initials , Responsibility decreasing from left to right				
1	<u>MK</u>	Susanne Beck			
2	<u>MK</u>	Susanne Beck			
S1	<u>MK</u>	Doris Schneider			
S2	<u>MK</u>	Susanne Beck			
S3	<u>MK</u>				
S4	<u>MK</u>	Doris Schneider			

Manuscript 2: Data Analysis Software (submitted, passed peer-review, under revision)

Martin Kuric, Regina Ebert (2024): plotastic: Bridging Plotting and Statistics in Python, **Journal of Open Source Software**

Figure	Author Initials , Responsibility decreasing from left to right				
1	<u>MK</u>				
Table	Author Initials , Responsibility decreasing from left to right				
1	<u>MK</u>				
2	<u>MK</u>				

Documentation	Author Initials , Responsibility decreasing from left to right				
README	<u>MK</u>				
Example Gallery	<u>MK</u>				
Features	<u>MK</u>				
Testing	Author Initials , Responsibility decreasing from left to right				
Test-Code (Pytest)	<u>MK</u>				
Continuous Integration	<u>MK</u>				

Explanations: All files are available on GitHub (<https://github.com/markur4/plotastic>) and installable via pypi.com. Documentations are found in the Readme, including example gallery and feature explanation. Software tests was written using pytest. Coverage of code by tests is reviewable with codecov (<https://app.codecov.io/gh/markur4/plotastic>). Continuous Integration is implemented using GitHub actions.

Manuscript 3: Research Letter (published)

Daniela Simone Maichl, Julius Arthur Kirner, Susanne Beck, Wen-Hui Cheng, Melanie Krug, Martin Kuric, Carsten Patrick Ade, Thorsten Bischler, Franz Jakob, Dirk Hose, Anja Seckinger, Regina Ebert & Franziska Jundt (2023): Identification of NOTCH-driven matrisome-associated genes as prognostic indicators of multiple myeloma patient survival, **Blood Cancer Journal** **13:134**

Figure	Author Initials , Responsibility decreasing from left to right				
1 a	Daniela Simone			Susanne Beck	
1 b	Daniela Simone			Susanne Beck	
1 c	Daniela Simone			Susanne Beck	<u>MK</u>
1 d	Daniela Simone			Susanne Beck	<u>MK</u>
Table	Author Initials , Responsibility decreasing from left to right				
1	Daniela Simone				

Explanations: Martin Kuric plotted multidimensional diagrams using python and fine-adjusted them using professional design software (Affinity Publisher, Serif Ltd).

Manuscript 4: Research Paper (under peer-review)

Wyonna Rindt, Melanie Krug, Shuntaro Yamada, Franziska Sennefelder, Louisa Belz, Wen-Hui Cheng, Azeem Muhammad, Martin Kuric (MK), Marietheres Evers, Ellen Leich, Tanja Nicole Hartmann, Ana Rita Pereira, Marietta Hermann, Jan Hansmann, Mohammed Ahmed Yassin, Kamal Mustafa, Regina Ebert, and Franziska Jundt (2024): A 3D bioreactor model to study osteocyte differentiation and mechanobiology under perfusion and compressive mechanical loading, **Acta Biomaterialia**

Figure	Author Initials , Responsibility decreasing from left to right				
1	Wyonna Rindt				<u>MK</u>
2	Wyonna Rindt				
3	Wyonna Rindt				
4	Wyonna Rindt				
5	Wyonna Rindt				<u>MK</u>
6	Wyonna Rindt				<u>MK</u>
7	Wyonna Rindt				<u>MK</u>

Explanations: Martin Kuric contributed by counseling on experimental procedures and data analysis, such as quantifying normalized fluorescence intensity of immunohistochemistry and qPCR.

Manuscript 5: Research Paper (under revision)

Marietta Herrmann, Jutta Schneidereit, Susanne Wiesner, Martin Kuric (MK), Maximilian Rudert, Martin Lüdemann, Mugdha Srivastava, Norbert Schütze, Regina Ebert, Denitsa Docheva, Franz Jakob (2024): Peripheral blood cells enriched by adhesion to CYR61 are heterogenous myeloid modulators of tissue regeneration with early endothelial progenitor characteristics, **European Cells and Materials**

Figure	Author Initials , Responsibility decreasing from left to right				
1	Marietta Herrmann				
2	Marietta Herrmann				
3	Marietta Herrmann				
4	Marietta Herrmann				
5	Marietta Herrmann				
6	Marietta Herrmann				
7	Marietta Herrmann				<u>MK</u>

Explanations: Martin Kuric scanned osteogenically differentiated MSCs in Fig. 7 for quantification of alizarin red staining.

Manuscript 6: Research Letter (published)

Marietheres Evers, Martin Schreder, Thorsten Stühmer, Franziska Jundt, Regina Ebert, Tanja Nicole Hartmann, Michael Altenbuchinger, Martina Rudelius, Martin Kuric (MK), Wyonna Darleen Rindt, Torsten Steinbrunn, Christian Langer, Sofia Catalina Heredia-Guerrero, Hermann Einsele, Ralf Christian Bargou, Andreas Rosenwald, Ellen Leich (2023): Prognostic value of extracellular matrix gene mutations and expression in multiple myeloma, **Blood Cancer J.** 13(1):43

Figure	Author Initials , Responsibility decreasing from left to right				
1	Marietheres Evers				
2	Marietheres Evers				

Explanations: Martin Kuric contributed indirectly through counseling and feedback on submitted manuscript.

I also confirm my primary supervisor's acceptance.

Doctoral Researcher's Name

Date

Place

Signature

C.2 Affidavit

Affidavit

I hereby confirm that my thesis entitled "Development and Semi-Automated Analysis of an in vitro Model for Myeloma Cells Interacting with Mesenchymal Stromal Cells" is the result of my own work. I did not receive any help or support from commercial consultants. All sources and / or materials applied are listed and specified in the thesis.

Furthermore, I confirm that this thesis has not yet been submitted as part of another examination process neither in identical nor in similar form.

Würzburg
Place, Date

Signature

Eidesstattliche Erklärung

Hiermit erkläre ich an Eides statt, die Dissertation "Entwicklung und semi-automatisierte Analyse eines in vitro-Modells für Myelomzellen in Interaktion mit mesenchymalen Stromazellen" eigenständig, d.h. insbesondere selbstständig und ohne Hilfe eines kommerziellen Promotionsberaters, angefertigt und keine anderen als die von mir angegebenen Quellen und Hilfsmittel verwendet zu haben.

Ich erkläre außerdem, dass die Dissertation weder in gleicher noch in ähnlicher Form bereits in einem anderen Prüfungsverfahren vorgelegen hat.

Würzburg
Ort, Datum

Unterschrift

C.3 Curriculum Vitae

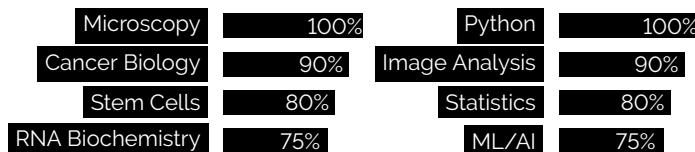
MARTIN KURIC

Cell Biologist | Data Scientist



WHO AM I?

As a cancer cell biologist with a strong passion for data analysis and machine learning, I am seeking a position where I can utilize my creativity to automate tasks, solve complex problems or handle big data.



SELECTED PROJECTS

2024	Python Software “ImageP” Accelerates batch processing of images of different sizes and types by >100%. <code>numpy</code> / <code>skimage</code> / <code>scipy</code>	GitHub Repository ⚡
2020-2024	Python Software “plotastic” Published a statistical library that self-configures based on intuitive plotting parameters. <code>pandas</code> / <code>matplotlib</code> / <code>pingouin</code> / <code>seaborn</code>	Journal of Open Source Software GitHub Repository ⚡
2018-2024	Cancer Research Project Worked in a team with up to three technical assistants and published a list of genes with relevance for survival of myeloma patients (under peer-review). <code>Time-Lapse Microscopy</code> / <code>RNAseq</code> / <code>Analysis of Patient Survival</code>	Journal: Cancer Research Communications
26.05.2022	Deep-Learning Assisted Image Cytometry Measurement of per-cell parameters from large automated microscopy scans. <code>Convolutional Neural Networks</code> / <code>Image Segmentation</code>	Poster at "Achilles Conference"

EDUCATION

28.01.2019 – 2024	Dr. rer. nat. in Biomedicine Research focus: Dissemination of multiple myeloma & mesenchymal stromal cell interactions	Prof. Dr. Regina Ebert University of Würzburg
01.04.2017 – 2024 parallel to M.Sc. & PhD	Elite Biological Physics Interdisciplinary & international study program for exceptional students of physics or biology.	University of Bayreuth
01.10.15 – 15.08.18	M.Sc. in Biochemistry & Molecular Biology Research focus: RNA biochemistry, small RNAseq, stem cells & piRNAs in <i>S. mediterranea</i>	Prof. Dr. Claus-D. Kuhn University of Bayreuth
01.10.12 – 14.12.15	B.Sc. in Biochemistry Research focus: Cell biology, mitochondrial inheritance in <i>S. cerevisiae</i>	Prof. Dr. Benedikt Westermann University of Bayreuth

LANGUAGES

German, English - C2
 Slovakian - passive
 French, Spanish - A2

SOFT SKILLS

Quality Management
 Project Management
 Violent Free Communication

HOBBIES

Coding - Python
 Music - Piano & Guitar
 Gym - Lift. Grow. Repeat

Würzburg

05.03.2024

Location

Date

Martin Kuric

Signature